UC Irvine
UC Irvine Electronic Theses and Dissertations

Title
Design and Control of a Hydrogen Fuel Cell Vehicle

Permalink
https://escholarship.org/uc/item/5jg115q0

Author
Bell, Joseph

Publication Date
2016

Peer reviewed|Thesis/dissertation

UNIVERSITY OF CALIFORNIA,
IRVINE

Design and Control of a Hydrogen Fuel Cell Vehicle

THESIS

submitted in partial satisfaction of the requirements
for the degree of

MASTER OF SCIENCE

in Mechanical and Aerospace Engineering

by

Joseph Kenneth Smithson Bell

Thesis Committee:
Professor Gregory N. Washington Irvine, Chair
Professor Jacob Brouwer
Professor K. J. Berry, Kettering University

2016

Table of Contents

List of Figures

List of tables

Acknowledgments

Abstract of The Thesis

Design and Control of Hydrogen Fuel Cell Vehicle
By

Joseph Kenneth Smithson Bell

Master of Science in Mechanical and Aerospace Engineering

University of California, Irvine, 2016

Dean Gregory N. Washington Irvine, Chair

Starting with the chassis of a 1969 Volkswagen Beetle, the goal of this project was to design and build a Proton Exchange Membrane Fuel Cell (PEMFC) hybrid vehicle that is powered by hydrogen. This thesis highlights the design process, modeling, and control of a Proton Exchange Membrane Fuel Cell hybrid drive train. Finally, the vehicle was built with many of the components assembled, fabricated, and functioning.

Introduction

The idea behind this project was to develop an alternative energy vehicle that can be sustained with minimum dependency on fossil fuels. As a society we are depleting the world's fossil fuel reserves far faster than they are being replenished, so it is inevitable that there will be a time in the not so distant future when our need for fossil fuels will be greater than our capacity to get them out of the ground. More importantly, there is poor air quality associated with fossil fuel combustion and the looming issue of anthropogenic (man-made) climate change. Because of this reality it is important that we develop transportation methods that do not rely on fossil fuel as the energy source. The vehicle power train architecture that is investigated and developed as a potentially sustainable concept in this thesis is the fuel cell hybrid design. The work outlined in this thesis is focused on the design and development of a proton exchange membrane fuel cell (PEMFC) vehicle that will operate on hydrogen gas or strictly on battery power. It will also have the ability to be a plug-in hybrid. In addition to being a platform for demonstrating the technology, the vehicle will be used to develop control algorithms and other systems related studies for future MS and PhD research. While the concepts developed in this thesis are for sustainable transportation, they are not necessarily correlated to zero emissions. The development in this thesis is also a plug-in hybrid due to the size of the battery. The common argument is that if it is a plug in hybrid then it is not truly independent of fossil fuels, since the vehicle requires electric energy that is likely harvested through generators that are powered by fossil fuels. This argument is valid; however, the counter argument is that the large scale generators that produce the energy on the grid that plug in hybrids utilize are much more efficient then the small internal combustion engines found in most vehicles. In addition, the grid can increasingly introduce renewable power generation to support the plug-in

electricity use and even the hydrogen production via electrolysis to make this type of vehicle a zero emissions vehicle. Also since Hybrids utilize an electric motor instead of an internal combustion engine they are actually using the energy more efficiently. Thus, plug-in hybrids, while not completely independent of fossil fuels, are a step in the right direction and as the development of solar energy harvesting gets better it is entirely possible that in the near future battery charging stations will be off the grid and completely powered by solar energy.

Ch. 1: What Is a Fuel Cell?

A fuel cell has a direct analogy to an internal combustion engine. An Internal combustion engine converts chemical energy stored in the fuel being supplied to the engine and produces rotational mechanical energy [1]. The rotational energy produced is then either used to propel a vehicle or focused through a generator and converted into electrical energy. A fuel cell acts much in the same way as an internal combustion engine; the fuel cell converts chemical energy directly into electrical energy [2]. Unlike a battery that drains while it is used to power electrical components, internal combustion engines and fuel cells act as continually operational power sources so long as fuel is being provided to them [3].

1.1 Introduction to Fuel Cells and How They Work

There are many different types of fuel cells however the principal behind how they all function is similar. For a fuel cell to work there are three things that are needed: an anode, a cathode, and an electrolyte. Depending upon the type of fuel cell the electrolyte will be different, in fact fuel cells are categorized by the electrolyte material that they use. A fuel cell can be composed of hundreds of individual cells. Each cell in the fuel cell is composed of an electrolyte, anode and a cathode. The cell essentially sandwiched the electrolyte between the cathode and the anode.
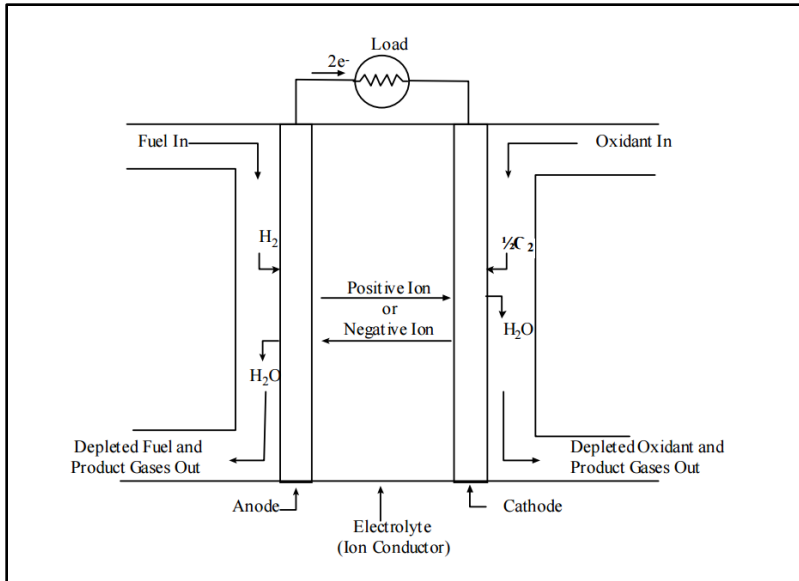
Figure 1: Fuel Cell Operation Diagram [4]

In Figure 1 above, the electrolyte material being used is a polymer electrolyte membrane, also known as a proton exchange membrane (PEM) electrolyte. This particular membrane is what's commonly used in mobile power applications. While the electrolyte material used varies depending on the type of fuel cell the general function of the fuel cell is as follows: Fuel (usually hydrogen) is fed into the anode compartment of the fuel cell while air or pure oxygen is fed into the cathode side of the fuel cell. On the anode side of the cell electrons are separated as the gas tries to make its way through the electrolyte membrane, the membrane basically filters out the electrons and only allows the $2H^+$ ions to pass through. In the cathode compartment the $2H^+$ ions that passed through the membrane combine with the oxygen atoms from the air supply to produce H$_2$O or water as a bi-product; heat is also produced as an off product to the reactions that take place [2], [4]. It should be pointed out that unlike internal combustion engines, where the fuel is mixed with air and combusted, in a fuel cell there is separation of the fuel and oxidant with no combustion of the fuel. As a result, with a fuel cell one does not get the same criteria pollutant by-

products that internal combustion engines produce; in fact, water and heat are the only byproducts from a fuel cell.

1.2 Types of Fuel Cells

As was previously stated fuel cells are characterized by the type of membrane they use. Listed below is a table of some of the more common fuel cells and the type of membrane each uses.

Table 1: fuel cell types

Fuel Cell	Abbreviation	Membrane
Solid oxide fuel cells	SOFC	Yttria-stabilized zirconia
Direct methanol fuel cell	DMFC	Solid polymer electrolyte (Nafion)
Phosphoric Acid fuel cell	PAFC	Phosphoric Acid (H_3PO_4)
Polymer electrolyte fuel cell Or Proton exchange membrane	PEMFC	Solid polymer electrolyte (Nafion)

Just like internal combustion engines fuel cells can operate on different fuels, while hydrogen is the chosen fuel for most mobile applications other fuel cells are more fuel flexible and can actually operate on a variety of different fuels. These types of fuel cells are usually used for stationary power since they often operate at higher temperatures which is partially what enables them to process different types of fuels [3].

1.2.1 Solid oxide fuel cell (SOFC)

A common stationary power fuel cell is a solid oxide fuel cell. Solid oxide fuel cells operate at elevated temperature ranges usually around $800°C - 1100°C$. An advantage to a solid oxide fuel

cell is that due to the elevated temperature ranges and oxidizing ion (O$^=$) transport these fuel cells are capable of handling a variety of fuels [4]. A common use for these fuel cells is back up power for cell phone towers. The reactions associated with solid oxide fuel cells are presented below.

Full reaction:

$$H_2 + \frac{1}{2}O_2 \rightarrow H_2O \tag{0.1}$$

Oxidation reactions (anode):

$$H_2 + O^{2-} \rightarrow H_2O + 2e^- \tag{0.2}$$

$$wgs - CO + O^{2-} \rightarrow 2CO_2 + 2e^- \tag{0.3}$$

$$sr - CH_4 + O^2 \rightarrow CO_2 + 2H_2O + 8e^- \tag{0.4}$$
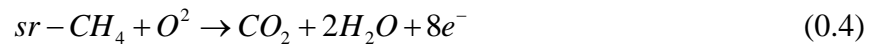
Reduction reaction (cathode):

$$\frac{1}{2}O_2 + 2e^- \rightarrow O^{2-} \tag{0.5}$$

1.2.2 Direct Methanol Fuel Cell (DMFC)

Direct methanol fuel cells are an example of a low temperature non-fuel flexible fuel cell. these fuel cell were initially implemented in small portable electronic devices such as laptops and cell phones [5].

Over all reaction:

$$CH_3OH + \frac{3}{2}O_2 \rightarrow CO_2 + 2H_2O \tag{0.6}$$

6
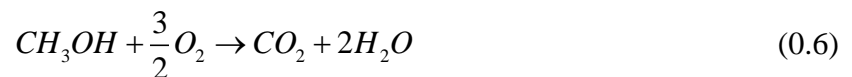
Half reactions associated with direct methanol

fuel cells are listed below

Oxidation:

$$CH_3OH + H_2O \rightarrow CO_2 + 6H^+ + 6e^-$$ (0.7)

Reduction:

$$-6H^+ + 6e^- + \frac{3}{2}O_2 \rightarrow 3H_2O$$ (0.8)
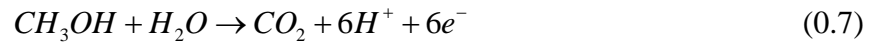
1.2.3 Phosphoric Acid Fuel Cell (PAFC)

Phosphoric Acid Fuel Cells (PAFC) are a medium temperature fuel cell that conducts hydrogen

ions so that they are not as fuel flexible as the high temperature fuel cells that conduct oxidizing

ions (e.g., $O^=$, $CO_3^=$). While PAFCs are predominantly used for stationary power, they have also

been implemented in some large scale vehicles such as public buses [6].

The overall reaction can be characterized as follows:

$$H_2 + \frac{1}{2}O_2 \rightarrow H_2O$$ (0.9)

The half reaction associated with the Phosphoric acid fuel cell is the following.

Oxidation reaction:

$$H_2 \rightarrow 2H^+ + 2e^-$$ (0.10)

Reduction reaction:

$$\frac{1}{2}O_2 + 2H^+ + 2e^- \rightarrow H_2O \qquad (0.11)$$

1.2.4 Polymer Electrolyte Membrane Fuel Cell (PEMFC)

Polymer electrolyte membrane fuel cells or proton exchange membrane fuel cells are low temperature fuel cells that conduct hydrogen ions (H^+) making them non fuel flexible. These fuel cells are easily the most widely used in the transportation sector because since they are low temperature fuel cells they operate around $80°C$ so they can start up and stop relatively quickly [7]. Another advantage to PEMFC's is that they have very high efficiency and power density in the vehicle engine size class [8]. These features are well-suited to a vehicle power source where power density is desired and the dynamic power demands are significant. Some of the drawbacks to PEMFC's include a higher risk of CO poisoning and they require cooling.

The overall chemical reaction for PEMFC is:

$$H_2 \rightarrow 2H^+ + 2e^- \qquad (0.12)$$

The chemical half reactions for the PEMF are:

Oxidation reaction:

$$H_2 \rightarrow 2H^+ + 2e^- \qquad (0.13)$$

Reduction reaction:

$$\frac{1}{2}O_2 + 2H^+ + 2e^- \rightarrow H_2O \qquad (0.14)$$

Ch. 2: Drive Train Architectures

2.1 : The First Drive Train Design

While the traditional single power source internal combustion engine is popularly thought to be the first major drivetrain orientation, this is actually incorrect. Some of the first cars built were powered by electric motors. In the early19[th] century pure electric powered vehicles were actually more common than internal combustion engines however limitations in battery technology and the ability for automotive companies particularly Henry Ford to produce internal combustion engines vehicles cheaply lead to the growth of the internal combustion engine in the automobile [9]. A pure electric drive train can be seen in Figure 2
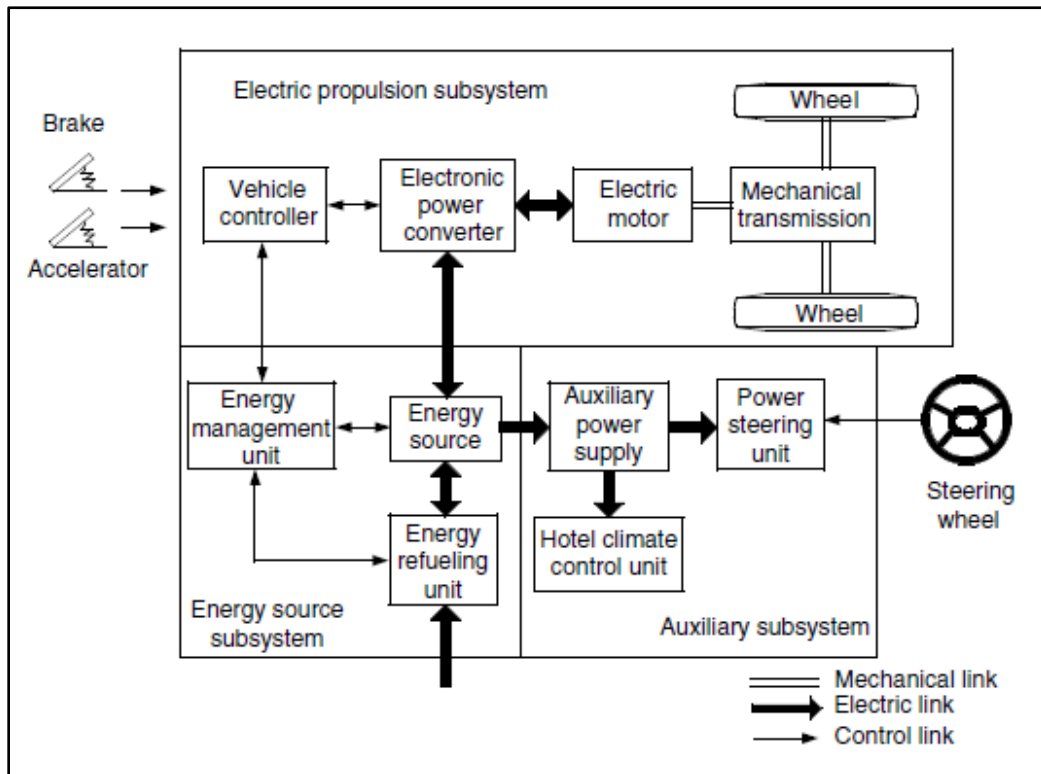
Figure 2: Electric Vehicle Drive Train Configuration [9]

9

2.2 : Classical Single Internal Combustion Engine Design

During the industrial revolution north America produced almost exclusively internal combustion engine vehicles and to this day the single internal combustion engine is still the most common vehicle drive train architecture. While there are slight variations such as number of cylinders and front, rear, or all-wheel drive, the single internal combustion engine is still in large part the dominate drive train worldwide. One of the shortcomings of the ICE however is that they produce very small amounts of torque at low speeds. To account for this low torque output, multiple speed transmissions must be used to magnify the torque and account for the speed difference in the engine that is required to meet the torque demand commanded at the wheels. Depicted below in Figure 3 is the drive train of a single ICE
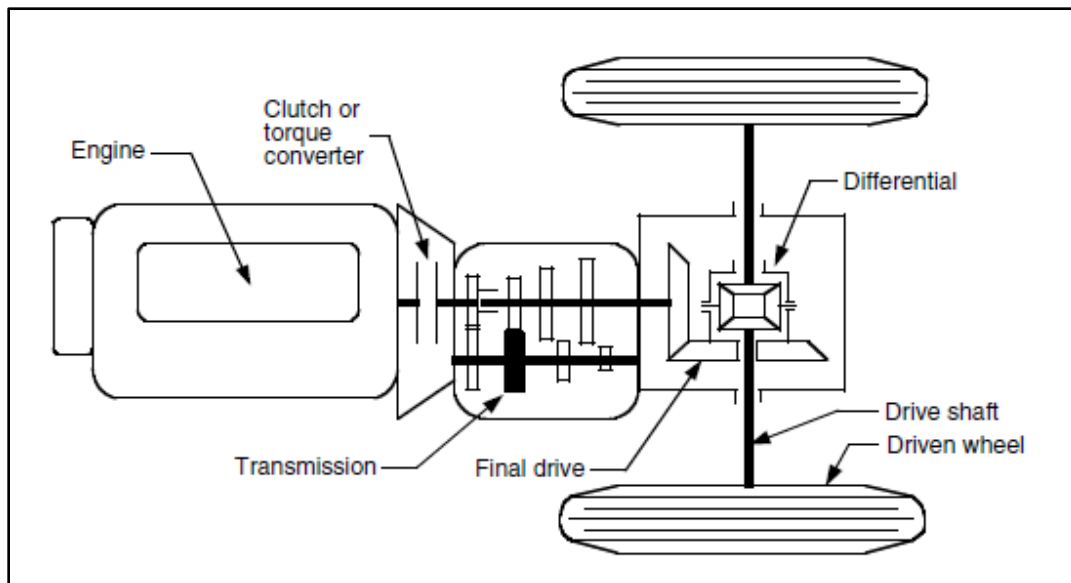
Figure 3: Internal Combustion Engine Drive Train [9]

2.3 Hybrid Drive Train Designs

From a performance standpoint the traditional internal combustion engine vehicle works well, however, there have been a number of other factors that have led to research into other drive train

architectures. Some of the primary motivations for alternative drive train architectures include the increasingly strict emissions requirements being imposed on manufacturers by the California Air Resources Board, U.S. Environmental Protection Agency (EPA), and other bodies concerned with air quality [10]. In addition, energy independence and fuel economy concerns have prompted the U.S. Congress to impose Corporate Average Fuel Economy (CAFÉ) standards that have prompted investment in alternative fuels and vehicle drive trains. An even broader perspective is the reality that the current fuel being used to power internal combustion engines is of a finite capacity [7]. These realities have led to the development of move efficient drive train designs.

2.3.1 Parallel Hybrid

One of the earlier hybrid drive train designs was the parallel hybrid architecture. In this configuration both the internal combustion engine and the electric motor can be used to power the vehicle independent of one another. This configuration includes the advantage that each power source can be used in the drive cycle when its most efficient [9]. As stated in section 2.2 the internal combustion engine has a low torque output at low speeds, this means that in stop and go drive cycles the internal combustion engine is extremely inefficient. However, electric motors provide almost instantaneous torque so in a stop and go drive cycle an electric motor will be more efficient then an ICE. Implementing a parallel hybrid system allows one to operate each power source or both of them to varying degrees when it is most efficient in the drive cycle. So, for example, during low speeds and stop and go cycles the electric motor would primarily be used and the internal combustion engine would be mostly off for efficiency reasons. Or, during steady state highway conditions the electric motor would be off and the ICE would power the vehicle to engender long range by using the high energy density of the fuel [11]. In the parallel configuration one also has the ability to operate both the ICE and the electric motor together when the torque demand is

11

greater than the torque produced by either the ICE or the electric motor independently [12]. Since both power sources can be operated in unison when torque demands are high it allows both the engine and the motor to be scaled down in size since the majority of the time the drive cycle will not have a high torque demand, which can further increase the overall efficiency of the parallel design. Another advantage to the parallel hybrid drive train architecture is the ability to harvest energy through deceleration in the drive cycle with the implementation of regenerative braking. Regenerative braking is not exclusive to parallel hybrid architecture, rather, almost all hybrids have the ability to deploy regenerative braking to harvest what would otherwise be wasted heat energy from the mechanical brakes [13]. Regenerative braking works by essentially converting the electric motor into a generator during stops and decelerations in the drive cycle; this energy then gets stored back into the batteries of the vehicle to be used later in the drive cycle [14]. On a traditionally single ICE this energy would be lost to heat in the braking system but with a hybrid one can capture a portion of it as stored electricity for later use. A visual representation of a parallel hybrid drive train is depicted below in Figure 4
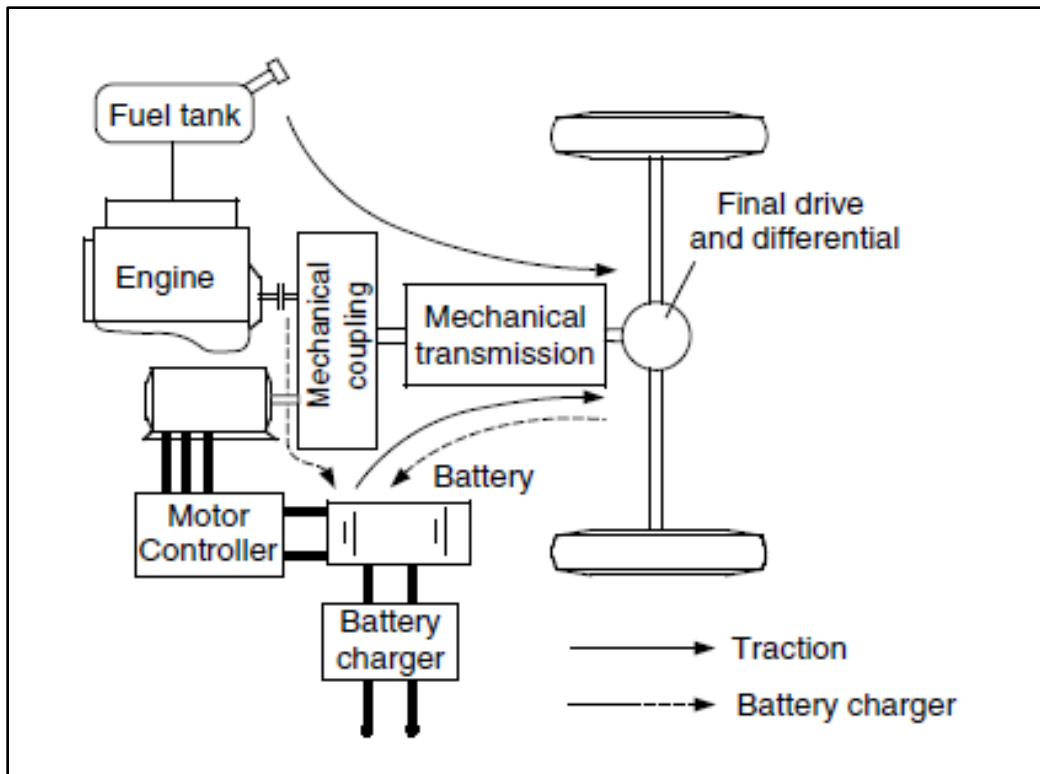
Figure 4: Parallel Hybrid Configuration [9]

2.3.2 Series Hybrid

A series hybrid drive train architecture differs from a parallel hybrid drive train in that the two power sources are no longer independently able to power the vehicle. Instead generally the ICE will act as a charger for the batteries while the electric motor is used as the only source to propel the vehicle [15]. One of the advantages to this design is that there is no need for a transmission since the ICE is not powering the vehicle directly. Since reducing the weight of the vehicle directly correlates to increasing efficiency the ability to totally eliminate the transmission in a series hybrid design is one benefit of the series hybrid over a parallel hybrid. In a series configuration the ICE does not have to account for any of the transient dynamics in the drive cycle like it would in a parallel configuration, because of this the engine can be operated at steady state at its most efficient rpm thus further increasing its efficiency[16]. In a series configuration one is also a little more

flexible in regards to implementing alternative energy devices. For example, for this project the ICE was replaced with a hydrogen fuel cell. Since in a series hybrid the ICE converts chemical energy to mechanical energy then to electrical energy it is actually more efficient to use a fuel cell to convert directly from chemical energy to electrical energy to charge the battery pack. This is one of the main reasons why for this project the decision was made to implement a series configuration. It should be pointed out that a fuel cell can also be used in a parallel configuration however to archive that the fuel cell would need to be robust enough to handle the transient dynamics created by the drive cycle. Most fuel cells do not handle transient dynamic well and so usually fuel cells are required to operate near steady state conditions which makes them ideal for series hybrid architectures [17]. An example of a series hybrid configuration is depicted below in Figure 5.
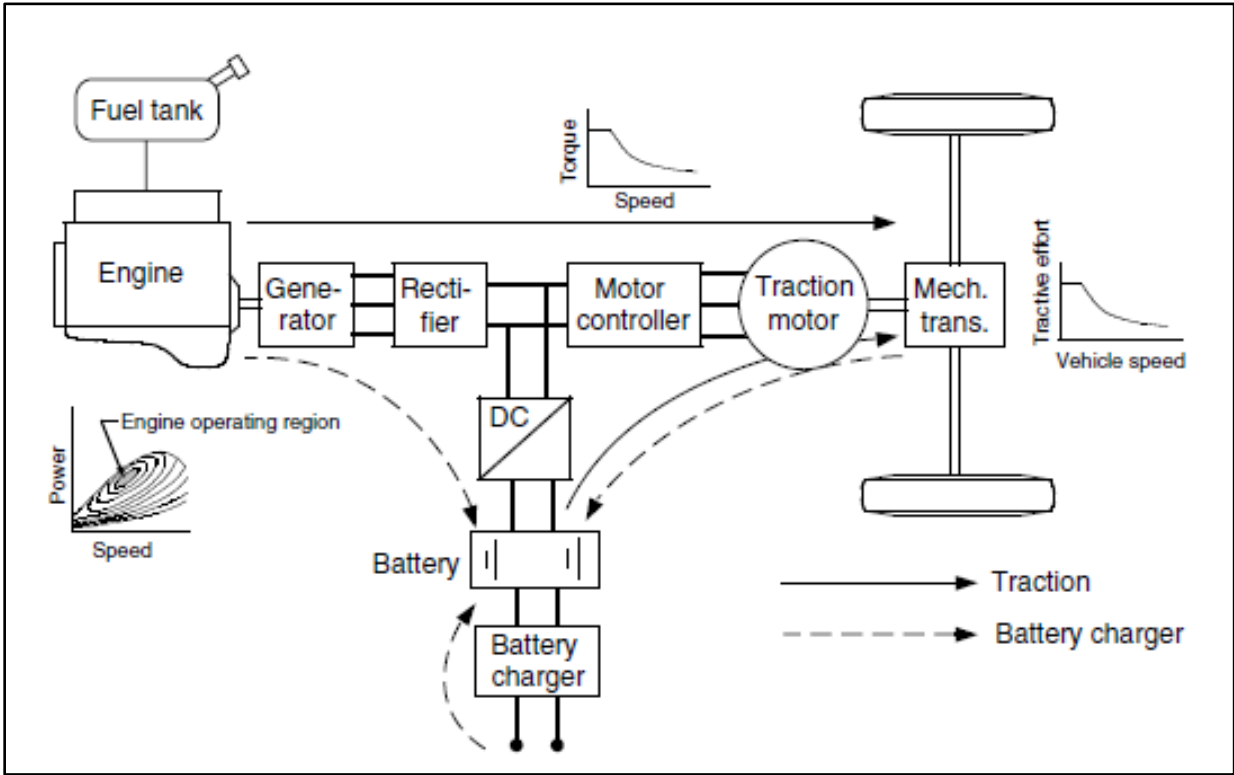
Figure 5: Series Hybrid Configuration [9]

The series hybrid design can also support regenerative braking to recover energy during stops and decelerations much the same way the parallel hybrid does by converting the motor into a generator during these instances in the drive cycle. A draw back to the series hybrid design can be that the motor is required to be larger since there is no way to use both power sources during a hard acceleration. For this project the decision was made to implement a transmission so that the motor would not have to be over-sized like it would in a traditional series design without a transmission.

2.3.3 Series-Parallel Hybrid

Series-parallel hybrid, like the name implies is a combination of both series and parallel hybrid drive train configurations. In a series-parallel hybrid both the electric motor and the ICE can power the vehicle independently or jointly. Also the ICE can divide its power between driving the car and charging the batteries at the same time [18]. This architecture provides the most control flexibility since the modes of operation can be switched to optimize whatever drive cycle is being driven. However, one of the drawbacks to this design is the amount of hardware required, since the ICE has to be able to drive the vehicle a transmission is required, and since the engine also needs to have the ability to charge the batteries a generator is also needed. The series-parallel design has all the benefits of both the series design and the parallel design which makes it more flexible to different drive cycles; however, it also has all the drawbacks of both designs so it's a compromise [19]. An example of a series-parallel hybrid architecture is shown below in Figure 6
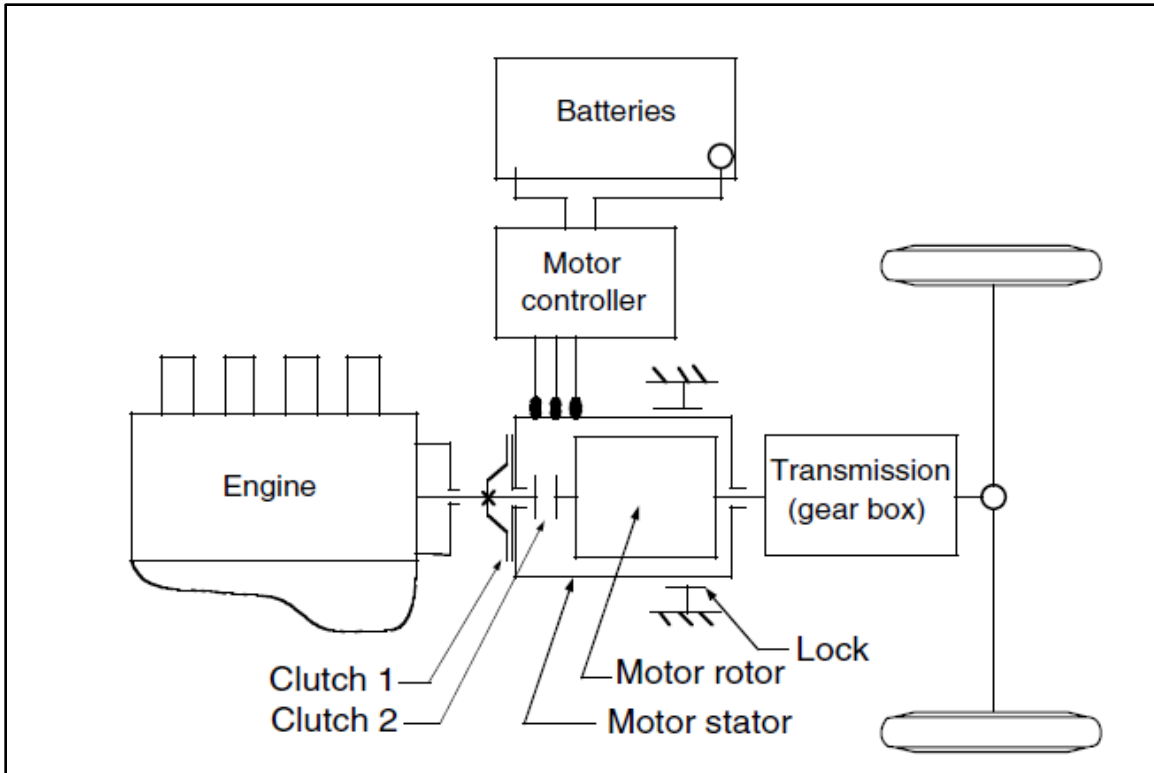
Figure 6: Series-Parallel Hybrid Configuration [9]

For this project the series-parallel design was not chosen because the fuel cell being used does not handle transient dynamics well and so would not be able to account for the load dynamics associated with different drive cycles when the car was in parallel mode.

Ch. 3: SolidWorks CAD Design

The starting vehicle for this project was a 1969 Volkswagen Beetle. Because of its lightweight design and simplistic unibody construction, the Beetle was chosen. The body was removed from the chassis as the intention was not to utilize the original steel body in an effort to cut down on weight. Once the body was removed and the chassis was painted measurements were taken to see where the major components would fit. The original VW Beetle was a two door four seater

however do to all of the balance of plant components that were spec out it was evident that the back seat would have to go, so the project became a two seater.

The five major components that needed to be designed into the vehicle were the:

1. fuel cell
2. hydrogen tank
3. power electronics
4. Battery
5. Conversion electronics

To decide on the placement of the major components two primary factors were considered: driving performance and optimization of component integration.

For driving performance, the goal was to look at the weight distribution of the vehicle. For optimum handling the ideal weight distribution is 50/50 front to back weight ratio however since the original Beetle has a rear mounted motor this was going to be a challenging task [20]. After analyzing the space available on the chassis the decision was made to mount the battery pack in the front of the vehicle just over the front axle, the conversion electronics are mounted directly over the battery box. The power electronic box was mounted just behind the passenger compartment; almost in the center of the vehicle. The hydrogen tank is just in front of the rear axle while the fuel cell sits directly over the hydrogen tank. This set up helps to compensate for the fact that the motor actually sits behind the rear axle. The second factor that was considered was the layout for integrating the components. Obviously the hydrogen tank had to be plumed to the fuel cell so by placing those two components near one another the plumbing of the necessary fuel lines is more efficient. In this regard, it is desirable to have the batteries as close to both the fuel cell

and the motor as possible so that the electrical cables could be as short as possible to prevent ohmic losses. But, the compromise we made from a driving performance point of view was to move the batteries to the front of the vehicle as stated earlier. The below figure shows the original CAD design of the chassis.

3.1 Chassis CAD Design
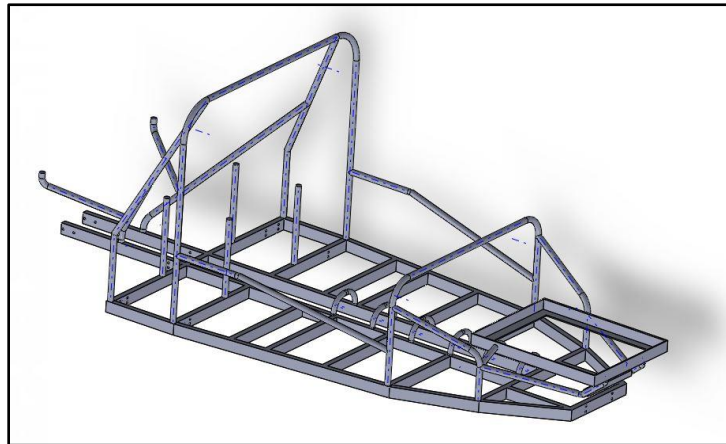
Figure 7: Chassis CAD Design

Since the original VW design used the actual unibody for structural rigidity, a lightweight chassis had to be developed that would act as a structural substitute for the body. In Figure 7 one can see a rectangular steel channel is implemented to provide some of this structural support. 0.125" thick Chromalloy tubing is also implemented in addition to the rectangular support to both acts to provide structural rigidity by reducing body twist but also to provides protection for the occupants of the vehicle in the event of a roll over. In the front of the chassis the rectangular battery box support bracket can be seen. The bottom battery box support bracket was built as part of the chassis since it was a component that would be welded and not bolted in for added security.

3.2 Heat Exchanger

Once the chassis was developed each of the major components were designed in SolidWorks. This process was critical since real-estate on the VW chassis was limited. The first major component that was designed was the heat exchanger. The heat exchanger is similar to the radiator found on most internal combustion engine it takes the cooling fluid from the fuel cell and uses air to cool it before delivering that fluid back to the fuel cell. Depicted below in Figure 8 is the design of the heat exchanger that was custom-built for this application.
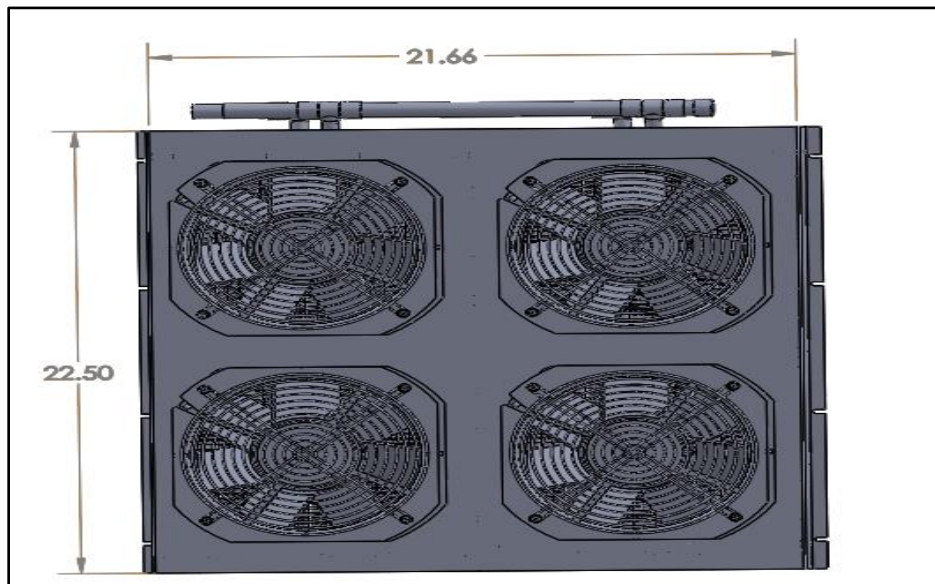
Figure 8:Heat Exchanger

On an ordinary internal combustion engine vehicle, the radiator has a single electric or mechanical fan that is used to provide the air flow needed to cool down the fluid going through the radiator to the appropriate levels. For this application the temperature gradient dictated the use of four electric fans in order to provide the necessary cooling; small details like this became important because of space limitations. This was again why designing the vehicle in SolidWorks was done prior to the actual construction of the physical vehicle.

3.2.1 Water Pump

While the major components of a fuel cell vehicle are obviously the fuel cell and the hydrogen tank to power said fuel cell; what can easily get overlooked is the packaging of the major components for the balance of plant. One of the critical balance of plant components for the fuel cell is the water pump for the cooling system. Having the right flow rate is critical to maintaining the right temperature of the fuel cell. The water pump that was used on this project was the CA Series Micro Pump. This pump has a 27 liter per minute flow rate yet is about the size of a coffee mug, so it was perfect for this project were space comes at a premium. Depicted below in Figure 9 is the schematic of the water pump.
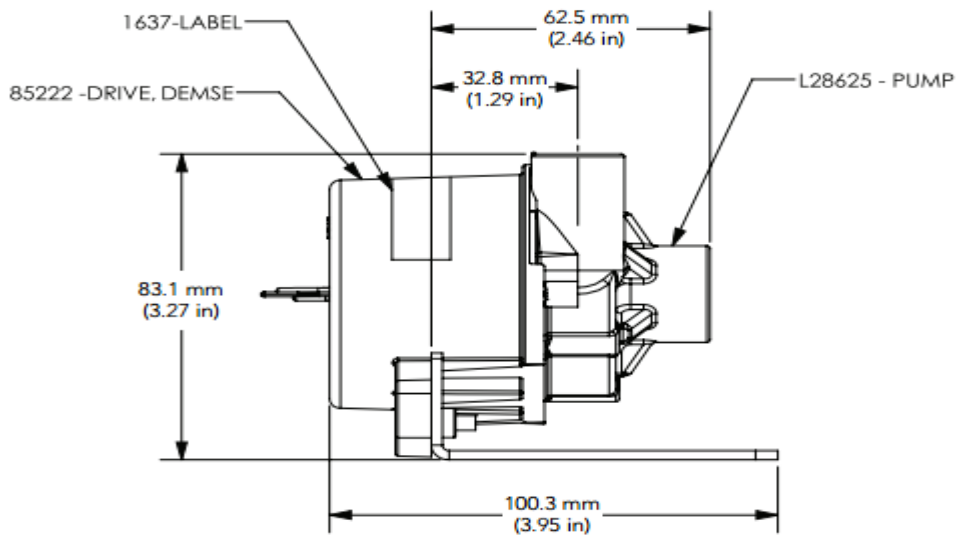
Figure 9: Water Pump [28]

3.3 Battery Box

Since the heat exchanger was in the front of the vehicle the major components were designed and integrated into SolidWorks from the front of the vehicle to the back. As was stated earlier the battery box was placed above the front axle so the next component to be designed was the battery box, which can be seen below in Figure 10

Figure 10: Battery Box

While there are a number of individual cells that make up the battery system it was not necessary to represent each individual cell in the SolidWorks design since the final battery box geometry is all that was needed to locate where on the chassis the system would be mounted. So, as the title explains, the battery box was designed literally as a 20" x 25" x 8" box. This was all that was really needed since the company manufacturing the battery pack also agreed to produce an aluminum box to integrate, package, and orient all the cells.

3.4 Power Electronics

After the battery box was designed the power electronics box was the next major component that needed to be oriented on the vehicle. As the name implies, this too was a box containing the integrated power electronics sub-system. Due to the amount of current that was being produced the size of the box needed to be sufficiently large in order to account for the amount of heat that

would be produced. The power electronics cabinet was specked out to be 3' x 1.5' x 1.5' this meant the power electronics box would be easily the largest component on the vehicle. The power electronics SolidWorks design is depicted in Figure 11
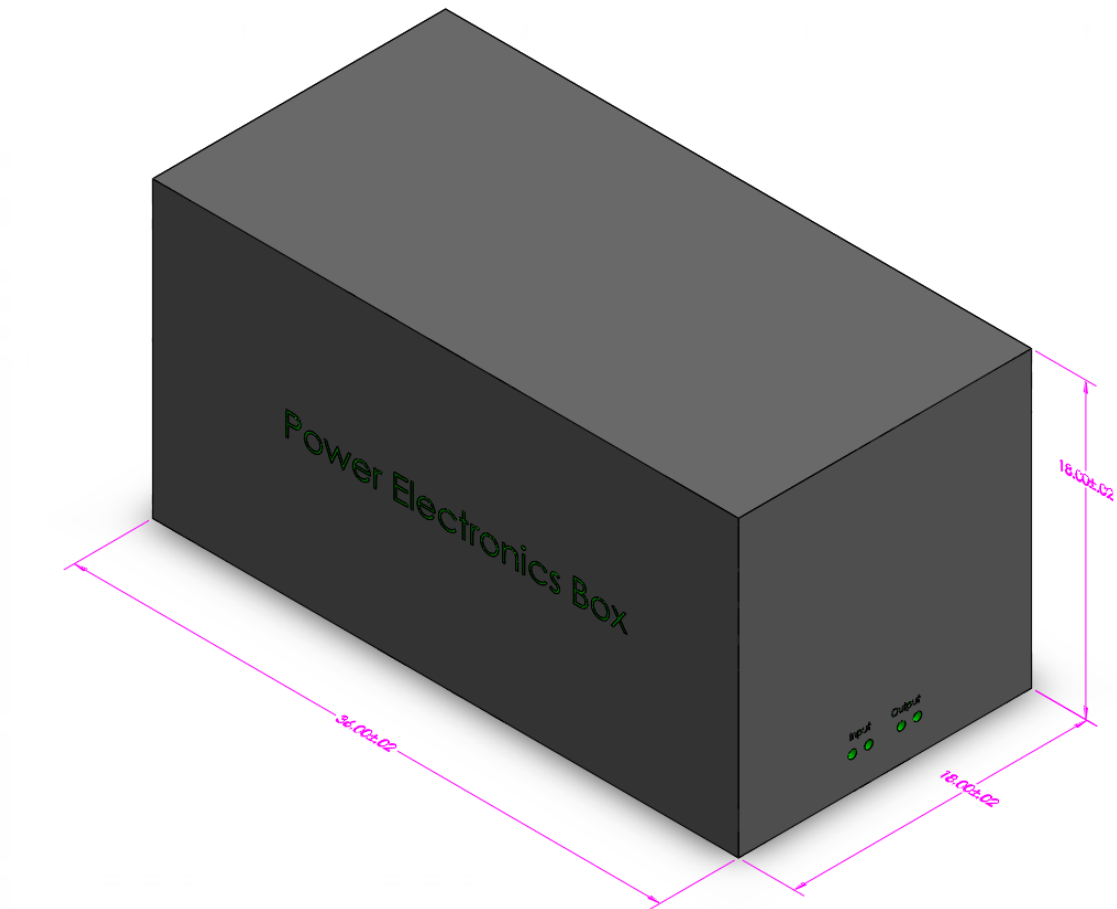
Figure 11: Power Electronics Cabinet

What made the placement of the power electronics box unique besides the fact that it was so large was, the box has vents that needed to be able to receive air, this of course is challenging since the box had to be mounted inside of a closed car. The solution to this challenge will be discussed in the body design section.

3.5 Hydrogen Tank

The item of most controversy was designed next. On a hydrogen fuel cell vehicle, the actual hydrogen tank is an area of interest since there is no real elegant way to store large volumes of hydrogen. In general, for passenger vehicle the tank pressure is generally around ten thousand pounds per square inch [21]. Having a tank of such high pressure is necessary to be able to store the required volume of hydrogen needed to reach comparable ranges as traditional internal combustion engines without turning the interior of the vehicle into a hydrogen tank. Since range is not a large component of this project, as the vehicle is intended for research purposes, the decision was made to use a standard 300 size DOT specification: 3AA2400, steel compressed gas tank. The range of the vehicle was of course diminished; however, the working pressure is only 2,400 pounds per square inch so it's safer for research purposes. The tank can be seen in Figure 12 below.
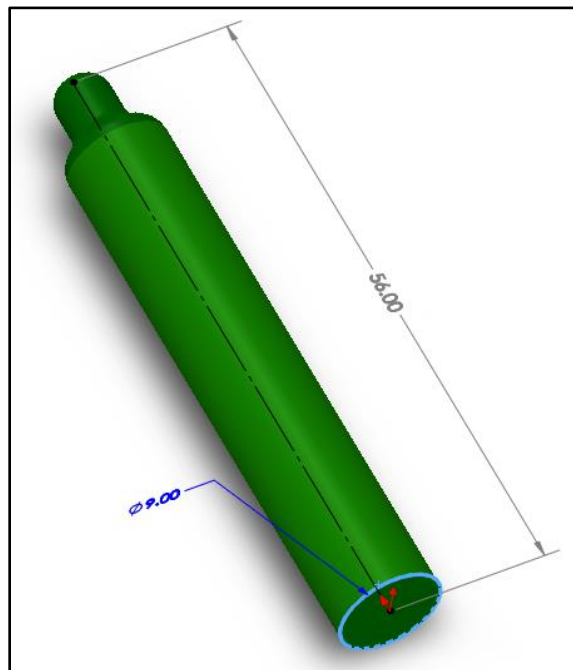
Figure 12: Hydrogen Tank

3.6 Fuel Cell

The Fuel cell for this project is: HyPM HD 12, model: 1037312 produced by Hydrogenics Advanced Hydrogen Solutions. This fuel cell is a 12KW PEMFC capable of automotive operations. Much like the battery box and power electronics cabinet the internals of the fuel cell had a lot going on in them but designing that was not needed. Instead, the outer dimensions of the fuel cell were designed. Depicted below in Figure 13 is the SolidWorks design of the fuel cell.
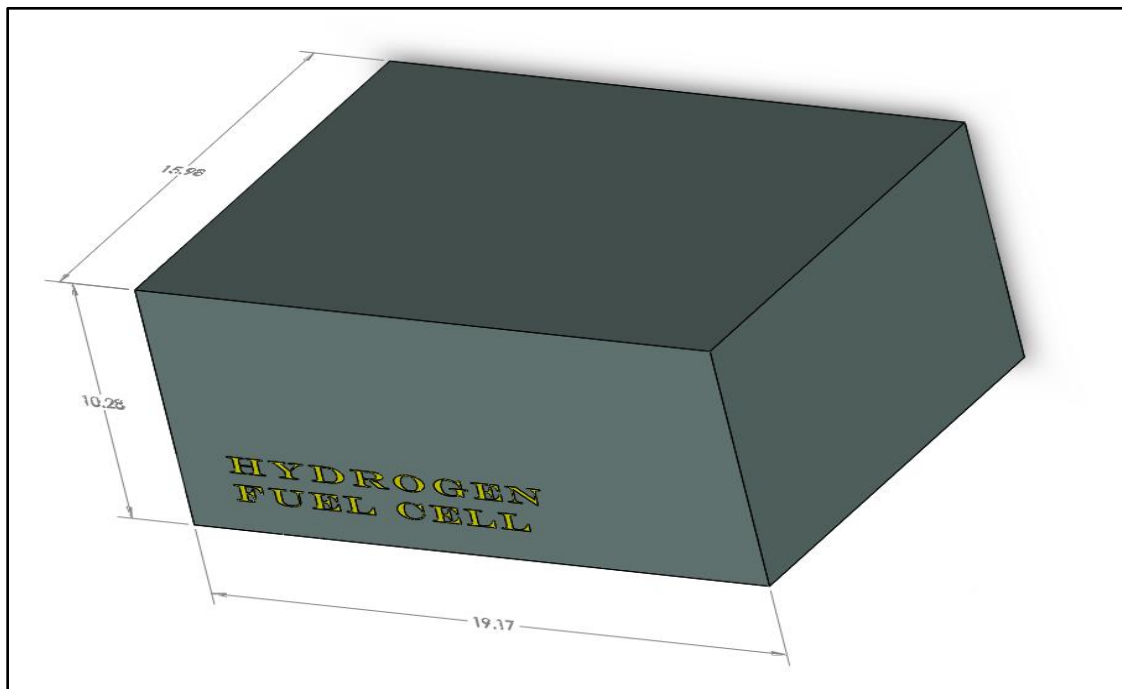
Figure 13: Fuel Cell

The fuel cell will be mounted directly above the hydrogen tank in an effort to reduce the extent of the pluming from the tank to the fuel cell. To mount the fuel cell in this location Chromalloy tubing was used to create bracket that would end up connecting to a plate that was positioned directly over the hydrogen tank.

3.7 Transmission

Due to the size of the fuel cell the plate in which it sits had to be extended to essentially cover the top of the transmission. To make sure there would be sufficient clearance the transmission needed to be implemented into the CAD design as well so in Figure 14 the original 1969 VW Beetle 4-speed transmission is designed.
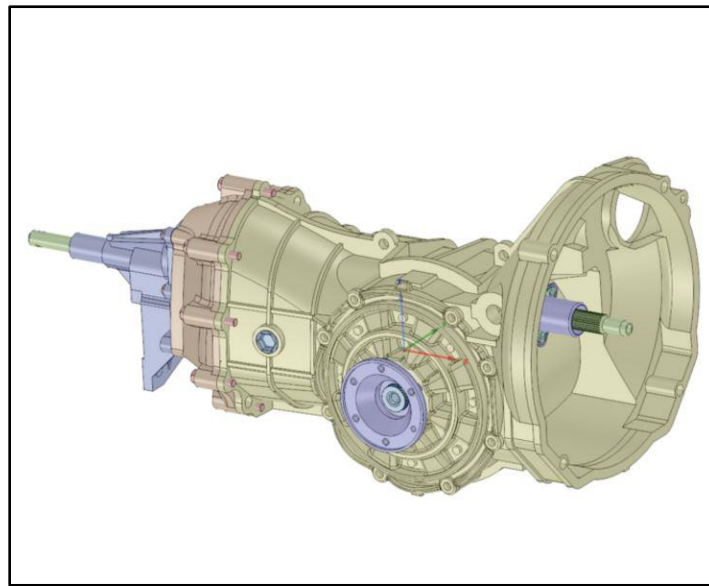
Figure 14: Transmission

3.8 Electric Motor

The final major component to be designed was the motor. The motor being used on this project is the AC-50. An AC motor was chosen for this project instead of a DC motor because of the higher power-to-mass ratio associated with an AC motor over a DC motor [22]. The original power train in a Volkswagen Beetle mounted the transmission to the chassis and then bolted the engine to the transmission. This part of the original drive train was un-altered; the only difference with the current design was that instead of bolting an internal combustion engine to the transmission an electric motor was mounted to it instead. This was achieved through the use of a custom aluminum

bracket that bolted to the face of the motor on one end and bolted to the bell housing of the transmission on the other end. To connect the output shaft of the motor to the input shaft of the transmission a forged steel adapter was used. This adapter received the input shaft of the motor and used a key way and set screw to create a solid connection to the motor. The opposite end of the steel adapter had the stock bolt pattern for a Volkswagen flywheel, so a standard flywheel, clutch and pressure plate were bolted on to the other side of the steel adapter. With this set up the motor was able to mount to the transmission and the standard clutch and transmission are able to keep their functionality, meaning one can still use the clutch and shift gears if one so desires. The design of the motor used is depicted below in Figure 15
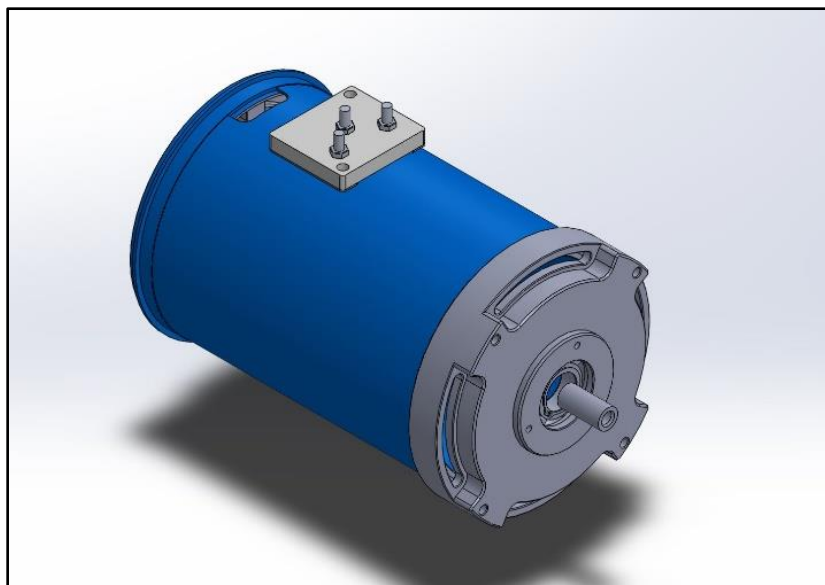
Figure 15: AC 50 Motor

Once all of the major components were designed a completed computer aided design (CAD) file was produced showing roughly where each component would be placed on the vehicle. This completed CAD file helped in the overall packaging of the components on the vehicle by providing

a visual aid of the real estate available on the chassis. The completed CAD is depicted below in Figure 16.
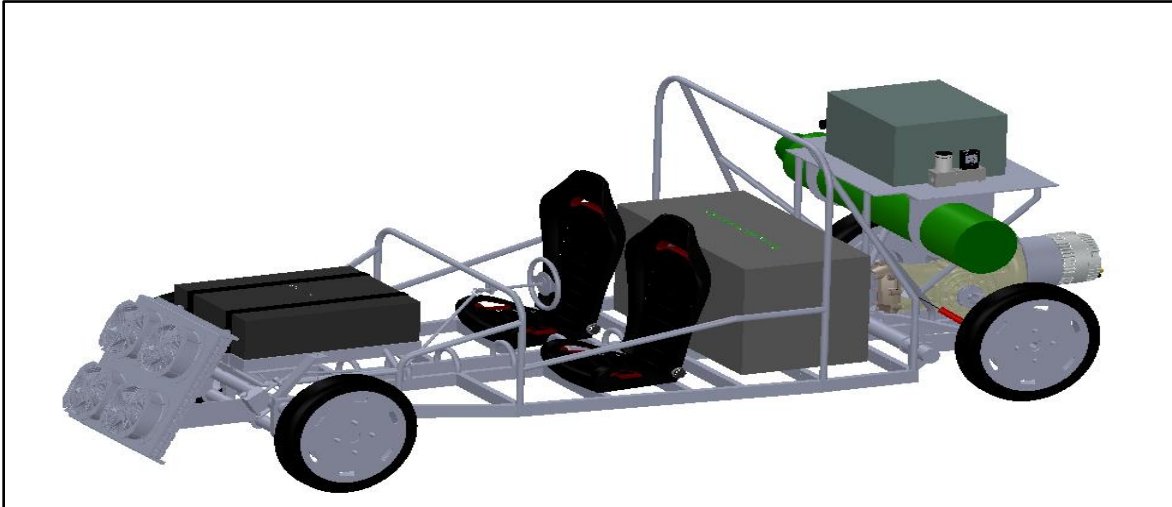
Figure 16: Completed CAD of Vehicle

Ch. 4: Vehicle Dynamics Equation & Power Calculation

To get an understanding of the power requirements needed for the vehicle and some of the dynamic forces the vehicle needed to withstand an analysis of the dynamic equation of a vehicle were performed [9]. The dynamic equation of the vehicle can be defined as follows:

$$M_v \frac{dv}{dt} = (F_{tf} + F_{tr}) - (F_{rf} + F_{rr} + F_w + F_g) \tag{0.15}$$

The variables in the dynamic equation of the vehicle are shown below in Table 2.

Table 2: Dynamic Vehicle Equation Variables

	Variable	Definition
(1)	M_v	Mass of the vehicle

(2)	$\dfrac{dv}{dt}$	Acceleration of the vehicle
(3)	F_{tf}	Tractive force of the front axle
(4)	F_{tr}	Tractive force of the rear axle
(5)	F_{rf}	Rolling resistance from front axle
(6)	F_{rr}	Rolling resistance from rear axle
(7)	F_{w}	Force from wind resistance
(8)	F_{g}	Force from gradient
(9)	C	Coefficient of rolling resistance
(10)	W	Weight of the vehicle
(11)	v	velocity
(12)	C_{d}	Coefficient of drag
(13)	A	Frontal area
(14)	ρ	Density of the air

A number of simplifying assumptions were made to this equation, the first being that since this particular vehicle is going to be rear wheel driven there would be no tractive force coming from the front axle and therefore the F_{tf} term equals zero. The next assumption was that since the weight distribution is nearly 50/50, the F_{rf} and the F_{rr} terms become equal, represented by F_r. The last assumption made is there is no elevation gradient so we make the assumption that the gravitational force in the propulsion direction, F_g, is equal to zero. The dynamic equation then simplifies down to:

$$M_v \frac{dv}{dt} = (F_{tr}) - (F_r + F_w) \tag{0.16}$$

This means the mass of the vehicle times the acceleration of the vehicle is equal to the tractive force at the rear wheels (which is what is needed to calculate motor power) minus the force of the sum of the rolling resistance and the force of the wind resistance. The mass of the vehicle is taken to be a known variable and the acceleration that was used was the stock VW Beetle acceleration. With the mass and the maximum acceleration, calculating the tractive force required for the motor becomes basic arithmetic; once the forces of rolling resistance and wind resistance is calculated. To calculate the rolling resistance, the following equation was used.

The rolling resistance force calculation:

$$F_r = cW \tag{0.17}$$

See Table 2 variables nine and ten for definitions to equation (0.17)

To calculate the coefficient of rolling resistance the following equation was used:

$$c = 0.005 + \frac{1}{tire\ pressure}(0.01 + 0.0095(\frac{v}{100})^2) \tag{0.18}$$

Where:

- Tire pressure = 51 psi or 3.516 Bars

However, the velocity is zero since the calculation is for the static force needed to overcome rolling resistance. Since the final mass was not yet known for the vehicle the curb weight of the stock VW Beetle (870kg) was used as a ball park figure.

$$c = 0.005 + \frac{1}{3.516}(0.01 + 0.0095(\frac{0}{100})^2) = 0.00784 \qquad (0.19)$$

The rolling resistance force then becomes:

$$F_r = 0.00784(870*9.81) = 66.91NM \qquad (0.20)$$

Next the wind resistance force was calculated, however to come up with this number a requirement for how fast the anticipated maximum speed of the vehicle will be was needed. For this calculation a highway speed of 80 miles per hour was chosen. The following equation was then implemented to calculate the wind resistance at that speed.

Wind resistance formula:

$$F_w = \frac{1}{2}(C_d A_\rho v^2) \qquad (0.21)$$

Where:

- C_d = Coefficient of drag = 0.159 (C_d from the VWXL1) 30% safety factor= 0.207
- A = Frontal Area = 1.34 m^2 (based on the body design we are developing)
- ρ = density of the air = 1.2041 kg/m^3
- V = Velocity = 80 mph = 35.76 m/s

The force due to wind resistance then becomes:

$$F_w = \frac{1}{2}(0.207)(1.34)(1.2041)(35.76)^2 = 213.55\frac{kg}{s} \qquad (0.22)$$

Now that the wind resistance force and the rolling resistance force are known they can be plugged in to the dynamic equation of an automobile to determine the tractive force required to power the vehicle.

$$870\frac{dv}{dt} = (F_{tr}) - (66.91 + 164.03) \tag{0.23}$$

To calculate the acceleration term in the equation the zero to sixty time of a stock 1971 Beetle was used for the design. This time was 15 seconds.

- $60mph = 26.822\frac{m}{s}$

- $\frac{dv}{dt} = \frac{26.822\frac{m}{\sec}}{18\sec} = 1.49\frac{m}{s^2}$

There for the tractive force needed is:

$$870(1.49) = (F_{tr}) - (66.91 + 164.03) \tag{0.24}$$

$$\boxed{F_{tr} = 1527.24N} \tag{0.25}$$

Now that the tractive force needed is known, the power output needed can be calculated. For simplicity, the power required was determined assuming there was a direct drive from the motor to the wheels, (i.e., no transmission) for this drive train orientation the following power calculation is:

$$Power = force(F_{tr}) * \frac{dis\tan ce}{time} \tag{0.26}$$

Therefore:

31

$$Power = force(F_{tr}) * velocity \qquad (0.27)$$

If our tires are roughly 24 inches in diameter, then at 80 miles per hour the wheel will be rotating at 1,400 rpm. This converts to 44.68 meters per second. Once this conversion is plugged into the power equation, the power needed is calculated to be:

$$Power = (1,527.24N)(44.68\frac{m}{sec}) = 68237.08$$
$$= \boxed{68.24KW} \qquad (0.28)$$

Ch. 5: Simulations

Once the power calculation was determined with the dynamic vehicle equation, the next phase in the project was to simulate the vehicle dynamics to verify that this calculation made sense in an actual drive cycle. The MATLAB based Advanced Vehicle Simulator (ADVISOR) was used to generate a standard drive cycle [23]. This drive cycle was then used to develop a drive cycle specifically for the hybrid fuel cell vehicle being designed. Once that drive cycle was developed, a whole vehicle simulation was developed from the ground up. Since the goal was to use Advisor to obtain the velocity profile of a standard drive cycle a generic vehicle was used from the ADVISOR library. Once a vehicle was selected the US06 drive cycle was chosen and the simulation of the generic vehicle was performed. The power calculation that was developed using the dynamic equation of the vehicle considered only the maximum power needed to propel the vehicle. Such a calculation does not take into consideration a complete drive cycle. This implies that only by examining the maximum power requirement one could design a drive train system that has more power than it needs. This is kind of like driving a 550 horse power Ferrari 10 miles per hour, one can do it but it's not the most efficient way to go 10 miles per hour. To verify that

the maximum power demand and the average drive cycle demand were not statistically to far apart a drive cycle analysis was preformed to determine the power requirement at each time stamp in the cycle.

From ADVISOR the US06 Supplemental Federal Test Procedure was chosen as the drive cycle. In Advisor after selecting the drive cycle and running the simulation of this drive cycle, the velocity profile that corresponds to each time stamp in the cycle gets saved as a vector in MATLAB.
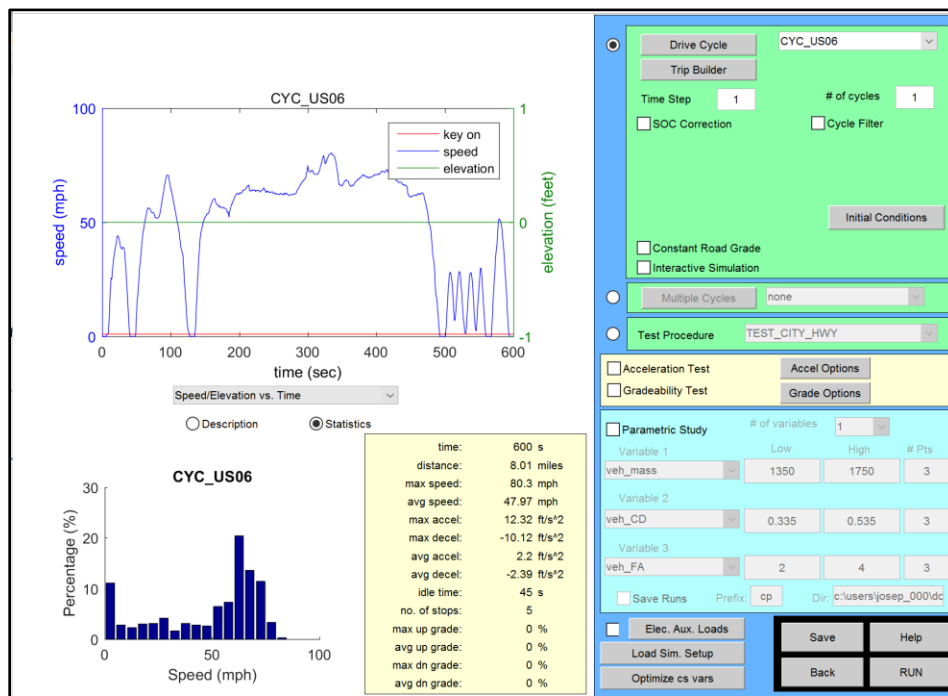
Figure 17: ADVISOR Display Window

From this velocity profile, using Excel, the acceleration and deceleration were calculated by dividing the velocity by the time step (dv/dt). The dynamic equation of a vehicle was then applied at each time stamp to generate a power requirement at every individual time. The power required at every step in the drive cycle is depicted in the figure below:
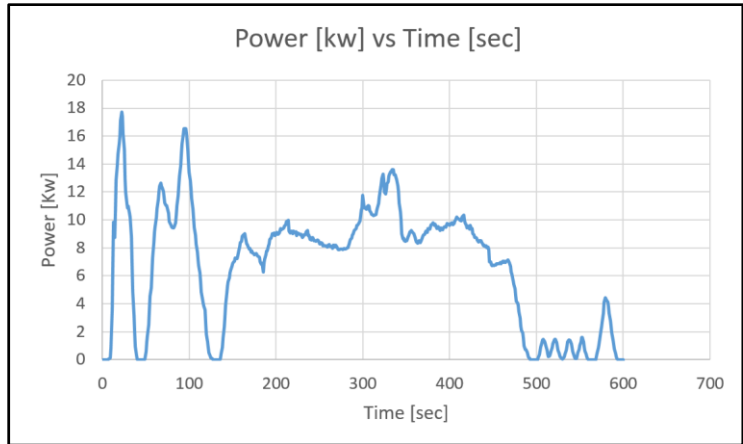
Figure 18: Power Required in US06 Drive Cycle

From Figure 18 the average power demand is about eleven kilowatts with a peak of about 18 kilowatts. This means that the simple power calculation that was developed using the dynamic vehicle equation is reasonable and comparable to the required maximum power that was determined by analyzing vehicle performance for the entire drive cycle.

5.1 MATLAB Code

Once the power calculation was verified in excel the next step was to construct a MATLAB routine that would input the velocity from any drive cycle along with the vehicle specifications and calculate the: power required, energy needed, and hydrogen consumption over the drive cycle [24]. The first step in the code was simply to list the vehicle specifications and their variable names. Table 3 lists the vehicle variables that were used in the code.

Table 3: MATLAB Routine Vehicle Parameters

Variable	Definition	Value
Gravity	Acceleration due to gravity (m/s)	9.81
Mass	Gross mass of the vehicle (kg)	870

weight	Mass*gravity (N)	8534.7
Tire_pressure	Inflation pressure of tires (bar)	3.516
Crr	Coefficient of rolling resistance	
Frr	Force due to rolling resistance	
Cd	Coefficient of aerodynamic drag	0.207
Af	Frontal Area of vehicle (m^2)	1.34
rou	Density of the air (kg/m^3)	1.2041
Fw	Force due to wind resistance	
Ft	Tractive force at rear wheels	

The code uses the dynamic equation of a vehicle to calculate the tractive force at each time step in the drive cycle. The tractive force vector that is produced then gets multiplied with the velocity vector from the drive cycle to produce the power needed at the wheels at each time step. It should be noted that this power is not the same as the power needed at the motor. One must account for the losses associated with every component in the drive cycle in order to calculate the power needed for each individual component. Below in Figure 19 is a schematic of the drive train components and their associated efficiencies; this system is oriented in a series configuration.
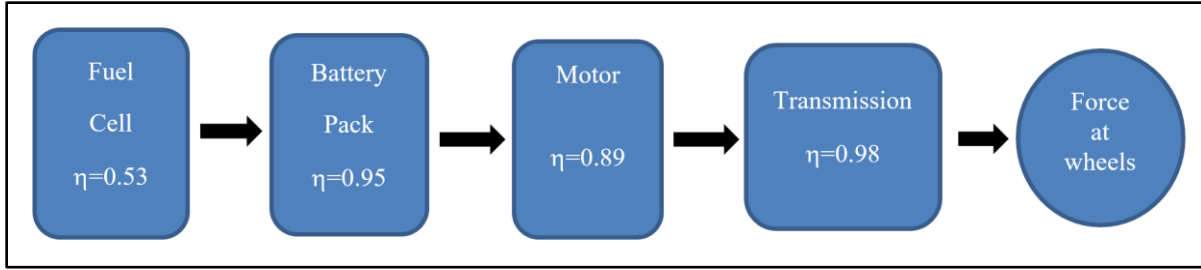
Figure 19: Drive Train Power Flow Chart

So far the power calculated is the power needed at the wheels, however as can be seen from Figure 19, due to the losses associated with each individual component in the drive cycle, the power needed from the fuel cell will be larger than the power needed at the wheels. A quick aside that should be pointed out here is that one of the motivations for hybrid fuel cell systems is that their energy conversion efficiency is much higher than traditional internal combustion engines. The best internal combustion engine only has an efficiency of about 30% compared to the 53% one can get from a fuel cell [25]. To calculate the power needed for each component the following equations were implemented in MATLAB:

$$power\ motor = \frac{power\ wheels}{efficency\ transmission} \tag{0.29}$$

$$Power\ battery = \frac{Power\ motor}{efficency\ motor} \tag{0.30}$$

$$power\ before\ battery = \frac{Power\ battery}{efficency\ battery} \tag{0.31}$$

$$Power\ FC = \frac{Power\ before\ battery}{efficency\ FC} \tag{0.32}$$

Calculating the power needed in each step of the drive train helps in determining the correct sizing for each of the components. The fuel cell power required (power FC) was then integrated so that

the energy needed by the fuel cell could be calculated for every time step in the drive cycle. Figure 20 presents the power and energy required over the drive cycle against each time step in the cycle.
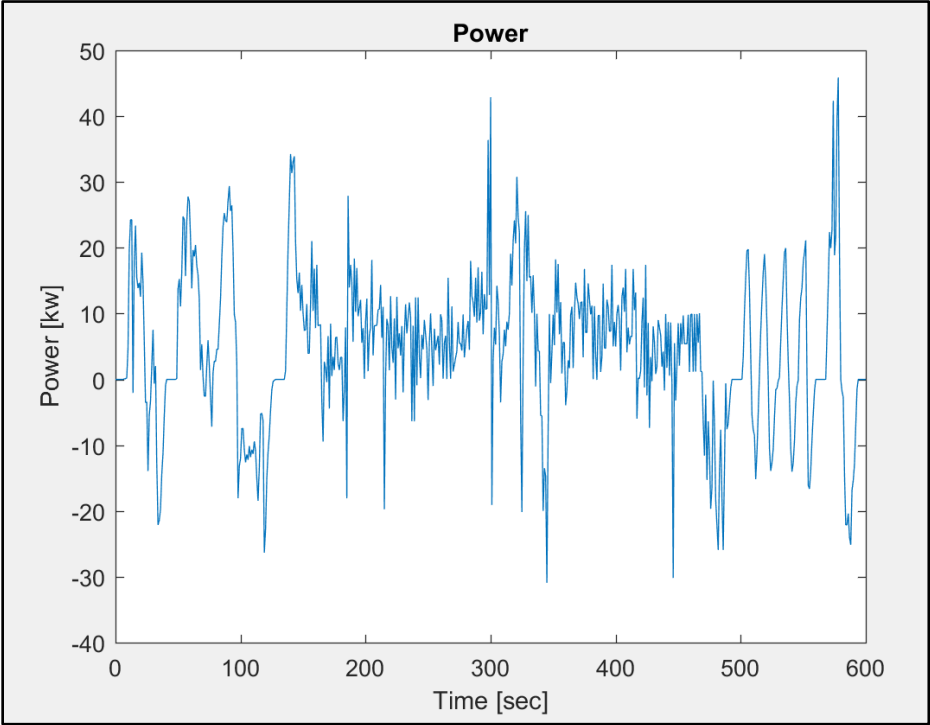
Figure 20: Power Requested from Fuel Cell
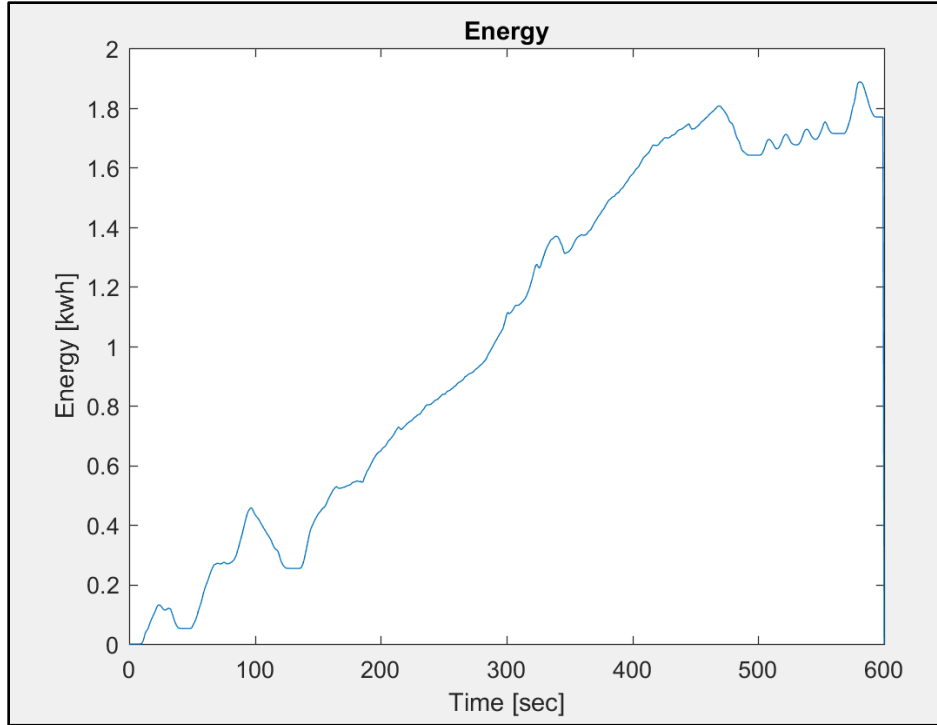
Figure 21: Energy Requested of Fuel Cell

Knowing the energy needed across the drive cycle and the energy density of hydrogen the fuel consumption over the drive cycle was then calculated using the following equation.

$$H_2 \ consumption = \frac{Energy \ [J]}{142,000 \ [\frac{J}{g}]} \qquad (0.33)$$

The fuel consumption over the drive cycle was then used to specify the size of the fuel tank for the vehicle. The fuel consumption rate over the drive cycle is plotted below in Figure 22.
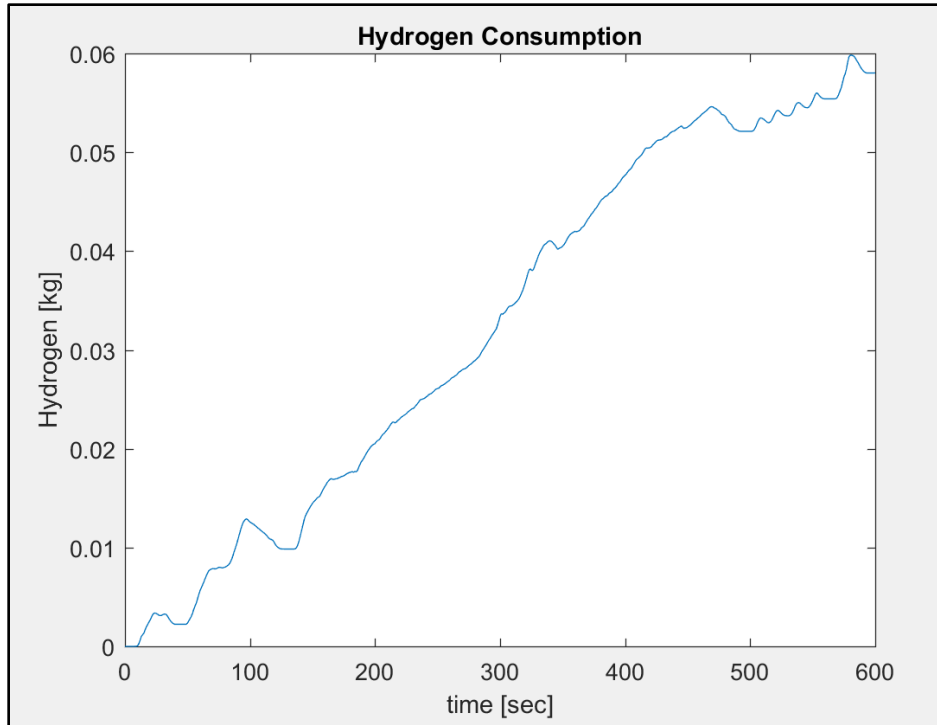
Figure 22: Fuel Consumption Over the Entire Drive Cycle

It should be noted that there was a simplifying assumption made before calculating the fuel consumption. The US06 drive cycle has both accelerations and decelerations and so on the decelerations regenerative braking was used to recapture some on the energy lost to powering the vehicle. However, this energy in practice gets stored in the battery so in equation (0.33) technically there would be no positive energy going back into the tank since hydrogen is not being produced. For this simplified model this fact was neglected, resulting in the simplifying assumption that hydrogen energy was "effectively returned." But in practice, it should be noted that the hydrogen consumption graph would really be a continuously smooth and increasing or flat (when only the battery was used to power the motor) line.

5.2 Simulink Model

Once the MATLAB script was created a Simulink model was produced to simulate the vehicle operating over a drive cycle. The Simulink model used the exact same inputs as the MATLAB routine and produced the same outputs (i.e., power, energy, fuel consumption). The Simulink model was essentially an object oriented model of the MATLAB scrip created in section 5.1 [26]. The Simulink model was constructed in three phases, each phase adding a level of complexity. The same vehicle parameters that are presented in Table 3 were implemented in the Simulink model as an initialization function that runs prior to the model. A version of this file can be found in the Appendix. The velocity vector of the drive cycle which is saved as its own script file gets called into the model from the initialization function. Once the velocity is in the model its derivative is taken to get the acceleration. The velocity and acceleration then get used in two subsystem blocks. The first subsystem blocks use the dynamic equation of a vehicle to calculate the tractive force at the wheels while the second subsystem takes the tractive force as an input and calculates the power required by the fuel cell. An over view of the model is depicted below in Figure 23 below.
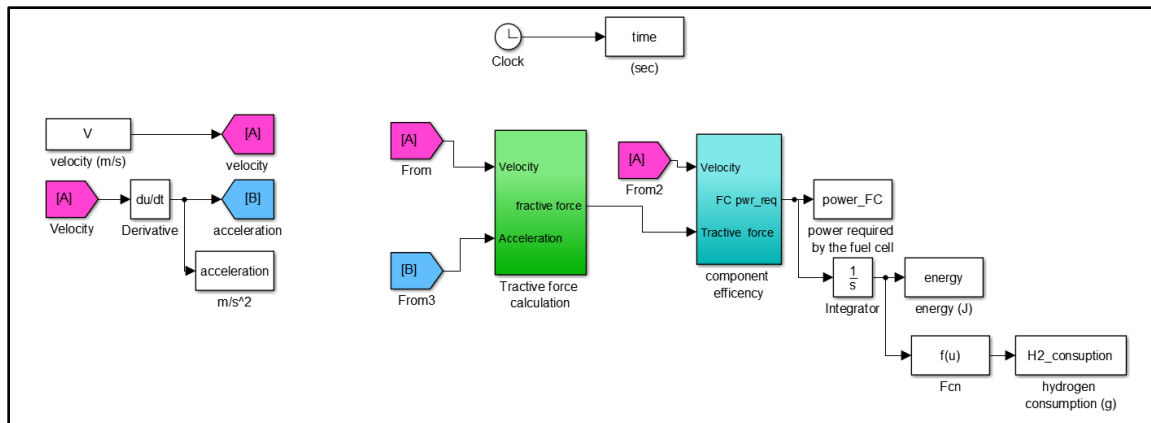
Figure 23: Simulink Model Overview

The inside of the tractive force subsystem block takes the velocity and the acceleration and uses mathematical operations and user defined functions to implement equations (0.19) through (0.25) this block then out puts the tractive force required at the wheels. The inside of the tractive force subsystem block is depicted in Figure 24.
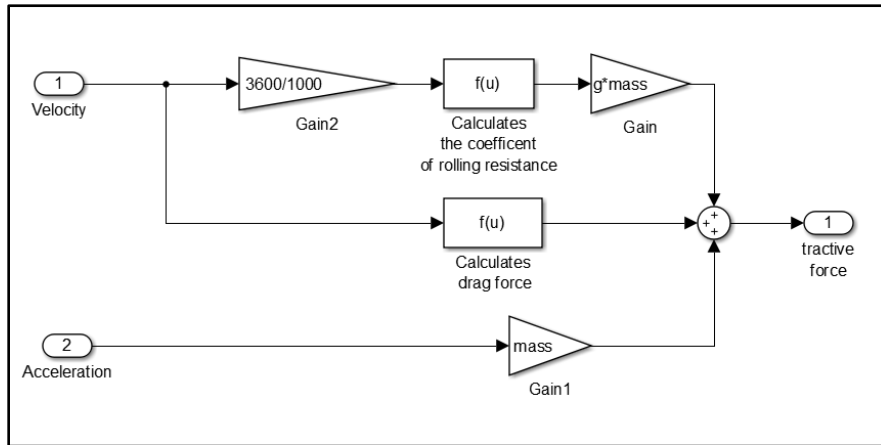
Figure 24: Tractive Force Calculation Subsystem

The output of the tractive force subsystem becomes the input to the component efficiency sub-system model. In the efficiency sub-model, the power at the wheels is calculated by multiplying the velocity with the tractive force. The efficiencies of each of the components are then applied by creating user defined functions that calculate equations (0.29) through (0.32). The output of this subsystem is then the power required by the fuel cell. This subsystem can be seen in Figure 25
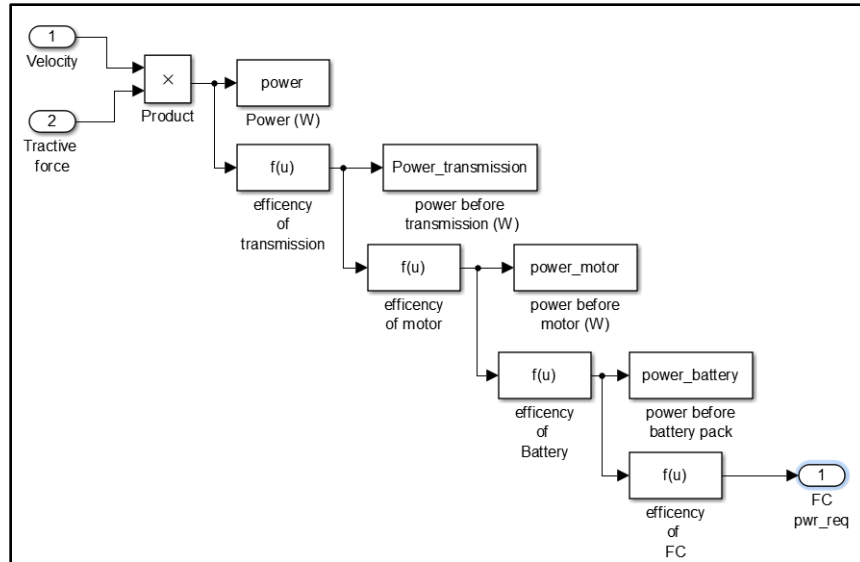
Figure 25: Efficiency Subsystem Block

The power required by the fuel cell is then integrated to give the energy required by the fuel cell and this energy is then divided by the energy density of hydrogen to give the hydrogen consumption over the drive cycle. This is essentially the right-hand side of the overview presented in Figure 23. After the model is executed there is a post function script that plots the power, energy, and hydrogen consumption; this function can be found in the Appendix. The results from the Simulink model are depicted below in Figure 26-28.
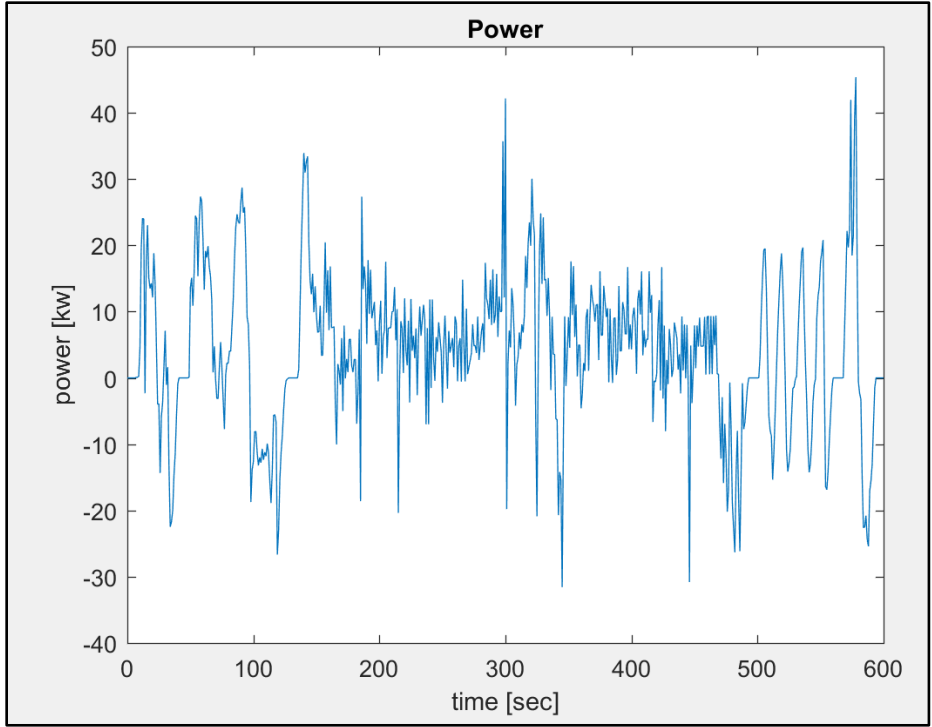
Figure 26: Power Over the Drive Cycle
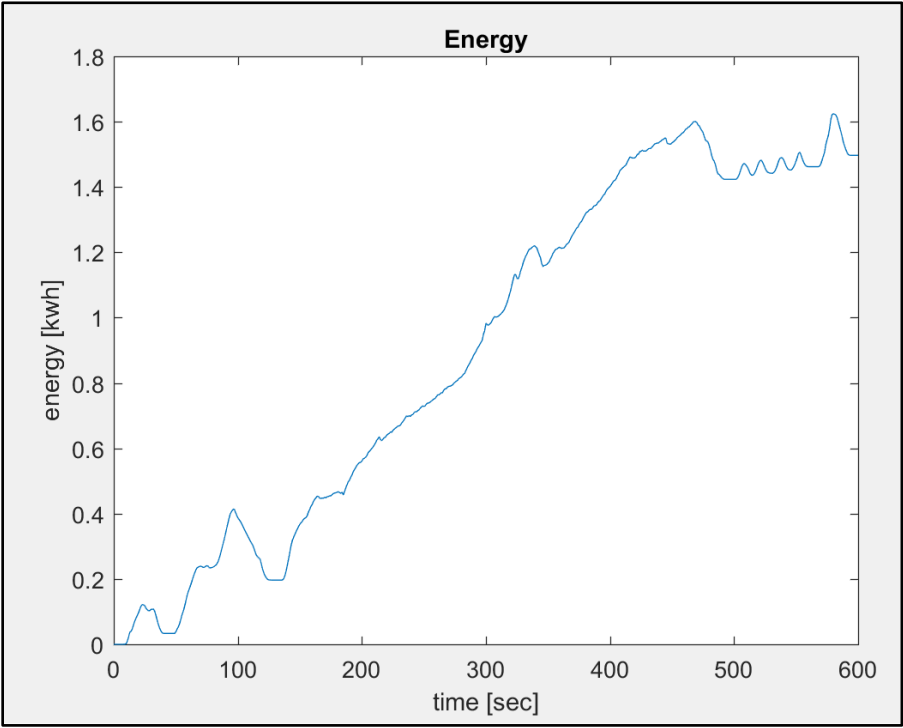
Figure 27: Energy Over the Drive Cycle
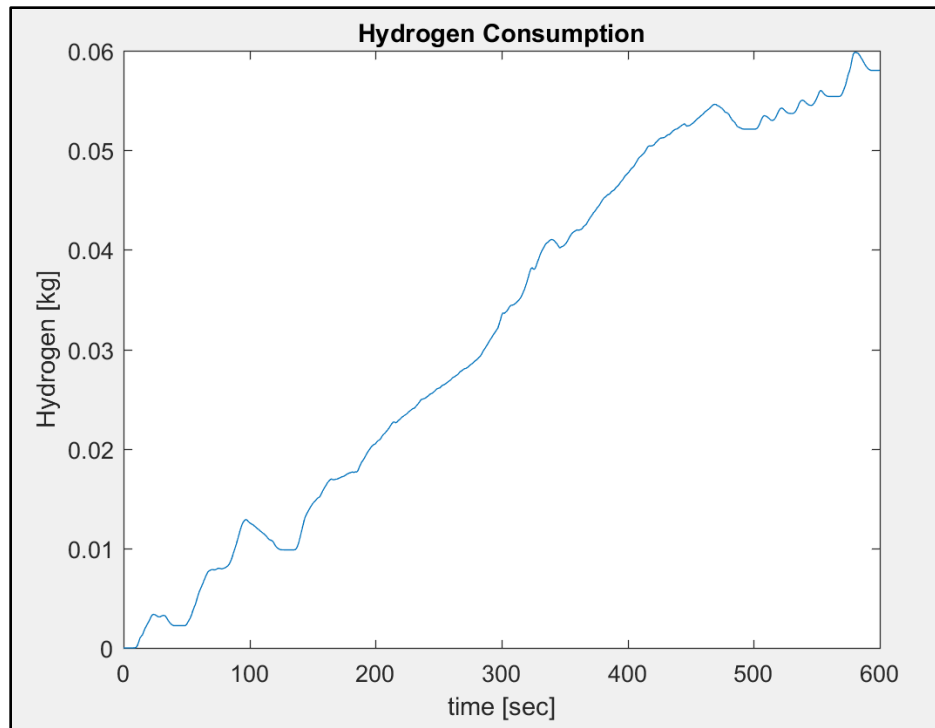
Figure 28: Hydrogen Consumption

As expected these results are exactly the same as the results achieved by using the MATLAB script.

Phase two of the Simulink model added a level of complexity to the design by considering both the state of charge and the voltage change as a function of the state of charge. The overview of phase two of the Simulink model is depicted below in Figure 29.
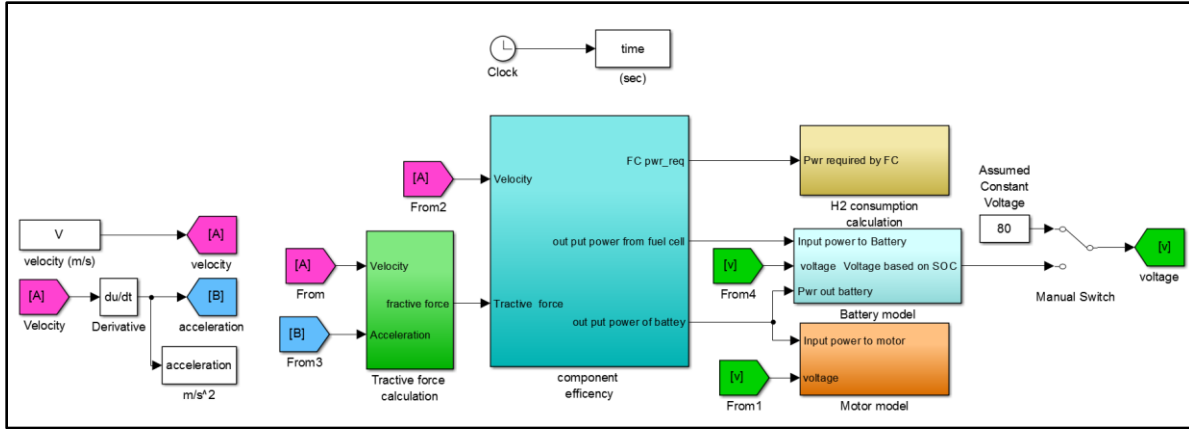
Figure 29: Overview of phase two of model

Three additional subsystems we added to the model: H_2 consumption Calculation, Battery model,

and motor model. The H_2 consumption subsystem is exactly the same as the right hand side of the

component efficiency portion of phase one of the model which can be seen in Figure 23. The

battery calculation and the motor model subsystems are the new additions to the model. For phase

two both the motor model and the battery model do not account for dynamics so they are zero

order models. The use of zero order models are common for automotive systems, which tend to

spend most of their time at steady-state values. The motor subsystem simply inputs the battery

output from the component efficiency subsystem and divides this value by the voltage of the

system, which is an input that is calculated in the battery subsystem. The inside of the motor

subsystem is depicted below in Figure 30.
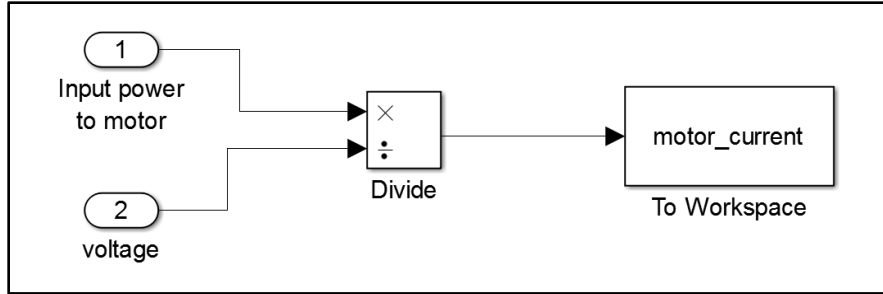
Figure 30: Zero order motor subsystem

From the motor subsystem the current for the motor can be calculated. Similar to the motor model, the battery is also simulated as a zero order system that inputs the power from the fuel cell and divides this power by the voltage of the system in order to get a current output from the battery. The inside of the battery subsystem is depicted below in Figure 31.
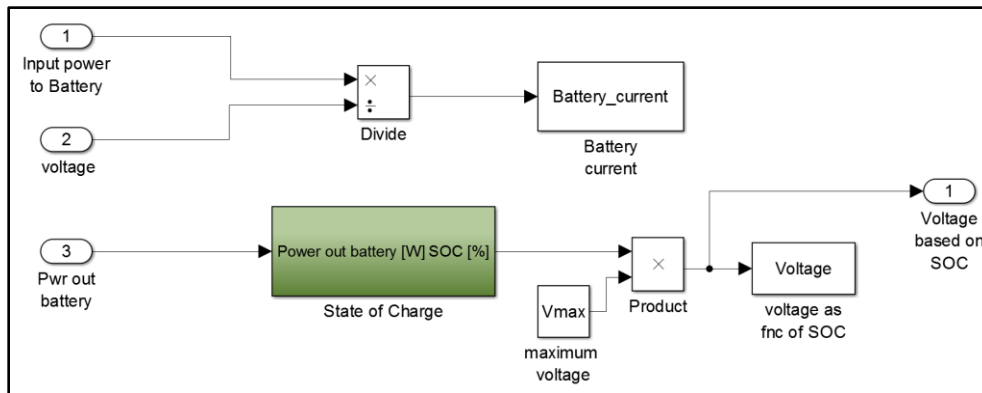
Figure 31: Battery subsystem

Up to this point the voltage was treated as a constant since the nominal voltage of the battery pack is 80 volts. In reality the voltage is a function on the state of charge of the system. To account for the voltage drop, a state of charge subsystem was created inside the battery model. The state of charge was calculated using equation (0.34)

$$SOC = \frac{(Capacity\_batt + FC\_ch\arg e - power\_out\_battery)}{Capacity\_batt} \tag{0.34}$$

46

Where:

- Capacity_batt: maximum capacity of the battery pack in kilowatt-hours

- FC_charge: Amount of charging the fuel cell will perform during the drive cycle in kiliwatts

- Power_out_battery: Input power to the motor in kilowatts

The inside of the state of charge subsystem in depicted below in Figure 32.
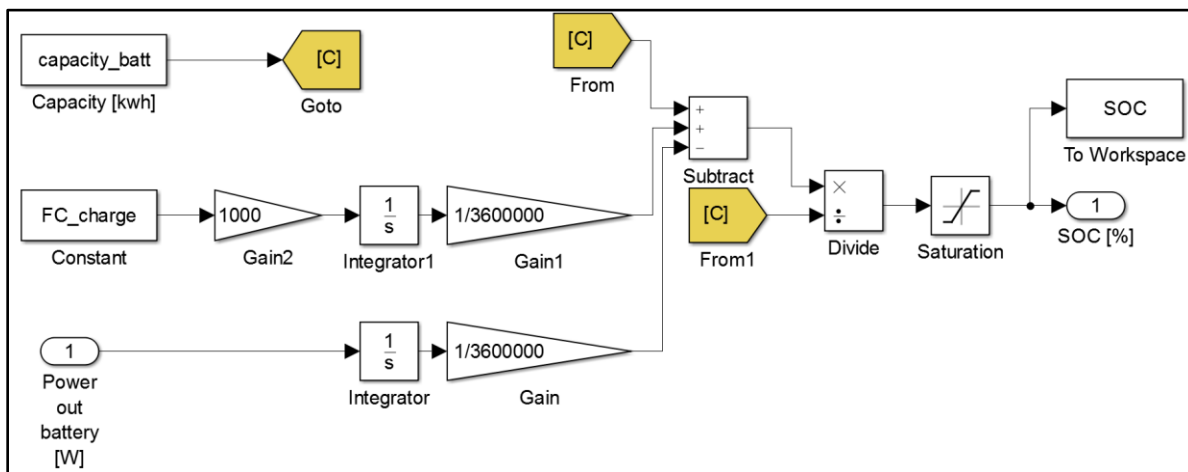
Figure 32: State of Charge Subsystem

Both the Capacity_batt and the FC_charge are listed as variables in the initialization script so that they can be adjusted and optimized based on the drive cycle. It is important to note that the state of charge of the battery pack has a range of zero to 1. In order to keep the state of charge in the allowable range a saturation block was implemented. The state of charge then gets multiplied by the maximum voltage of the battery which produces an accurate voltage based on the state of charge of the battery [27]. This voltage now gets distributed and used in both the battery model and the motor model by the implementation of a manual switch, this switch can be seen in Figure 33.

47
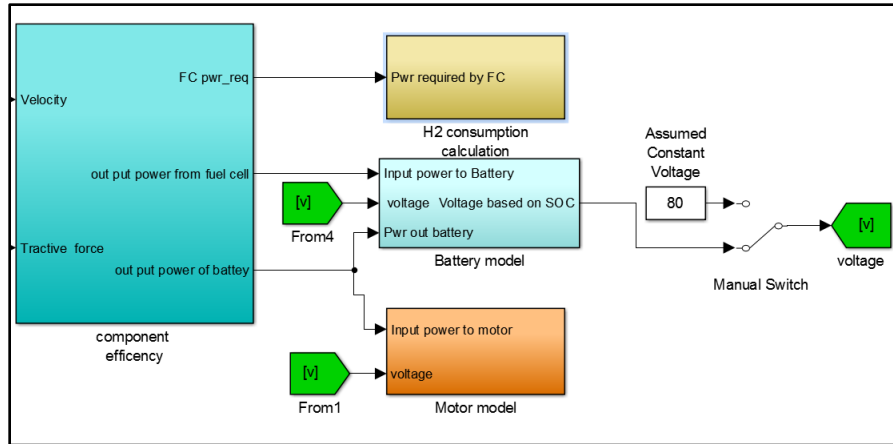
Figure 33: Voltage Routing

The model now no longer assumes the voltage is constant but instead calculates the voltage as a function of the state of charge of the battery pack. Now that the state of charge of the system is known the range of the vehicle can be calculated. The range of the vehicle is going to depend largely on the amount of charging the battery receives from the fuel cell. At this point in the simulation, the hydrogen supply is assumed to be infinite so the amount of charging of the fuel cell can do is not completely accurate since it does not account for the limitations in the size of the hydrogen tank. With the infinite hydrogen assumption two range plots were produced one showing the range in miles while the other shows the range as a function of time. Both plots can be seen below in Figure 34 and 35.
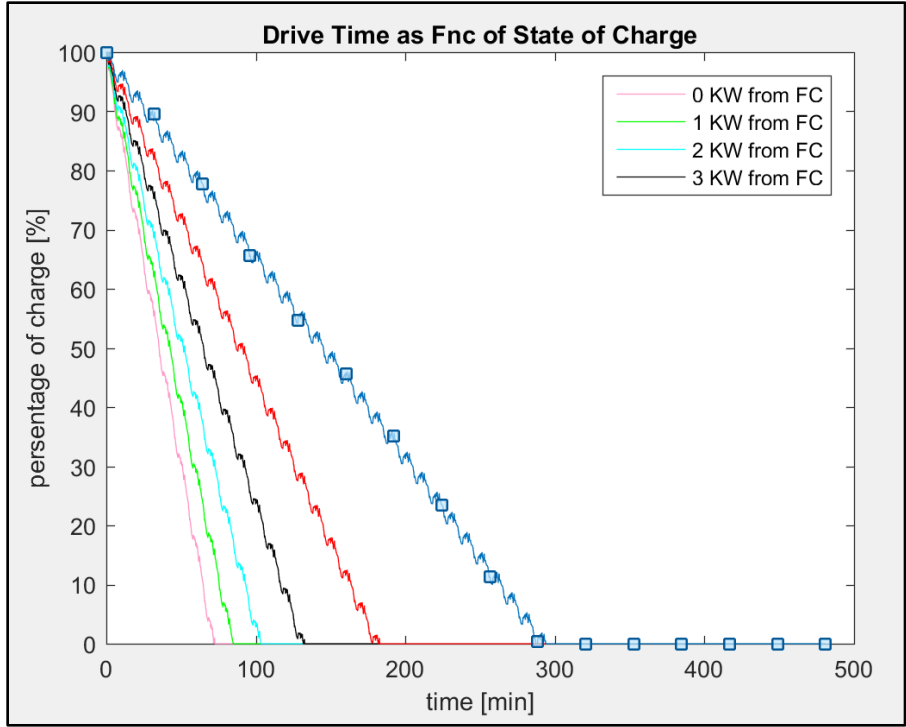
Figure 34: Drive Time as A Function of State of Charge
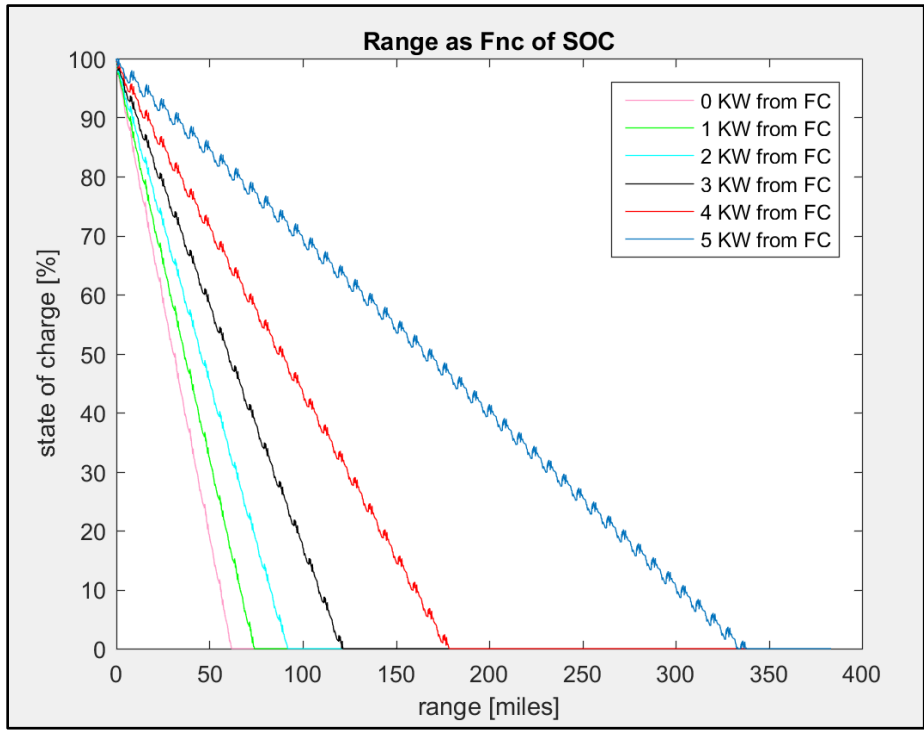
Figure 35: Driving Range as A Function of State of Charge

These plots compare the range starting with the fuel cell not providing any charging so operating as a pure electric vehcicle. As can be seen in the plot the range is limited to just over 50 miles with out any charging from the fuel cell. With incremental increases of 1kw of charging from the fuel cell the corresponding range increases. With a maximum of five kiliwatts of charging from the fuel cell the range reaches about 340 miles which is compariable to the range of one tank of gas in an internal combustion engine vehicle. Once the range calculation is known the optimal charge configuration from the fuel cell can be chosen based on the drive cycle or drive time desired. This can be a useful fuel saving strategy since the fuel cell would not be required to provide much charging on short distance trips and so, for example, a driver could request an input of only one kiliwatt of charging from the fuel cell if the desired trip is under 50 miles.

Phase three of the model took into consideration the limitations of the motor's output torque and speed and calculated how well the vehicle would follow the drive cycle with in the limitations of the motor's abilities. An overview of phase three of the model is shown below in Figure 36.
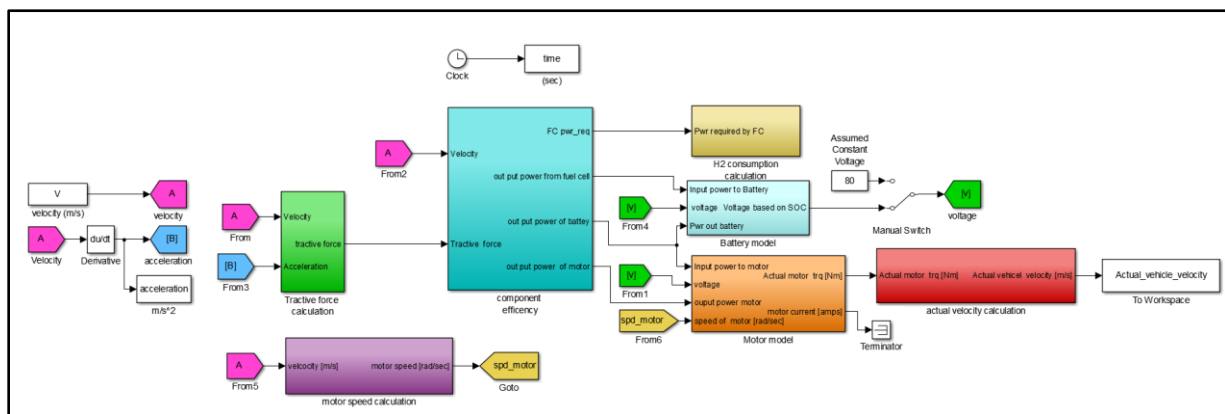
Figure 36: Over View of Phase Three of the Model

The obvious change in phase three of the model are the addition of the motor speed sub model and the actual vehicle velocity sub-model. The motor speed sub model is presented in Figure 37.
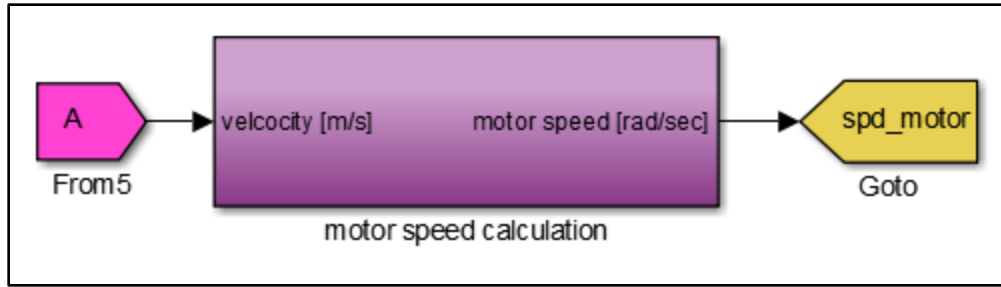
Figure 37: Motor Speed Calculation Sub Model

This model took into consideration the fact that the motor for the project has a maximum speed of

8,000 Revolutions Per Minute (RPM) and thus if the drive cycle ever requested a speed above that

maximum the motor would be saturated to its limit of 8,000 RPM. The inside of the motor speed

calculation sub-model is depicted below in Figure 38.
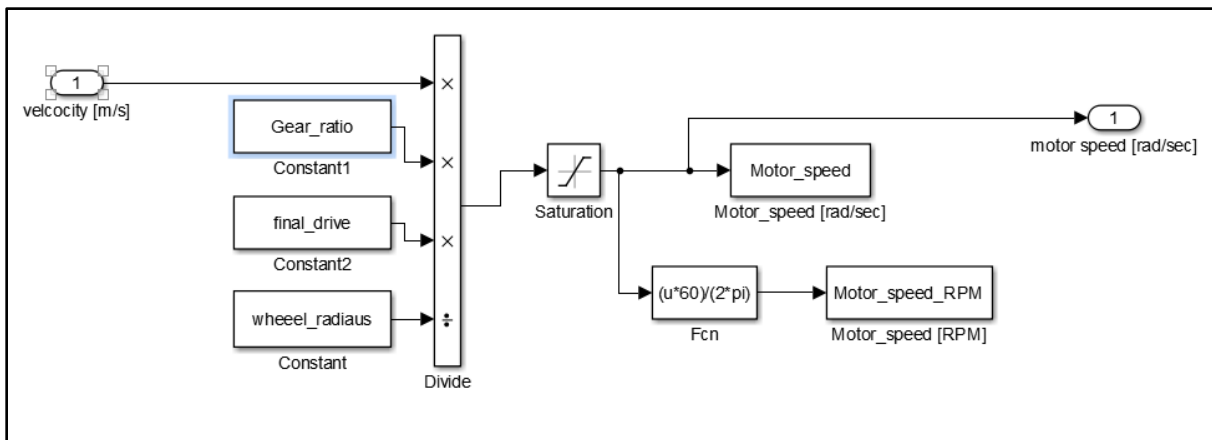
Figure 38: Motor Speed Sub Model

In this model the drive cycle velocity is fed in as an input, this velocity then gets multiplied by a

fixed gear ratio. It should be pointed out that although the motor is attached to a 4-speed

transmission this simulation was calculated with the assumption that the vehicle would be left in

the same gear during all driving operations since there is no need to shift gears with an electric

motor. This simplifying assumption is why the velocity can be multiplied by a fixed gear ratio.

The signal is then multiplied by the final drive ratio and then divided by the wheel diameter to

produce an angular velocity in radians per second. Lastly this velocity is converted into RPM and compared to the motor's peak RPM. The simulation was then executed and the speed of the motor throughout the drive cycle can be seen in the plot of Figure 39 below.
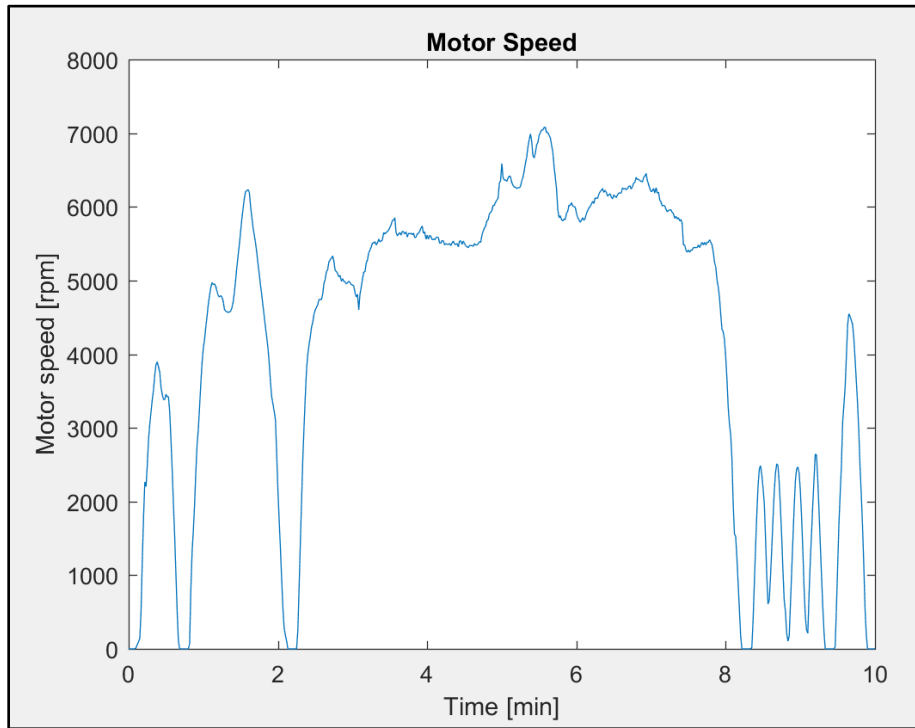
Figure 39: Motor Speed Throughout the Drive Cycle

From the plot it is clear that with the US06 drive cycle the motor is never required to go above its maximum speed. However, to make the model more robust it was important to consider how to construct the model to account for a drive cycle that demands that the motor spin faster than its maximum speed. To account for this possibility a saturation block was implemented in the motor speed calculation sub-model. The saturation block limits the maximum speed of the motor so that even if the demand from the drive cycle is larger than the maximum speed the motor can achieve the model will only out put the achievable motor speed.

The other limitation that was considered with phase three of the model was the fact that the motor has a maximum torque it can produce depending on the speed of the motor. To account for this maximum motor torque a motor torque requested calculation was added into the motor sub model. The inside of the motor sub model is depicted below in Figure 40.
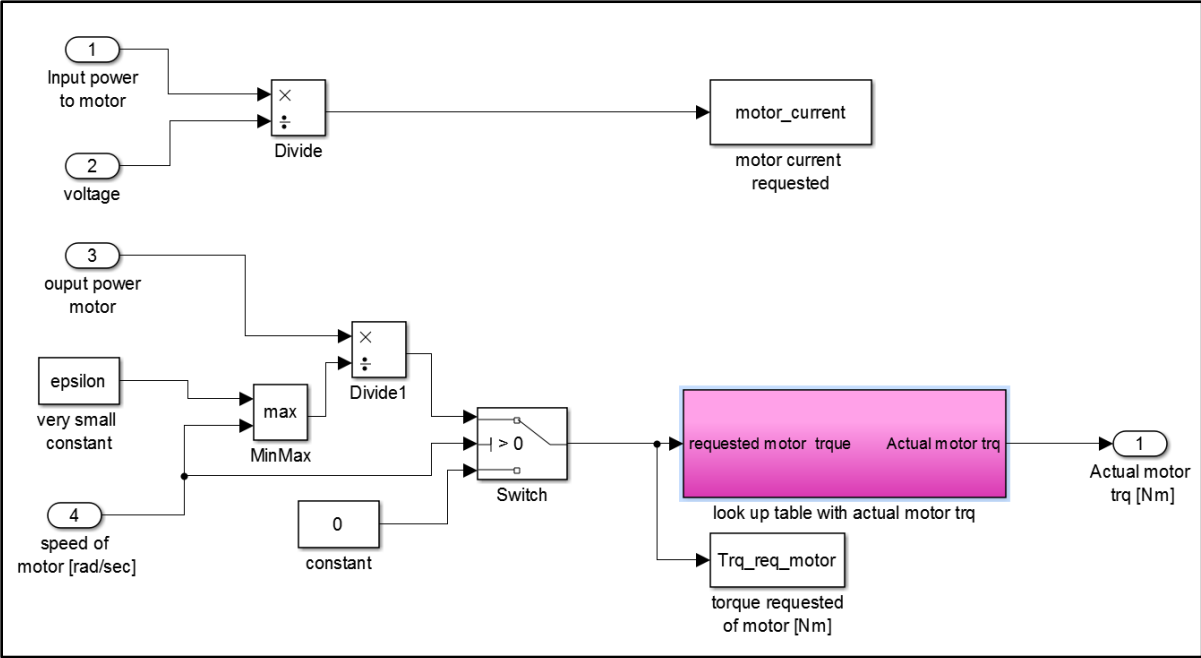
Figure 40: Inside Motor Sub Model

Previously the Motor model only calculated the motor current however two more inputs were added to the motor model, the output power in watts from the motor and the speed of the motor in meters per second that was previously calculated in the motor speed sub model. The power is then divided by the speed in order to get the torque requested of the motor. To prevent division by zero the speed of the motor was compared to a very small number epsilon and the maximum of the two is what the output power of the motor is divided by. When the requested speed is zero the requested torque is also zero so a switch was implemented that checks the speed request and then determines whether to divide the power by the speed to get the torque request or to send a value of zero as the

torque request when the speed is zero. So far, the torque requested by the drive cycle has been determined however it is still unknown if the motor being used is capable of meeting that torque request. In order to verify if the motor was able to actual achieve the requested torque at the requested speed a look-up table subsystem was implemented. The inside of the look-up table sub system in depicted below in Figure 41.
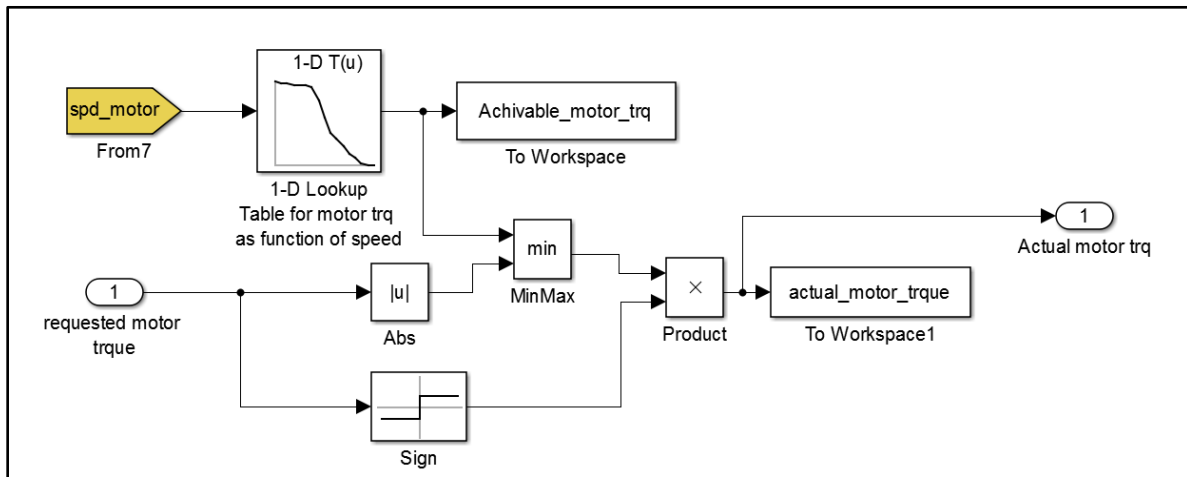
Figure 41: Inside Torque and Speed Look-Up Table Sub-System

The two inputs to this sub system are the requested motor speed and torque. In order to verify if the motor can achieve the torque requested of it a look-up table was populated with the manufacturer's dynamometer results that compared the maximum torque the motor can achieve as a function of the motor speed. The requested speed is then fed into this look-up table and the achievable torque is interpolated from the table. This torque is then compared with the requested torque and if the requested in less than the achievable the requested torque is used The requested torque and the achievable torque are plotted in Figure 42 below.
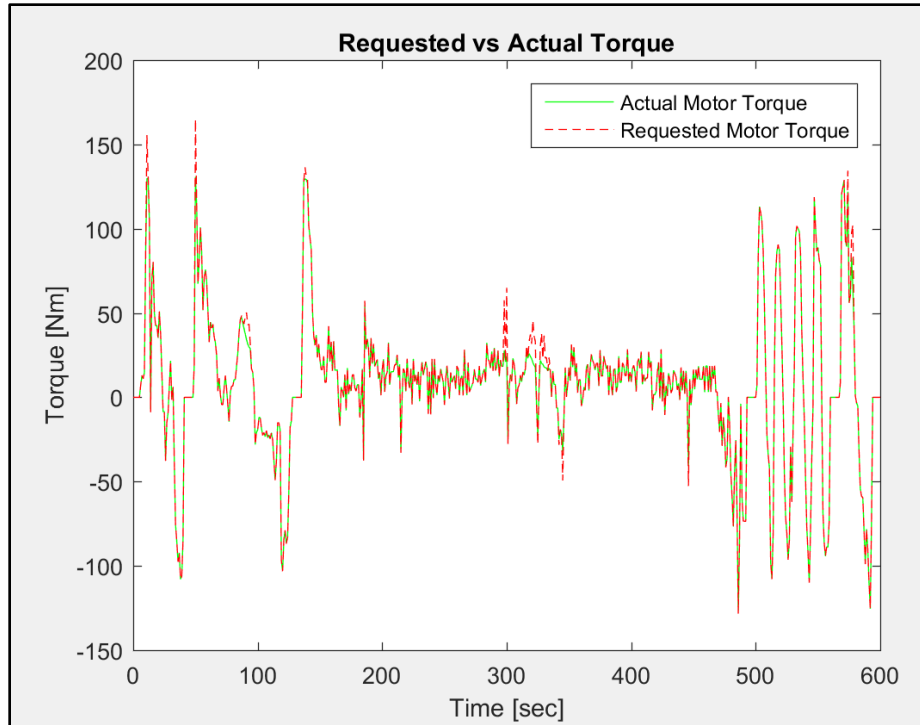
Figure 42: Requested Compared to Achievable Torque

As can be seen from the plot the motor is able to match most of the requested torque demand but the interesting case is when the requested torque is larger than the achievable torque, which can be seen in a few instances during the drive cycle. When the requested torque is larger than the achievable torque the achievable torque gets used. These conditions imply that the motor is not capable of producing the forces needed to maintain the velocity of the drive cycle.

To account for the instances where the motor cannot match the torque demand requested by the drive cycle the actual velocity calculation sub-model was created to calculate what the vehicles actual speed will be during the drive cycle based on the actual torque the motor is capable of achieving. The inside of the actual velocity calculation sub-model can be seen in Figure 43.
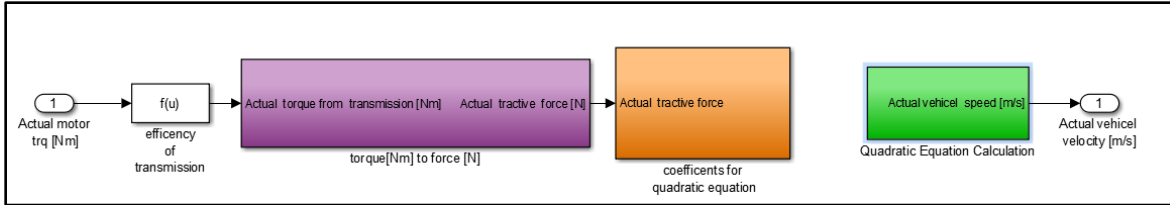
Figure 43: Actual Velocity Calculation Sub Model

In this model the actual motor torque is fed in as an input and the vehicles achievable speed is then

back calculated from the motors achievable torque. This is done by first multiplying the motors

torque by the transmission efficiency then sending that into the torque to force sub system which

can be seen below in Figure 44.
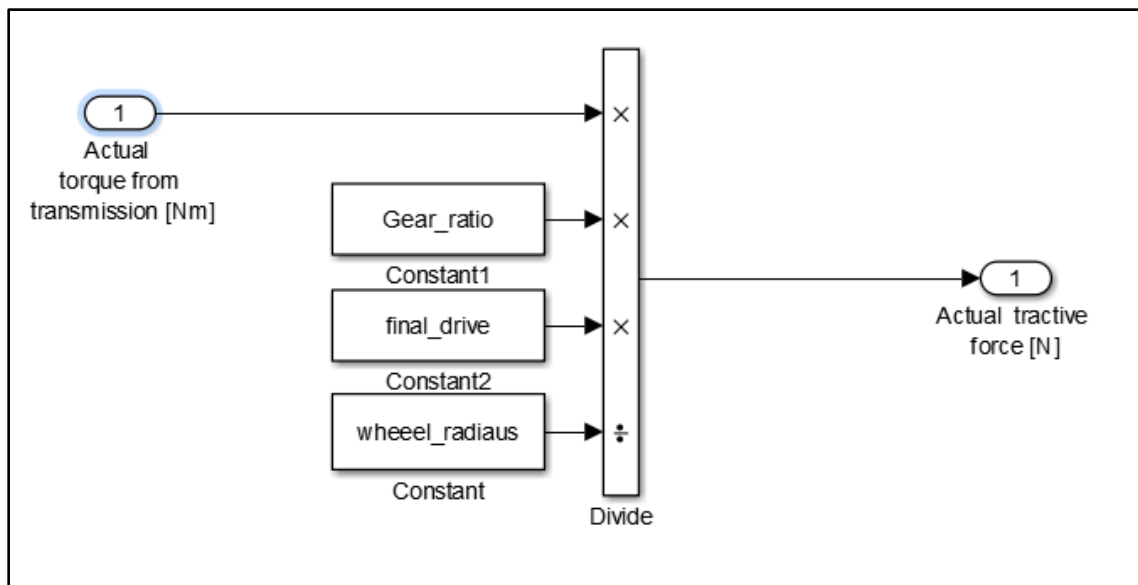
Figure 44: Torque to Force Sub System

In this sub-system the actual motor torque gets multiplied by the gear ration and the final drive

ratio then divided by the wheel radius to produce the achievable tractive force. This tractive force

was then used in the dynamic equation of a vehicle to back out the velocity of the vehicle. It should

be noted that one simplifying assumption was made to perform this calculation. That assumption

was that the portion of the coefficient of rolling resistance equation that depended upon velocity

could be neglected since the drive cycle being used did not reach speeds that would significantly affect the rolling resistance. The next portion of the model back solves for the actual velocity of the vehicle based on the motors achievable torque. This is done by solving the quadratic equation that is formulated after inputting the motors torque into the dynamic vehicle equation. The coefficients for this equation are calculated in the sub-model depicted in Figure 45.
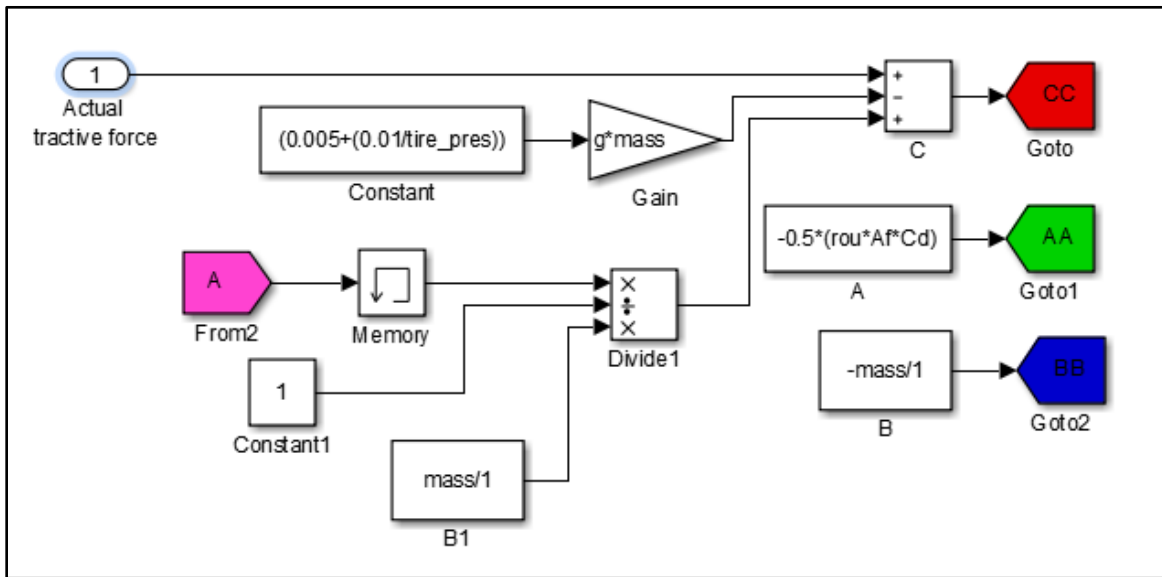
Figure 45: Coefficient for Quadratic Equation Sub Model

After the coefficients to the equation are calculated they are sent to the quadratic equation calculation sub-model through the use of signal routing blocks. In this sub-model as the name implies the quadratic equation is calculated and the velocity is determined. The inside of this sub-model can be seen in Figure 46.
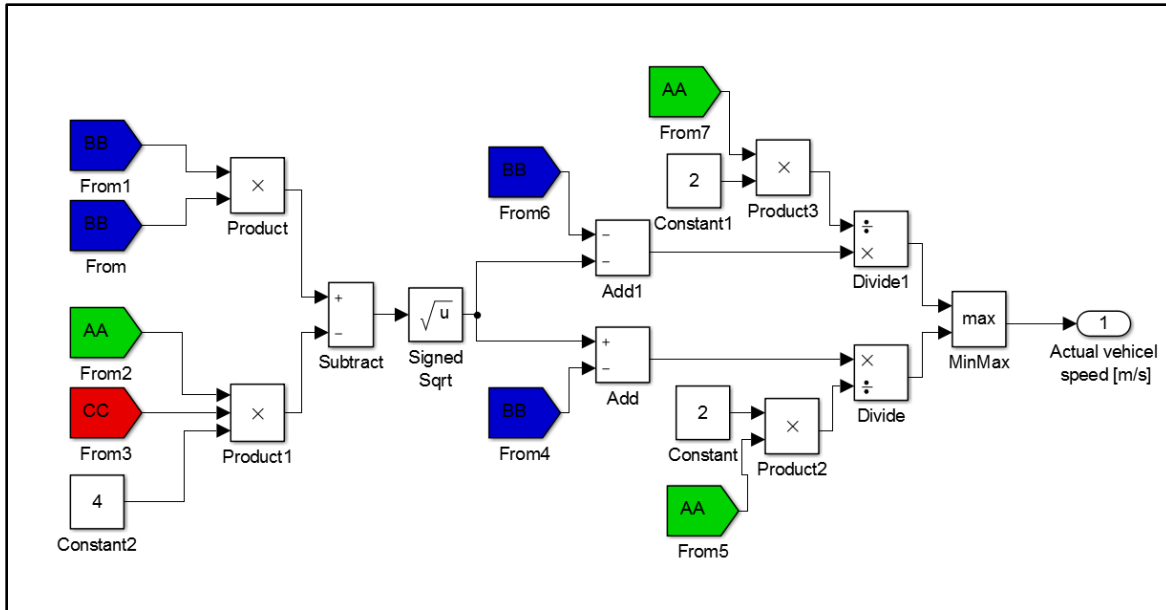
Figure 46: Quadratic Equation Calculation Sub Model

From these calculations the actual velocity of the vehicle is produced; but, as can be expected when solving any quadratic equation, the model produces two answers for the velocity. For this model the larger of the two answers is chosen as the actual velocity since the goal is to get as close to the drive cycle speed, which is faster than the actual speed. The results of how well the modeled vehicle can follow the drive cycle is shown in Figure 47.

58

Figure 47: Drive Cycle Trace

The vehicle is able to follow the drive cycle relatively well with the exception of a few peaks. These results were expected because of how well the motor was able to follow the requested torque, which was presented in Figure 42. Had the motor not been able to follow the requested torque demand then it would have been expected that the drive cycle trace would not match as well as it does. In practical applications the majority of time the drive cycle will not be known ahead of time so it was imperative to test how well the model handled different driving patterns. To evaluate how well the model handled different driving patterns ADVISOR was again implemented to obtain the velocity vector for two different drive cycles. The goal hear was to see how well the model followed the two most common driving patterns, the first being a steady state highway pattern and the second being an urban city pattern with multiple stop and go conditions. In order to evaluate how well the model held up in a highway condition the US06-HWY drive cycle was selected. This drive cycle starts off with a constant acceleration until the vehicle reaches highway speeds. The

59

beginning of the US06-HWY drive cycle simulates how one would accelerate when entering a freeway; it then stays at highway speeds of between 60 and 80 MPH. Below in Figure 48 is the plot of the torque for the US06-HWY cycle.
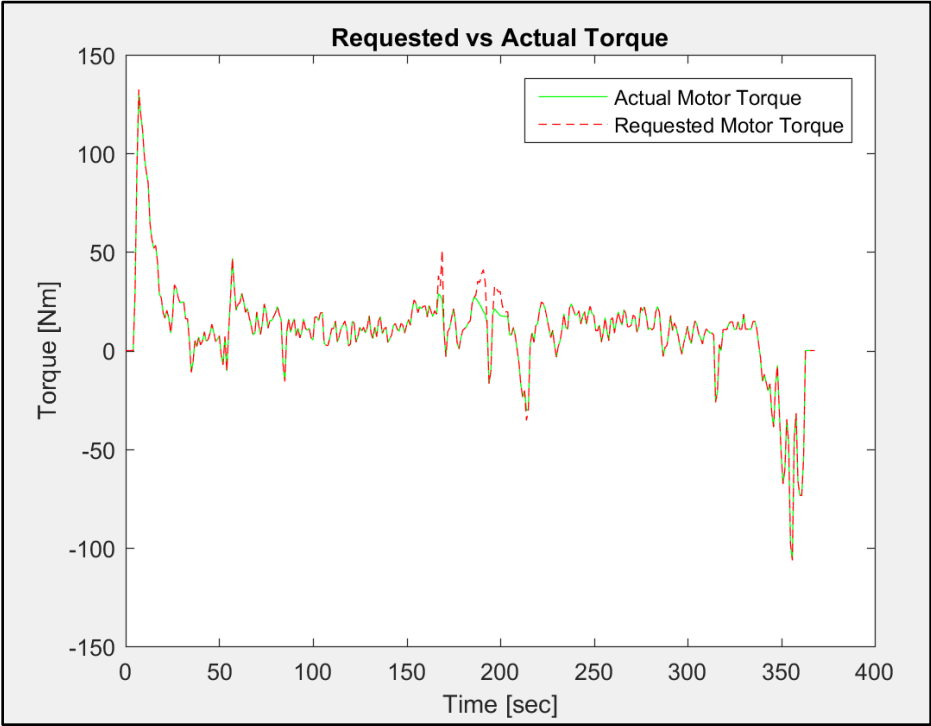
Figure 48: Torque Map for US06-HWY Drive Cycle

The initial sharp torque spike that is seen in Figure 48 comes from the constant acceleration associated with the drive US06-HWY drive cycle as the vehicle quickly attempts to reach highway speeds. From the graph it can be seen that the motor model is capable of following the torque request almost perfectly, because of this it is expected that the velocity trace should match almost identically to the drive cycle. Below in Figure 49 is the resulting plot of the velocity trance.
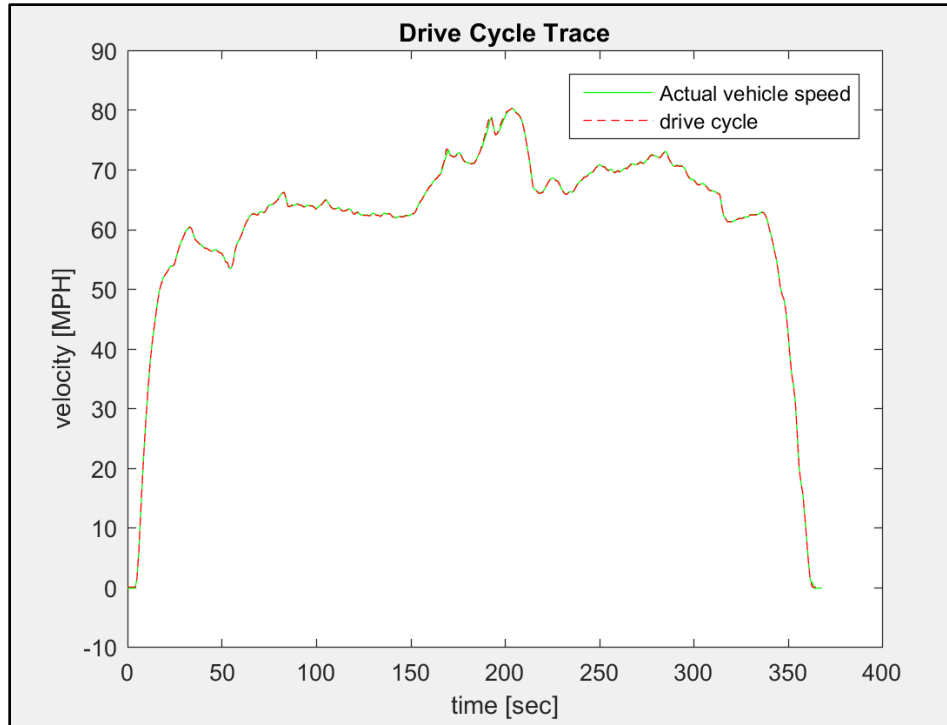
Figure 49:Drive Cycle Trace for US06-HWY Drive Cycle

As was hypothesized based on the torque map results the modeled velocity is almost identical to

the requested velocity. The Urban Dynamometer Driving Schedule (UUDS) was used to evaluate

how the model stood up to the second most common driving pattern. The UUDS is a low speed

driving cycle with a lot of stop and go patterns; this of course simulates driving in a congested city

with traffic and multiple stop lights. Below in Figure 50 is the plot of the torque request based on

UUDS.
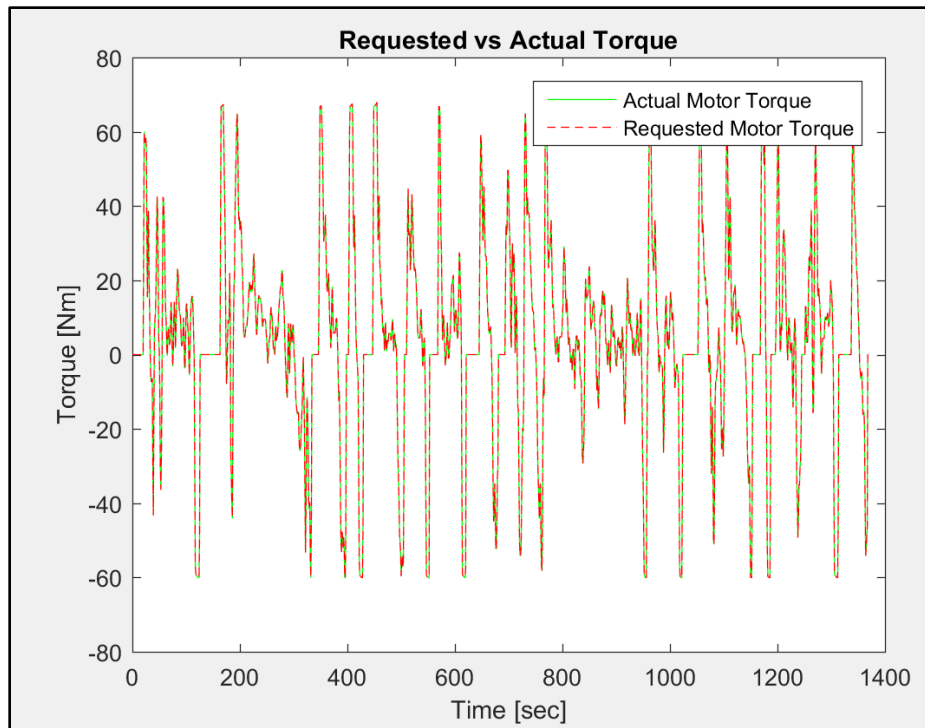
Figure 50: Torque Map for UDDS

Contrary to the US06-HWY cycle where the torque reached an almost steady state range in the UUDS the torque request is constantly changing. The constant change between negative and positive torque requests is a result of the decelerations cause by the stops in the drive cycle. The points where the torque request is zero for multiply seconds correlates to the velocity being zero, for example like at a stop light. The model seems to again match the torque request pretty well so it is anticipated that the velocity trance will again line up very closely to the request velocity. Below in Figure 51 is the velocity trace for the UDDS.
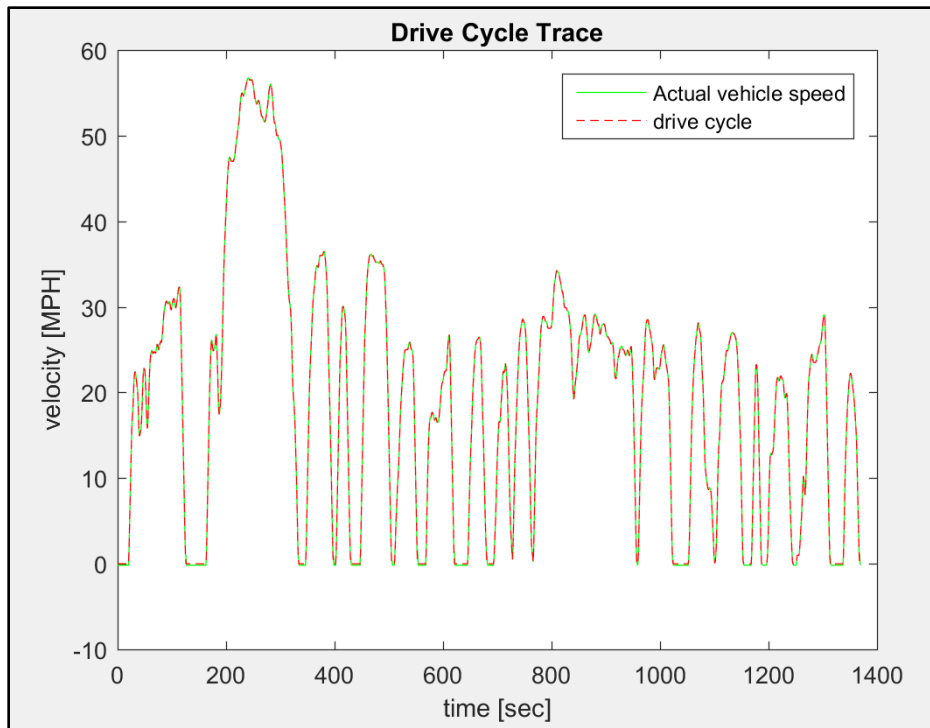
Figure 51: Drive Cycle Trace for UDDS

The velocity for trace matches very well to the requested velocity from the drive cycle, this is expected since the UDDS does not have large accelerations and so even though the entire drive cycle is filled with transient torque requests none of them are larger than the maximum torque in the lookup table for the motor model. Once the model was completed the focus for the project was shifted to the physical components needed to actual construct a prototype vehicle, as such the balance of plant components were analyzed next.

Ch. 6: Balance of Plant Components

Effective balance of plant components are necessary for a fuel cell to function properly. For example, the fuel cell being utilized on this project requires a specific coolant flow rate and in fact, as a safety precaution, the fuel cell will not turn on until the required flow rate is detected. In order to make sure all of the necessary balance of plant components functioned as required for the fuel

cell, tests of each individual components we taken in the lab prior to their integration on to the vehicle.

6.1 Heat Exchanger

One of the quickest ways to ruin a fuel cell is to operate the fuel cell at elevated temperatures. To prevent overheating a custom heat exchanger was designed to reject the heat that the fuel cell creates. This, of course, is a direct analogy to how the radiator of an internal combustion engine vehicle rejects the heat created from the combustion of fuel that takes place inside the cylinder of the engine by circulating antifreeze through the cooling chambers of the engine. In a fuel cell heat is also produced but it results from electrochemical reactions not combustion. Another crucial difference with the heat exchanger of a fuel cell is the type of material the heat exchanger is composed of. Unlike internal combustion engines which utilize a mixture of both antifreeze and tap water as the cooling fluid, fuel cells must use deionized water as their cooling fluid. The reason that fuel cells are restricted to using deionized water is because the membrane in the fuel cell will react and corrode if the fluid is impregnated with certain ions and current could flow through the coolant instead of the fuel cell stack if it contained sufficient conductivity. This of course means that the heat exchanger cannot be composed of certain materials as well since the cooling fluid that will be circulating through would get contaminated if the heat exchanger was composed of the wrong materials. It should be pointed out that this implies that not just the material the heat exchanger is composed of matters but every component in the cooling loop that comes into contact with the deionized cooling fluid must be a particular material. Stainless steel is very corrosion resistant and so all of the fittings in the cooling loop for this project were made from stainless steel. Depicted below in Figure 52 is the heat exchanger for this project.
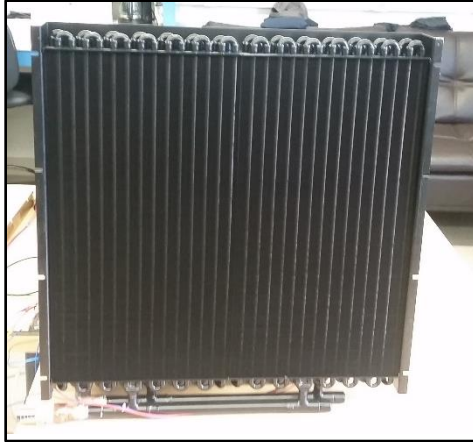
Figure 52: Heat Exchanger

The heat exchanger is 23 inches by 22 inches so it has a substantial surface area for cooling. For proper heat rejection air flow through the fins of the heat exchanger is crucial. With a traditional internal combustion engine cooling system, the radiator is usually assisted by either a mechanical fan that is coupled to the engine though the use of the engines serpentine belt or an electric fan that is triggered by the thermostat reading of the motor. The same principal of moving cool air across the heat exchanger applies for this project as well and, in fact, the heat exchanger for this project utilizes four 24-volt variable speed fans that are attached via a custom radiator shroud to help maximize air flow. Depicted below in Figure 53 is the front of the heat exchanger.

Figure 53: heat exchanger cooling fans

From the front of the heat exchanger one can see the four cooling fans and the custom shroud that connects them to the heat exchanger.

Each cooling fan is powered by a 24-volt direct current (DC) supply and takes a zero to ten-volt variable control signal to adjust the speed. Since there was no need to run the fans at independent speeds since the goal is for them to work in unison to cool the radiator they were wired in parallel and a potentiometer was used to vary the control signal, i.e., adjust the speed of the fans. A bench test of the cooling fans is depicted below in Figure 54.
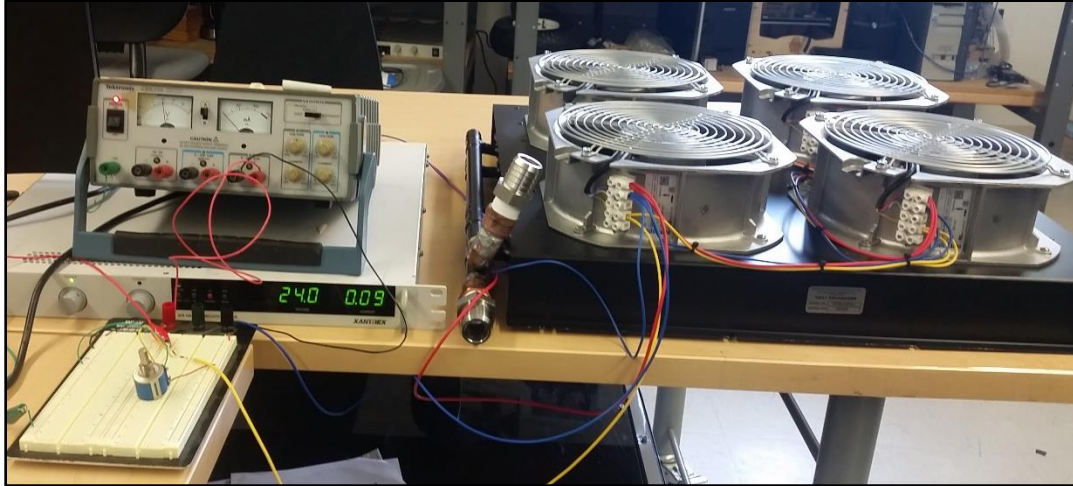
Figure 54: Bench test of cooling fans

The bottom power source with the digital display in Figure 54 is supplying the 24-volt supply to

the fans and the top power source in Figure 54 with the analog gauge is supplying the 10-volt

supply to the bread board, which is then being adjusted by the blue potentiometer which can be

seen on the bread board. In this bench test the maximum speed of the fans was actually achieved

at a control signal of 7.68 volts.
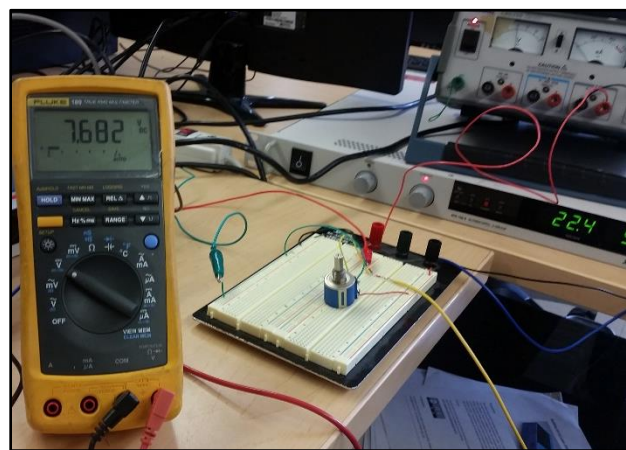
Figure 55; Control voltage that produced max fan speed

This result was due to the fact that the power supply being used could not supply the demanded

current that the motors were drawing when the control signal was at its maximum of 10 volts.

6.2 Water Pump

The heat exchanger is only effective if the fluid that it is extracting the heat from is flowing through the heat exchanger at the right flow rate so after testing the fans for the heat exchanger the water pump was bench tested next. Since real estate was on high demand for this project a micro pump was actually utilized to supply the pumping needs. The CA series micro pump, which is an Eagle Drive pump was implemented do to its small size and reduced sound when operating. The water pump can be seen in Figure 56.

Figure 56: CS Series Micropump [28]

The pump has a maximum flow rate of 27 liters per minute which is plenty of power for this application [28]. Just like the cooling fans, the pump operates on a 24-volt direct current (DC) power supply. The water pump also has a variable flow rate, which is adjustable through a 0-5 volt control signal. A bench test was performed on the water pump in lab similar to the test that was performed on the fans. A 24-volt power supply was used to test the pump while a smaller 5 volt supply was used in junction with a potentiometer to vary the control signal (ie speed/flow rate of the pump). The bench test set up can be seen in Figure 57.
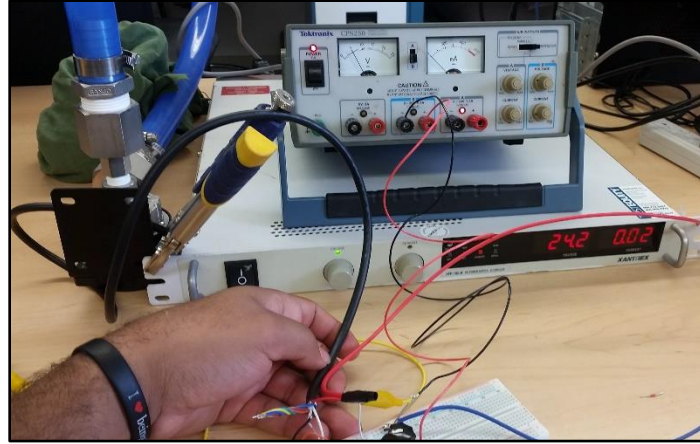
Figure 57: Water Pump Bench Test

Blue hoses were connected to both the inlet of the water pump and the outlet of the pump and a 9.5 Liter buckets was used to draw from while a five-gallon bucket was used to collect the water during the test. The test was timed and the water was measured so that the flow rate could be verified with the manufacturer's specifications. At 24 volts and at maximum speed, the pump was able to achieve a flow rate of 9.5L/37.6 sec. However, it was noted that the pump drew more power than the power supply could provide during the test and so the voltage dropped to only 14.4 volts during the test. Below in Figure 58 is an image of the bench test.
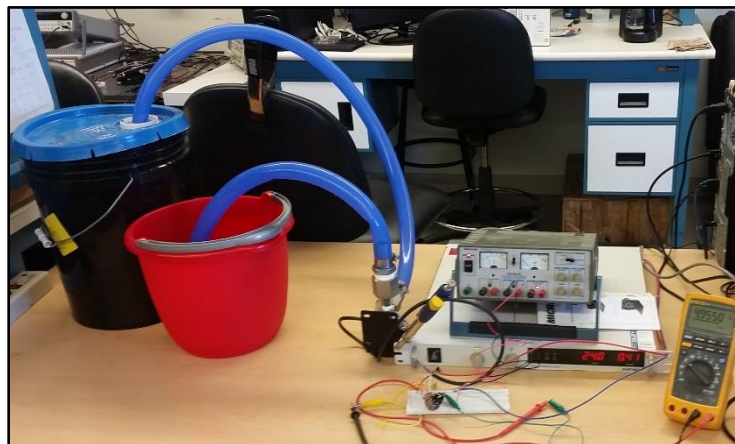
Figure 58: Water Pump Bench Test

The red bucket was the 9.5L liter bucket used as the supply and the black five-gallon bucket was the collection bucket. One-inch diameter high temperature hose was used to connect the pump to the supply and drain buckets respectively.

6.3 Battery Pack

The next major component to be evaluated was the battery pack. The battery pack for this project was a joint design between Kettering University in Flint Michigan and a company called e-Transportation Luxembourg Europe. The battery pack is comprised of more than just batteries, the pack consists of: the individual battery cells, the Battery Management System (BMS), controls hardware, and Controller Area Network (CAN) communications. There are 20 individual cells being used each of which produces 4.17 volts. And the chemical composition of the battery cells is Lithium Polymer. The cells were made in Korea by a company called KOKAM. All the cells put together generate 80 Volts DC when fully charged at 100 amps' charge continues, 200 amps' discharge continues, and 400 amps' peak. All of the components that make up the battery pack were housed in a custom built aluminum box to make mounting the pack to the vehicle easier. E-Transportation did all of the actual assembly of the battery box and its components. Below in Figure 59 and 60 are pictures of the battery pack.

Figure 59: Battery Box
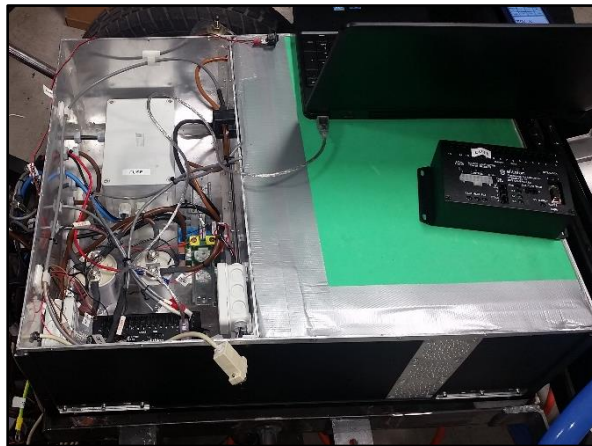
Figure 60: Inside of Battery Box

Since this vehicle is going to be powered by a series hybrid drive train, the battery pack will be required to provide all of the power to the motor. Because of this, it is important that the state of charge of the battery pack be maintained throughout the drive cycle. In order to maintain the state of charge of the battery system a power electronics box was developed to receive variable input power from the fuel cell and output a constant charge to the battery pack.

6.4 Power Electronics

In theory, in a fuel cell series hybrid drive train architecture the fuel cell would charge the battery directly however in practice the power coming from the fuel cell is not constant. In order to account

for the fact that the power coming from the fuel cell fluctuates, a power conditioning unit (power electronics box) is implemented between the fuel cell and the battery pack to condition the signal sent to the battery pack for charging. The design of the power electronics box for this project was again a joint collaboration, this time between Kettering University and Zahn electronics in Franksville Wisconsin. The power electronics box is designed to take a variable input signal from the fuel cell between 50-70 volts at 400 amps' and amplify this signal to output a constant 80 VDC at 400 amps' to charge the battery pack. The power electronics box can be seen below in Figure 61 and 62.

Figure 61: Power Electronics Box

Figure 62: Outputs to Power Electronics Box

6.5 Conversion Electronics

Once the high power electrical components were taken care of (i.e. the motor, battery, power electronics) the next phase was to work on the electrical system for the balance of plant electronics. This portion of the electrical system was entitled the conversion electronics because it provided power to all of the other necessary components to convert the vehicle into an electrically propelled car. The power electronics board's basic function was to take the 80volts that the battery was outputting and drop that voltage to the necessary voltages needed to operate all of the smaller electrical devices on the vehicle. The conversion electronics board provides a 24-volt signal for the water pump and the cooling fans on the heat exchanger. Both the heat exchanger cooling fans and the water pump are variable speed units that operate off of a 0-10-volt and 0-5-volt control signal respectively so the conversion electronics also accommodates these variable voltage signals. The Curtis motor controller requires a 12-volt ignition signal so the conversion electronics board also handles this power supply. The standard voltage on most cars for things like interior light, tail, lights, head lights, and brake lights are all 12-volts so even though currently these items are not on the car eventual once the body for the vehicle is built and they are added the conversion electronics board will also supply the 12-volt power needed for these components. Below in Figure 63 is a picture of the power electronics board.
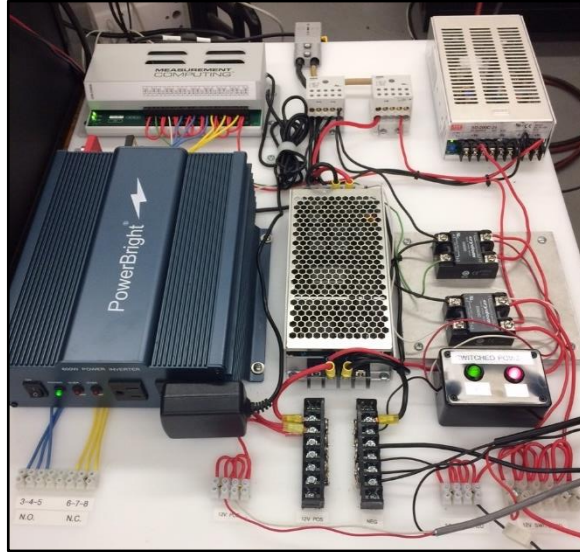
Figure 63: Conversion Electronics Board

Once the majority of the electrical components were specified and there was a common consensus on the major components the next task in the project was to see what type of a chassis platform could be used to house and integrate all these components.

Ch. 7: : Chassis Design

7.1 Classics Never Go Out of Style

After analyzing the dynamic equations of a vehicle it was evident that the lighter and more aerodynamic the vehicle the more efficient it will be. Using this knowledge, it was clear that the best vehicle to create would be a completely composite vehicle constructed out of lightweight materials such as carbon fiber and fiberglass however budget limitations dictated that an existing vehicle be used as a starting platform and that it be updated to fit the unique needs of the fuel cell.

With these requirements in mind the decision was made to bring back a German classic. A 1969 Volkswagen Beetle was purchased as the starting platform for the project.

Figure 64: 1969 Volkswagen Beetle

 The 1969 Beetle seen above in Figure 64 was the perfect plant to start with because unlike most vehicles it does not have a ladder frame architecture; its structural rigidity comes from its unibody design; this enables the VW Beetle to be extremely lightweight. Furthermore, since the intent is to implement an original control strategy for the hybrid system being designed it was easier to start with a vehicle with no electrical control system as opposed to having to tap in to the controls that come standard on most new vehicles.

While the Beetle body is certainty a classic in automotive design it was the chassis the body sits on that will be used for this project. With that said the first order of business was to detach the body from the chassis; this is illustrated in Figure 65.

Figure 65: Fenders and Body Removed from Chassis of the Beetle

After removing the body, the chassis condition was able to be analyzed. Being that the vehicle was created in 1969 there were some things that needed to be upgraded right away, the first being the braking system. The VW Beetle came standard with drum brakes which for their time worked okay as long as you kept them adjusted correctly but since the intent for this project was to produce what will be the future automobile it was decided to upgrade the braking system to self-adjusting disk brakes at all four wheels with a duel reservoir master cylinder for safety [29]. All the rubber and hard brake lines on the car were also replaced, more so as a precaution since they were almost 50 years old. This can be seen in

Figure 66 and 67.

Figure 66: Disk Brake Upgrade

Figure 67: Duel Master Cylinder Upgrade

The next step was to have the chassis media blasted to get rid of the 47 years of dirt and grease that was present on the chassis. Because the car spent its life in California it had minimal rust damage. After the media blast the chassis was painted to keep it from rusting. The new canvas was now ready to be molded into a fuel cell vehicle.

Figure 68: Freshly painted VW Beetle chassis

As stated earlier the VW platform is ideal for this project do to its light weight construction and unibody design however since the original Beetle body was not going to be used, this mint the

structural rigidity that the body provided would be lost. To account for this we implemented body pan stiffeners and a full rectangular tube body lifts kit. Both the pan stiffener and the lift kit are composed of two inch by one-inch mild steel rectangular tubing, each with a wall thickness of 0.12 inches. The pan stiffeners coupled with the body lift kit provide some of the structural rigidity that the body originally provided. The body lift kit was also used so that there would be a solid support to mount the roll cage and other major components to. In Figure 69 and Figure 70 you can see the pan stiffeners and the body lift kit respectively.

Figure 69: Floor pan stiffeners
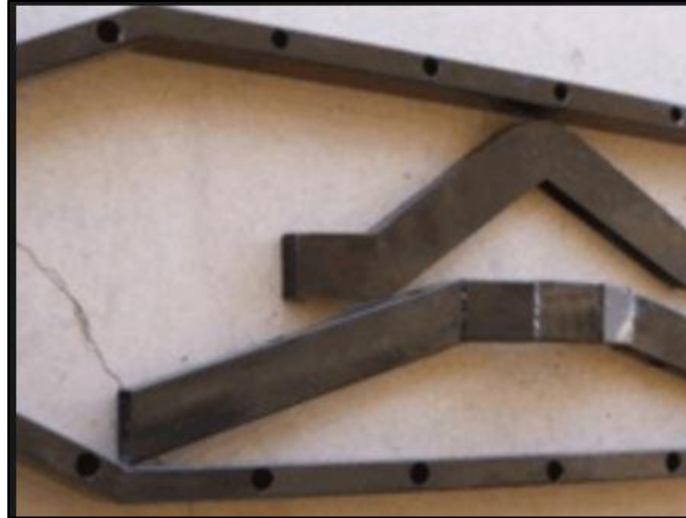
Figure 70: body lift kit

The pan stiffeners mount under the VW chassis and utilized the same mounting holes as the body. The body lift kit mounts on the top of the chassis so essentially the combination of the body lift kit and the pan stiffener sandwich the chassis together creating a much more ridged frame structure. The complete assembly can be seen in Figure 71 below.

Figure 71: Pan Stiffeners and Body Lift Kit Attached to Chassis

Now that the chassis was stiff enough to support significant loads, the suspension rigidity was tested by simply applying weight to the corners of the vehicle and measuring the compression of the suspension. As one might expect on a 50-year-old vehicle the original suspension had seen

79

better days. The suspension was bottoming out far before applying the original load capacity it was rated for in 1969 when it was new. The vehicle also continued to oscillate after taking the load off, this indicated that the shocks had gone bad as well. Since the fuel cell and the balance of plant components accompanying the fuel cell would be adding a substantial amount of weight to the vehicle, upgrading the suspension seemed like a logical next step. Beetles originally came with a torsion bar suspension so the easiest option would be to simply replace the original torsion bars with stiffer one. However torsion bar suspension does not have a multitude of adjustments and since the final weight calculation was not yet determined making an educated guess would have been the only way to choose replacement torsion bars [29]. Instead of replacing the torsion bars the decision was made to use adjustable coil over shocks. This way the suspension can be adjusted to account for varying loads and since the shocks also needed to be replaced this solution would kill two birds with one stone. Depicted below in Figure 72 are the adjustable coil over shocks on the back axle.

Figure 72: Adjustable Coil Over Shocks

The same adjustable coil over shocks were also used on the front axle to account for the extra battery weight being placed over the front axle. Once the suspension was taken care of the next phase in the project was to determine how the steering system would be reconnected.

7.2 Steering Integration

The original steering column from the VW Beetle was integrated into the original Beetle body; essentially the steering column connected strait from the internal dash board of the Beetle body directly to the steering box that is mounted onto the chassis through the use of a rubber rag joint. For weight reasons, as stated earlier no part of the original body would be reused; this meant that from the steering box on, the steering system would need to be completely redesigned. The first step in the redesign of the steering was to mount the seats into the vehicle so that a measurement could be obtained for the relative location of the steering wheel. Once the seats were in place a light weight dashboard was constructed out of a one inch Chromalloy tube. A tub bender was utilized to create a hoop that could then be weld to the body lift kit that was installed earlier. To get the correct measurements for the tube the height of both the original dashboard and the measurements we took with an average size driver seating in the vehicle. The dimensions that were calculated were 28 inches high by 44 inched across. The Chromalloy dash after a little time with thee tubbing bender is depicted below in Figure 73.

Figure 73: Chromalloy Dash Board

Once the correct bends were in place, the dash was tack-welded to the body lift kit and a 5'9" person was used to sit in the vehicle to make sure the driver still had adequate leg room. The next objective was to locate the steering wheel in a location comfortable to the driver while also allowing for the greatest driver size variation. The seat is adjustable so it was determined that by mounting the wheel in a location about at the right height for a 5'4" person by adjusting the seat either forward or backwards we could comfortably fit a 6'3" individual all the way down to a 5'0" tall person. Once the desired location was found a custom steering column bracket and heim joint rod ends were implemented to hold the column in place. The steering column was also custom

Side connecting to steering column

Spline connection to steering box

made ... lly was ¾" by 0.230 wall thickness tube that was ... te l... ion of the battery box bracket the steering column c... ly to the steering box as VW had done with the original steering system. To account for some of the odd geometry's that were created with the custom dash and the interference caused by the location of the battery box two universal U-joints were implemented. The first U-joint was right at the steering box; this joint replaced the original rag joint with a U-joint so that the steering rod could be angled around the battery box while still having the ability to mechanically connect to the steering box without binding. This particular U-joint enabled a connection strait to the steering box shaft thru the original mechanical spline connection. The U joint that was used is depicted below in Figure 74:

Figure 74: U-Joint Connecting Steering Column to Steering Box

The second U-joint was implemented to account for the angle that was created due to the custom dash. This joint differed from the first because it did not require mechanical connections that had to be able to separate as the first joint did; instead this joint simply welded directly on to the steering column. An image of this joint can be seen in Figure 75 below:

Figure 75: Weld on U-joint

Once the Joints were taken care of the connection of the steering wheel to the steering column was the next area of interest. To create the connection of the steering wheel to the steering rod a quick release steering wheel Hub and weld on sleeve were implemented. The sleeve welds directly on to the column while the steering wheel bolts to the hub, then the hub can be quickly connected or disconnected from the sleeve through the use of a collar button on the hub. The weld on collar, hub, steering wheel adapter, and steering wheel are depicted in Figure 76.

Figure 76: Steering Hub, Weld On Collar, Steering Wheel Adapter, And Steering Wheel

The complete steering linkage assembly minus the steering wheel, before being welded together

is depicted below in Figure 77 and 78.

Figure 77: Exploded View of Steering Linkage

Figure 78: Steering Linkage Assembled

After the steering linkage was TIG welded together and the supporting brackets were welded to the dash the linkage was installed using heim joint rod ends to attach the linkage to the brackets. The heim joint rod ends used are depicted below in Figure 79:

Figure 79: Heim Joint Rod End

The complete steering assembly mounted to the vehicle can be seen below in Figure 80 and 81.
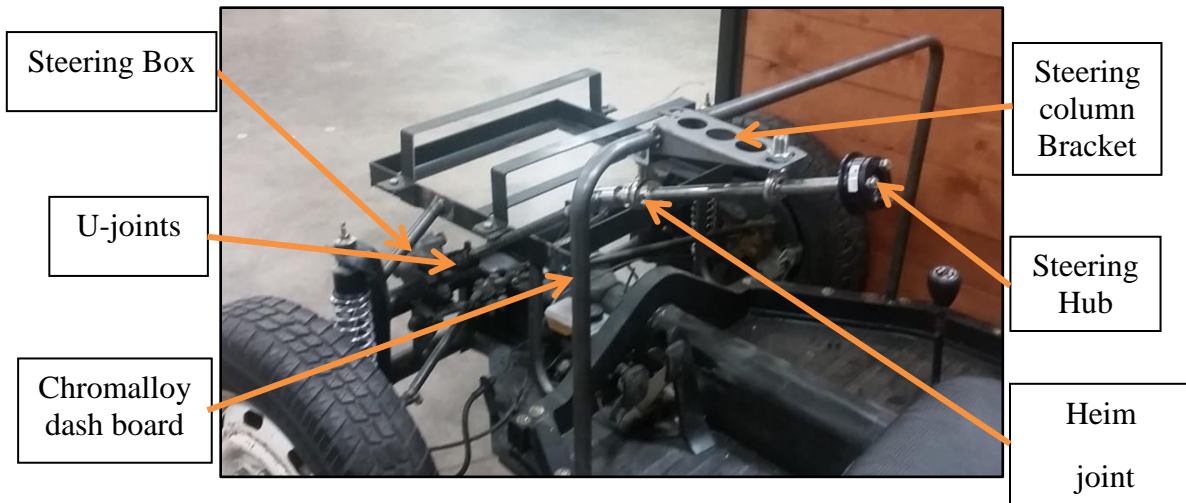
Figure 80: Steering Linkage Assembly On Vehicle

Figure 81: Completed Steering Assembly

Ch. 8: Motor Spec and Installation

8.1 Motor Specifications

The motor that was chosen for this project was the High Performance Electrical Vehicles (HEPV) AC-50. Based on the power calculation from the vehicle dynamics equations the AC-50 would be adequate for powering this size vehicle.

The motor was purchased from a company called High Performance Electric Vehicles (HPEV) and they provide engine speed verse current graphs for their motors because they test all of their motors on a dynamometer before shipping them out. Below is the graphical dynamometer results for the AC-50 powered with a 72-volt system:
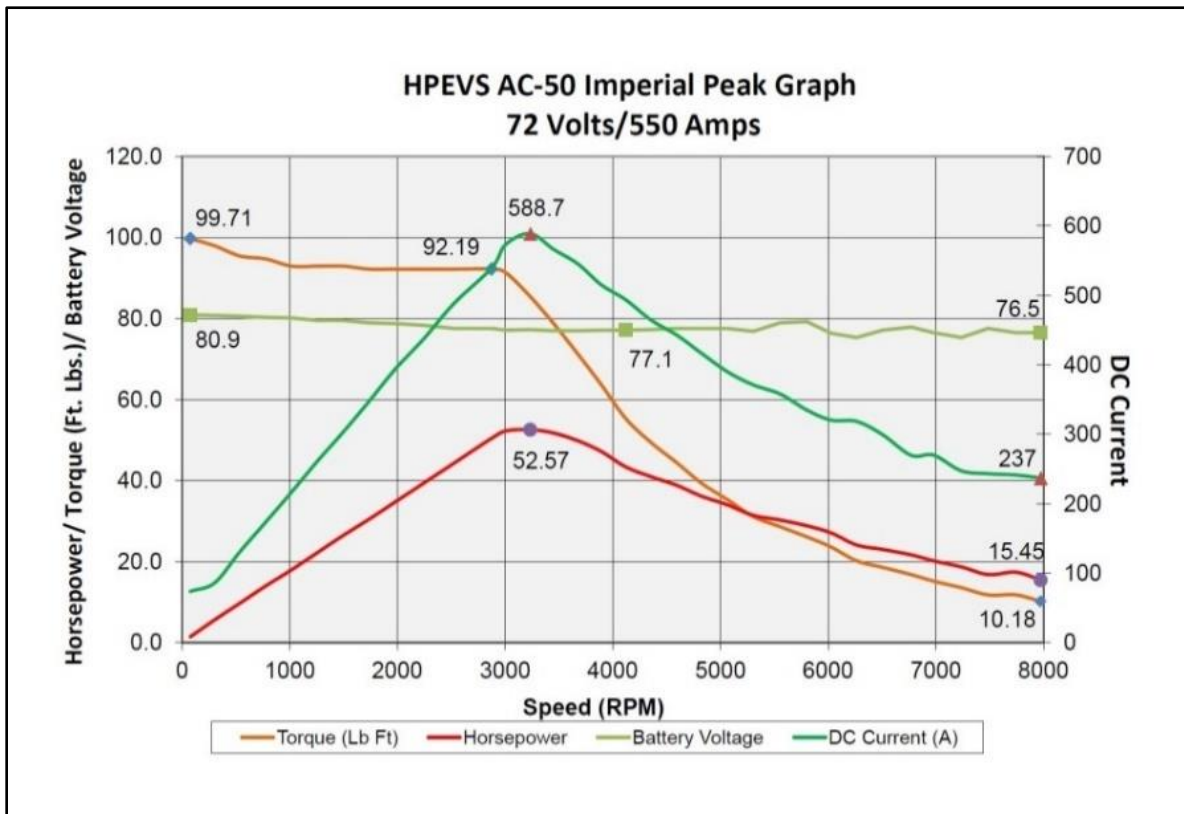
Figure 82: Dynamometer Results

8.2 Motor Installation

In a traditional internal combustion engine one needs a clutch to allow for the engine speed to be higher than the transmission speed in order to prevent the engine from stalling due to the low torque output of internal combustion engines at low speeds; this is not the case for an electric motor, since electric motors have essentially an instantaneous torque at all speeds. So it is conceivable that one could couple the output shaft of the transmission directly to the output shaft

of the electric motor. The only drawback to this set up is the lack of a safety check should something go wrong with the electric motor.

The desired design for this project was to connect the motor and transmission such that they could be decoupled in the case of a system failure. Achieving this design required the implementation of some sort of clutch set up so that the motor could be disengaged from the transmission in the event of a stuck throttle. The goal then became to develop a coupling system that would enable the coupling of the electric motor to the transmission in the same way the internal combustion engine was attached.

It just so happened that a company in Sacramento called EV4U now specialized in engineering couplers specifically for VW Beetle style transmissions. Their couplers utilize lightweight flywheels and performance clutches that enable one to shift gears using an electric motor and use the clutch to disconnect the electric motor should there ever be a stuck throttle situation.

The installation of the motor adapter that was implemented is illustrated in Figure 83, 84, 85, 86, 87, and 88.

Figure 83: AC-50 Motor

Figure 84: Flywheel to Motor Shaft Coupler

Figure 85: Motor to Transmission Coupler

Figure 86: Fly Wheel Installation

Figure 87: Clutch Instillation

Figure 88: Pressure Plate Instillation

Once the adapter and clutch were mounted on the motor, the motor was installed on to the transmission of the VW chassis the same way one would an internal combustion engine making use of the four factory mounting locations on the transmission. The transmission has a large hole in the back of it designed for the starter to fit into when utilizing a traditional engine however since

an electric motor is being used there is no need for a starter so to save weight we simply removed

it and fabricated an aluminum plate to cover the hole where the starter would have been.

Figure 89: Electric Motor Installed On Transmission

Figure 90: Starter Whole Cover Plate

8.2.1 Motor Controller Installation

Once the motor was installed the next logical phase in the project was to install the motor

controller. The motor controller used for this project was the Curtis 1238-6501. The Curtis 1238

can handle up to 96 volts and 650 amps so it is plenty capable for working with our system. Depicted below in Figure 91 is an image of the Curtis controller that was used:

Figure 91: Curtis 1238-6501 Motor Controllers

The motor controller takes a 0-5 volt reading from the throttle and then transfers the power from the battery pack directly to the motor. The operating nominal voltage for this system is 72 volts at 550 amps so to prevent losses it would be ideal to reduce the length of the wires; this was achieved by mounting the control as close to the motor as possible. However, what makes mounting the Curtis controller complex is the cooling supply pluming associated with the chill plate. The Curtis controller being used needs to be water cooled to prevent it from overheating, this meant the bracket to hold the controller needed to allow the controller to be mounted close to the motor but also be positioned so that cooling lines could be connected to bottom of the controller. The image below in Figure 92 depicts the cooling plate:

Figure 92: Aluminum Controller Chill Plate

There is a company called EV West that produced controller brackets that mount the controller directly over the engine, drastically reducing the length of the wires that run from the controller to the motor. The EV West bracket was utilized but modified to allow for the attachment the cooling lines to the bottom of the chill plate. The chill plate bolted directly under the controller and then has two water fittings that come out of the bottom of it, so holes were cut into the EV west bracket to allow for the water fittings to fit through. The bracket was then bolted to the back of the motor so that the chill plate basically gets sandwiched in-between the mounting bracket and the motor controller as can be seen in Figure 93 below.
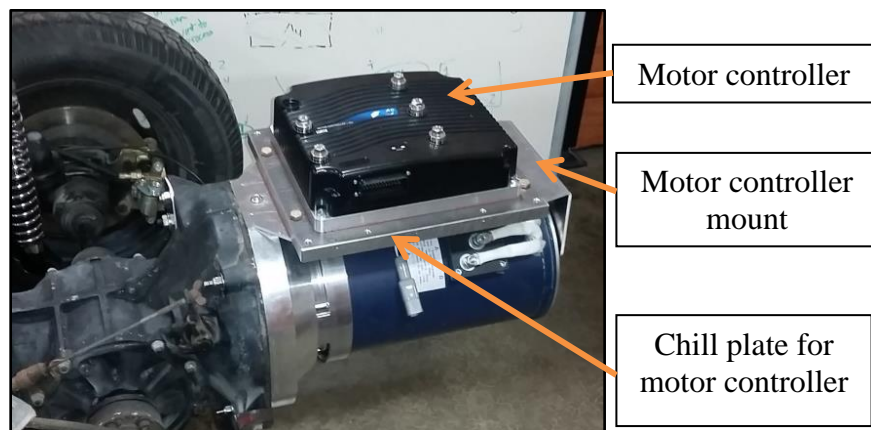
Figure 93: Motor Controller Mount Assembly

It is not visible from the above figure but the water fittings for the chill plate come out with 90 degree fittings under the controller mount right over the motor. Once the controller was securely in place, the controller was wired to the motor. Since the voltage and current traveling from the controller to the motor were pretty high, two gage double shielded cable was used, the cable used was rated for 600 volts at 1,000 amps and up to 220 degrees Fahrenheit. This allowed for the incorporation of a factor of safety with the main wiring to the motor which is why 2 gage cable was implemented. Below in Figure 94 is a picture of the three main wires from the motor controller to the motor:

Two gage double insulated cables
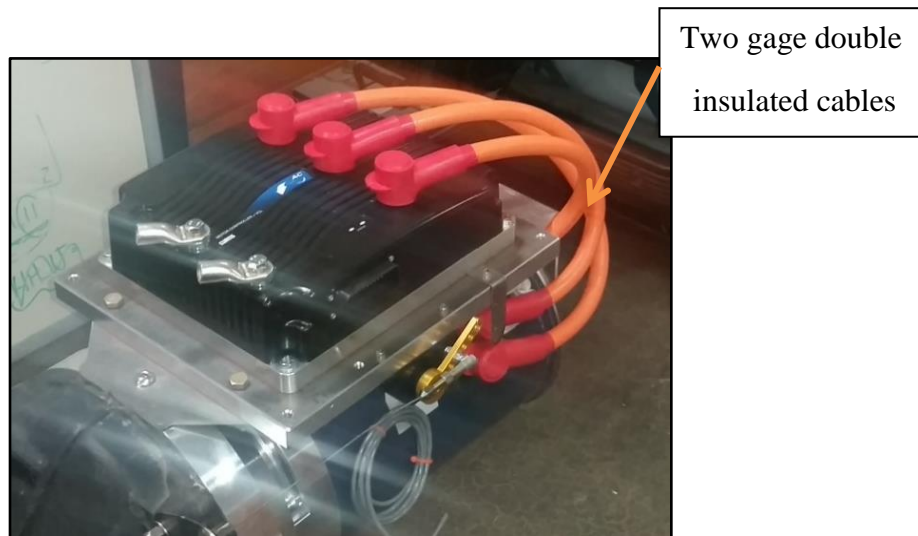
Figure 94: Wiring from Controller to Motor

8.2.2 Throttle Instillation

The throttle used for this project was EV West's billet aluminum throttle potentiometer. This throttle supplies a 0-5 volt reading to the controller and comes with its own built in return spring.

The throttle is depicted below in Figure 95:

Figure 95: Billet Aluminum Throttle

Once the right throttle was specked out for the Curtis controller the next thing to do was to consider where to mount the throttle. Ordinarily on an electric vehicle the accelerator pedal is basically just a lever arm hooked up to a potentiometer mounted to the floor. However, the original 1969 VW Beetle was carbureted and therefore had a cable that ran through a guide tube from the front of the car through the center tunnel all the way to the back of the car into the engine compartment and onto the carburetor. The elegance and simplicity of the original design was so neat the decision was made to utilize the original concept by simply mounting the throttle back by the controller and using the original cable that was in the car to connect the throttle pedal in the car to the throttle potentiometer. The throttle potentiometer was mounted to the side of the motor controller bracket and connected the throttle cable using a socket ball linkage joint. This can be seen below:

Throttle potentiomete

Throttle cable to connecting to accelerator pedal

Socket ball link joint
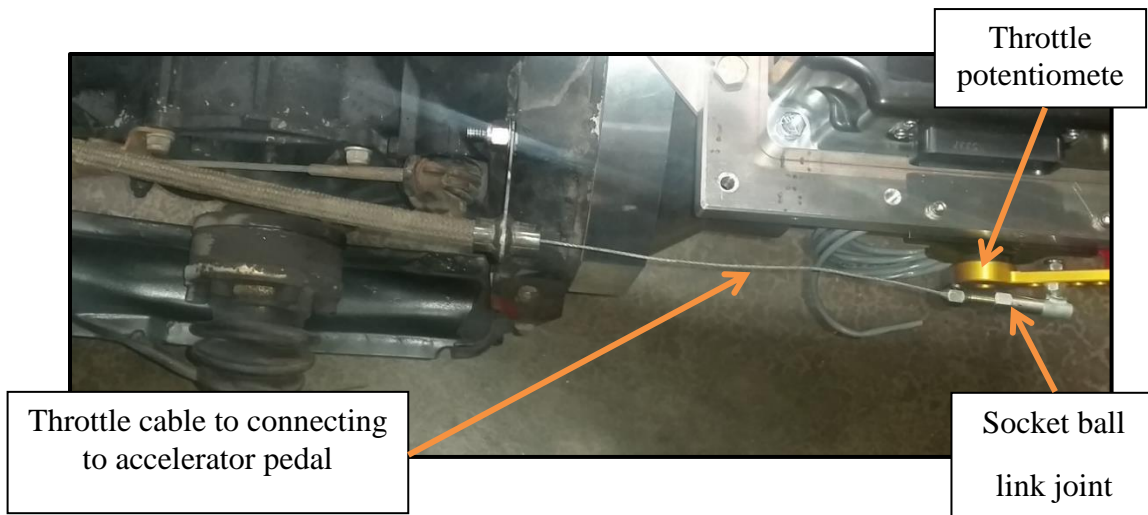
Figure 96: Throttle Mount

Aside from the elegant and simplistic design the other benefit to mounting the throttle right next to the controller is that the wires from the throttle connect directly to the controller having them close to one another makes routing the wires super easy. As mentioned before the throttle has its own internal return spring however since we are using a cable that runs the length of the car there was a substantial amount of friction and so the internal spring was not strong enough to accommodate for this excess friction. To account for this we mounted a bracket behind the throttle where we attached two return springs to in order to counter act the friction that was in the line. This can be viewed in Figure 97:

Throttle return spring bracket

Figure 97: Throttle Spring Return Bracket

Ch. 9: Major Component Bracket Designs And Installation

9.1 Battery Bracket Fabrication

After the motor, motor controller, and throttle were all mounted and wired, the next step in the project was to test the electrical components without the complication associated with the integration of the of the fuel cell. Basically the idea was to operate the car as a pure electric vehicle, to do this the battery pack would need t be installed, so naturally the fabrication of the battery pack mount was the next step in the build process.

The individual batteries are housed in a 20" x 25" x 8" aluminum box, the complete battery pack has a weight of 85 pounds so the mount for the pack had to account for this load. To build the bottom support for the box we used 3/16th by 2-inch angle iron to fabricate a rectangular support that the box could sit on, a 3/16th by 1.5-inch brace was then welded across the center of the rectangle for mid support. To keep the battery box securely in the bottom support two 1/8th by 1.5-inch steel straps we used to go over the top of the battery box and bolt to the bottom support structure using grade-8 3/8th inch bolts. The battery support can be seen in Figure 98 and 99.

Figure 98: bottom battery support bracket
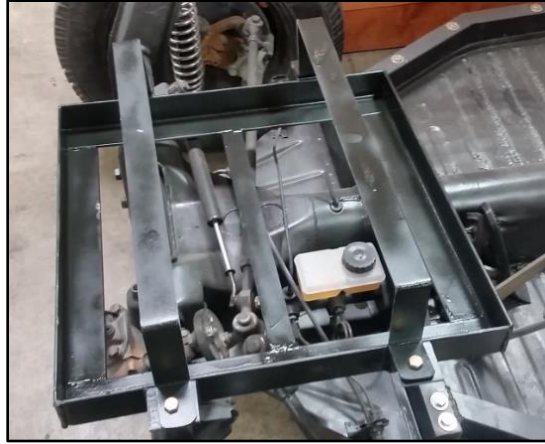
Figure 99: Battery box bracket with mounting strap

At this point the bracket for the battery box was completed however the bracket was not attached to the actual chassis. For better front to back weight distribution and to lower the cars center of gravity it would be ideal to mount the battery pack under the front axle of the car. However, mounting the battery pack under the pan of the chassis would have reduced our ground clearance to only four inches. Not wanting to risk damaging the battery pack by having it so close to the ground the decision was made to mount the battery pack above the front axle. The other factor that came into play when considering the location of the battery pack was the fact that this was going to be a research and development vehicle and as such mounting the batteries in a hard to access location would not make since for the purpose of the vehicle. Instead we decided to mount the battery bracket directly above the front axle, this orientation still helped with creating a 50/50 front to back weight ratio and allowed for easy access once the body was put on since the pack would essentially be accessed through the trunk however it did raise the cars center of gravity slightly. For the attachment of the battery box bracket to the chassis one inch Chromalloy tubing with 0.120 wall thinness was used. The bracket was welded to the strut towers of the chassis using the Chromalloy tubing and also to the body lift kit again utilizing the Chromalloy tubing. See Figure 100, 101, and 102for further detail:

98

Chromalloy tubing support bracket

Body lift kit (chassis frame)
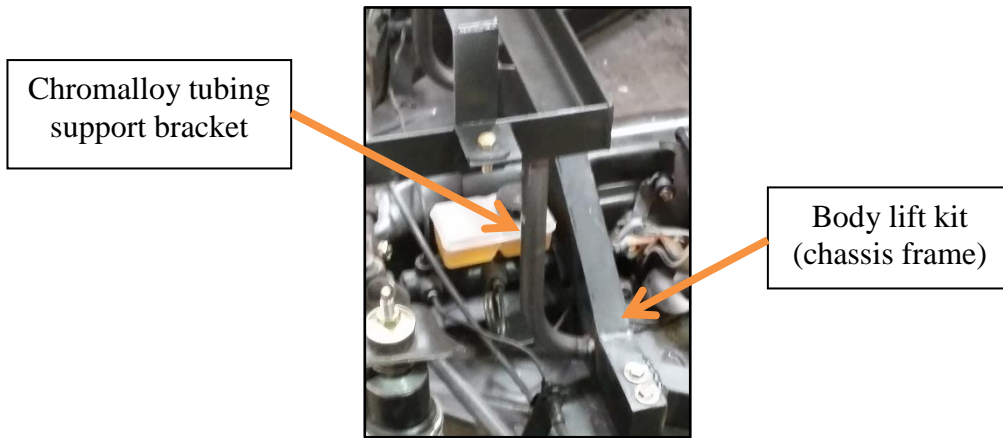
Figure 100: Battery Bracket Rear Support

Battery box bracket

Chromalloy tubing support bracket

Strut tower
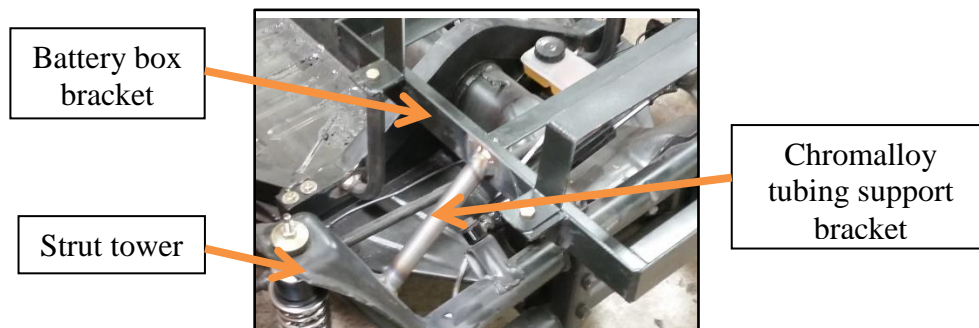
Figure 101: Battery Bracket Front Support

Figure 102: Battery Box Bracket Mounted to The Chassis

9.2 Component Installation

After the brackets for all the major components were attached the actual components themselves were integrated on to the vehicle. The following figure shows the assembled vehicle.

Figure 103: Passengers Side View of Assembled Vehicle

In Figure 103 all of the major components and their placement on the vehicle can be seen. The motor and motor controller are at the very back of the vehicle while the hydrogen tank and the fuel cell sit right over the back axle. The silver power electronics box is right behind the seats and the black battery box is under the conversion electronics board just over the front axle. From the driver's side view in Figure 104 the battery box, power electronics board, and the heat exchanger can be easily seen.

Figure 104: Drivers Side View of Assembled Vehicle

A close up view of the conversation electronics board can be seen in Figure 105 3/8-inch acrylic

is used to insulate the conversion electronics board and its components from the battery box.

Figure 105: Conversion Electronics Board

Ch. 10: Conclusion & Future Work

10.1 Conclusion

The goal of this thesis was twofold, the first portion of this thesis was to develop a simulation of a

series hybrid fuel cell vehicle. this was accomplished by starting with the dynamic equations of a

vehicle then making simplifying assumptions in order to then calculate the force needed to power said vehicle. For this calculation the stock 1969 Volkswagen Beetle vehicle parameter were used as a base line for the model. The standard US06 drive cycle was used to run the simulation. Once the power requirements were calculated based on the drive cycle velocity demand then the drive train component efficiencies were integrated into the model to provide an accurate calculation for the amount of power the fuel cell would need to be capable of providing. The motor specs were then factored in to the model and the actual torque the motor was able to produced was compared to the requested torque from the drive cycle. Finally, the velocity of the vehicle was then back calculated based on the achievable torque from the motor.

The second portion of this thesis was to build an actual prototype fuel cell hybrid vehicle. the simulation was used to specify some of the sizing for the components on the prototype. The reason that the 1969 Volkswagen Beetle vehicle parameters were used in the simulation was because the actual prototype vehicle was going to use a Volkswagen Beetle chassis as its base. As such the first order of business was to strip the Beetle chassis free from the Beetle body and prep the chassis for its new life as a fuel cell hybrid. This endeavor required upgrading the entire braking system, media blasting and painting the chassis, creating a rigid support structure for mounting the major components to, and developing custom brackets to hold all of the major components and all of the balance of plant components. Once everything was mounted in place the next phase in this portion of the project was to create a custom wiring harness for the vehicle once everything was mounted and wired the vehicle was tested in lab on jack stands.

Future work includes comparison studies comparing the simulation results to the actual vehicle performance in urban and highway driving. This will be discussed in the future work section.

10.2 : Future Work

This thesis focused on the mechanics behind the design and development of a prototype fuel cell hybrid vehicle however having a functioning vehicle is only part of building a car. The next phase of the project will be to develop a light weight aerodynamic body that can encompass the hybrid chasses that was developed in this thesis. To achieve this task, the future intention is to work with a company called South End Kustoms out of Hemet California. Owner and operator of South End Kustoms, Keith Dean is the son of Dick Dean who designed the Shalako in 1967, which was a custom fiberglass body made to fit a Volkswagen chassis. Depicted below is the Shalako Dick designed.
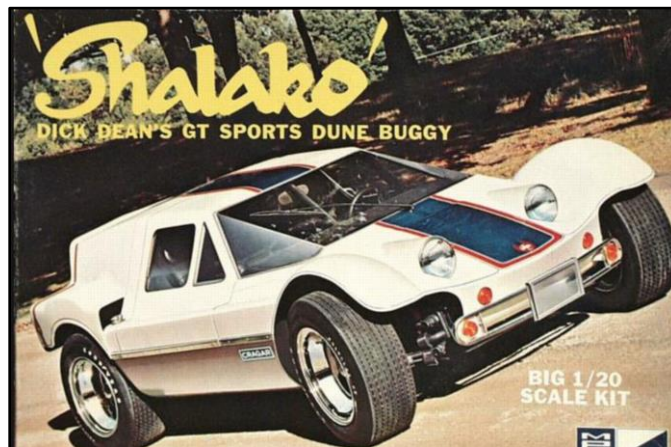
Figure 106: 1967 Shalako Body

Keith believes the chassis developed in this thesis can be merged with the Shalako body his father designed to produce a stylish one off eye catching concept car that will peak consumer appeal in alternative energy vehicles.

The simulation that was done in this thesis does not consider the physics or electrochemical dynamics associated with the battery or the fuel cell. The next phase in the simulation portion of this thesis will be to account for the current dynamics associated with the battery and fuel cell. For

the battery this will require the consideration of the battery temperature since the battery current is a function of temperature. In order to simulate the current dynamics of the fuel cell the flow rates of both the fuel and the oxidant will need to be taken into consideration as well as the temperature of the fuel cell.

Once a more comprehinsive model has been established, experimental validation of said model will be the next step. Eventual the plan will be to take the actual physical vehicle to a dynamometer testing facility and preform the US06 drive cycle on the vehicle so that the simulation results can be verified with actual experimental test data.

The actual experimental test will be important so that an accurate assessment of the hydrogen consumption rate can be verified. A higher pressure composite hydrogen tank will be needed in order to achieve driving ranges comparable to today's ICE vehicles. The next phase in the project will be to integrate a high pressure hydrogen tank on the vehicle or multiple hydrogen tanks onto the vehicle in an effort to achieve comparable driving ranges.

10.2.1 Works Cited

[1]   J. B. Heywood, *Internal Combustion Engine Fundamentals*. McGraw-Hill, 1988.

[2]   T. J. Bvumbe, P. Bujlo, I. Tolj, K. Mouton, G. Swart, S. Pasupathi, and B. G. Pollet, "Review on management, mechanisms and modelling of thermal processes in PEMFC," *Hydrog. Fuel Cells*, vol. 1, no. 1, pp. 1–20, 2016.

[3]   L. Giorgi, "Fuel Cells: Technologies and Applications," *Open Fuel Cells J.*, vol. 6, no. 1, pp. 0–0, Jul. 2013.

[4]   R. O'Hayre, S.-W. Cha, W. Colella, and F. B. Prinz, *Fuel Cell Fundamentals*, 3 edition. Hoboken, New Jersey: Wiley, 2016.

[5]   D. S. Cameron, G. A. Hards, B. Harrison, and R. J. Potter, "Direct Methanol Fuel Cells," *Platin. Met. Rev.*, vol. 31, no. 4, pp. 173–181, Oct. 1987.

[6]   V. S. Bagotsky, "Phosphoric Acid Fuel Cells," in *Fuel Cells*, John Wiley & Sons, Inc., 2012, pp. 99–106.

[7]   F. Barbir, *PEM Fuel Cells: Theory and Practice*. Academic Press, 2013.

[8]   S. Srinivasan, *Fuel Cells: From Fundamentals to Applications*. Springer Science & Business Media, 2006.

[9]   "Modern Electric, Hybrid Electric & Fuel Cell Vehicles - Mehrdad Ehsani.pdf." .

[10]   U. EPA, "Regulations and Standards: Light-Duty | Transportation and Climate." [Online]. Available: https://www3.epa.gov/otaq/climate/regs-light-duty.htm. [Accessed: 23-Aug-2016].

[11]   A. Emadi, K. Rajashekara, S. S. Williamson, and S. M. Lukic, "Topological overview of hybrid electric and fuel cell vehicular power system architectures and configurations," *IEEE Trans. Veh. Technol.*, vol. 54, no. 3, pp. 763–770, May 2005.

[12]   G. Maggetto and J. V. Mierlo, "Electric and electric hybrid vehicle technology: a survey," in *Electric, Hybrid and Fuel Cell Vehicles (Ref. No. 2000/050), IEE Seminar*, 2000, p. 1/1-111.

[13]   J. K. Ahn, K. H. Jung, D. H. Kim, H. B. Jin, H. S. Kim, and S. H. Hwang, "Analysis of a regenerative braking system for Hybrid Electric Vehicles using an Electro-Mechanical Brake," *Int. J. Automot. Technol.*, vol. 10, no. 2, pp. 229–234, Mar. 2009.

[14]   Y. Gao, L. Chen, and M. Ehsani, "Investigation of the Effectiveness of Regenerative Braking for EV and HEV," 1999.

[15]   J. Walters, H. Husted, and K. Rajashekara, "Comparative Study of Hybrid Powertrain Strategies," 2001.

[16]   "Drive Cycle Analysis of the Performance of Hybrid Electric Vehicles." [Online]. Available: http://www.academia.edu/26630391/Drive_Cycle_Analysis_of_the_Performance_of_Hybrid_Electric_Vehicles. [Accessed: 23-Aug-2016].

[17]   W. Hogarth and J. Benziger, "Dynamics of Autohumidifed PEM Fuel Cell Operation," *Journal of The Electrochemical Society*, vol. 153, no. 11, 2006.

[18]   S. Grammatico, A. Balluchi, and E. Cosoli, "A series-parallel hybrid electric powertrain for industrial vehicles," 2010, pp. 1–6.

[19]   W. Xiong, Y. Zhang, and C. Yin, "Optimal energy management for a series–parallel hybrid electric bus," *Energy Convers. Manag.*, vol. 50, no. 7, pp. 1730–1738, Jul. 2009.

[20]   J. Reimpell, H. Stoll, and J. Betzler, *The Automotive Chassis: Engineering Principles*. Butterworth-Heinemann, 2001.

[21]   L. Klebanoff, *Hydrogen Storage Technology: Materials and Applications*. Taylor & Francis, 2016.

[22] F. Giri, *AC Electric Motors Control: Advanced Design Techniques and Applications*. John Wiley & Sons, 2013.

[23] "APPENDICES–ADVISOR Documentation." [Online]. Available: http://adv-vehicle-sim.sourceforge.net/advisor_appendices.html#Appendix%20E. [Accessed: 09-Jun-2016].

[24] *MATLAB*. Natick, Massachusetts, United States: MATLAB.

[25] M. Eberhard, "The 21st Century Electric Car Tesla Motors." 24-Sep-2007.

[26] S. Wilkins and M. U. Lampérth, "An Object-Oriented Modeling Tool of Hybrid Powertrains for Vehicle Performance Simulation," in *ResearchGate*, 2002.

[27] O. Tremblay, L. A. Dessaint, and A. I. Dekkiche, "A Generic Battery Model for the Dynamic Simulation of Hybrid Electric Vehicles," in *2007 IEEE Vehicle Power and Propulsion Conference*, 2007, pp. 284–289.

[28] "User's Manual for Magnetic Drive Centrifugal Pump CA Series fMicropump." Micropump, Inc.

[29] "VOLKSWAGEN 1969 MODEL OWNER'S MANUAL Pdf Download." [Online]. Available: http://www.manualslib.com/manual/187844/Volkswagen-1969-Model.html. [Accessed: 23-Aug-2016].

[30] "History of the Electric Automobile." [Online]. Available: http://books.sae.org/r-187/. [Accessed: 22-Aug-2016].

10.2.2 Appendix: MATLAB Scrip File

```matlab
%% FC system model

clear all;
clc;
close all;

gravity=9.81;
mass=870;
time=[0:1:600]';
run ('velocity_file.m');
t1=[0; time(1:end-1)];
% calculates change in time
dt=time-t1;
%calculates the change in velocity
v1=[0;velocity(1:end-1)];
dv=velocity-v1;

acceleration=[dv./dt];
acceleration(1)=0;

weight=mass*9.81;
tire_pressure=3.516;

%Calculate the coeffecent of rolling resistance
crr=0.005+(1/tire_pressure)*(0.01+0.0095*((velocity./100).^2));

%calculate rolling resistance force
Fr=crr*(mass*9.81);

%calculate the wind resistance force (fw=1/2(Cd Av^2))
Cd=0.207;
Af=1.34;
rou=1.2041;

Fw=0.5*(Cd*Af*rou*(velocity.^2));

%calculate the tractive frce
Ft= (mass.*acceleration)+Fw+Fr;

%calculate the power after the transmission which equals the power at the
%wheels
power=Ft.*velocity;

%calculate the power before the transmission
```

```matlab
efficency_transmission = 0.98;
Power_transmission = power./efficency_transmission;

%calculates the power before the motor
efficency_motor = 0.89;
power_motor=Power_transmission./efficency_motor;

%calculates power before the battery pack
efficency_batttery = .95;
power_battery=power_motor./efficency_batttery;

%calculate the power before the Fuel Cell
efficency_FC= 0.53;
power_FC=power_battery./efficency_FC;

%calculating energy by integrating the power before the fuel cell, integrat
%in a loop to get the enrgy at each time step
energy=zeros(size(time));
for t2=2:time(end)
    energy(t2)=energy(t2-1)+trapz(time(t2-1:t2),power_FC(t2-1:t2));
end

%calculate the hydrogen consumption in grams, knowing that that the energy density of
%hydrogen is 142MJ/kg which is equal to 142,000J/g
H2_consuption = energy./142000;




figure(1)
plot(time,acceleration)
xlabel('Time [sec]')
ylabel('Acceleration [m/s^2]')
title('Acceleration')

figure(2)
plot(time,velocity)
xlabel('Time [sec]')
ylabel('Velocity [m/s]')
title('Velocity')

figure(3)
plot(time, power/1000)
xlabel('Time [sec]')
ylabel('Power [kw]')
title('Power')
```

```matlab
figure(4)
plot(time, energy/1000/3600)
xlabel('Time [sec]')
ylabel('Energy [kwh]')
title('Energy')

figure(5)
plot(time, H2_consuption/1000)
xlabel('Time [sec]')
ylabel('Hydrogen [kg]')
title('Hydrogen Consuption')
```

10.2.2.1 Simulink Initialization function

```matlab
% initialization file
tire_pres=3.516;
run ('velocity_file.m');
run ('Range_file.m');
run('mc_spd.m') %[rad/sec]
run('mc_trq_motor.m') %[Nm]
t=[0:1:600]';
V=[t, velocity];
regen_efficency=0;
epsilon=10^-6;
tend=t(end);
mass=870;
g=9.81;
Cd=0.207;
Af=1.34;
rou=1.2041;
efficency_transmission=0.98;
efficency_motor_pos = 0.89;
efficency_motor_neg=0.80;
efficency_batttery_pos =0.95;
efficency_batttery_neg=0.90;
efficency_FC= 0.53;
energy_density_H2=142000;
Vmax=80;
wheeel_radiaus=0.1778; %[meter]
Gear_ratio= 0.89; % 4th gear 1.26; % 3rd gear
final_drive= 4.125; %final drive gear ratio
capacity_batt=8; %KWh
FC_charge=2; %KW
```

10.2.2.2 : MATLAB. files called out in the initialization function

Velocity file:

% the velocity is in [m/s]

velocity=[0
0
0
0
0
0
0.089405556
0.312919444
0.491730556
0.759947222
2.682166667
6.213686111
9.164069444
11.48861389
11.17569444
12.69558889
14.43899722
15.46716111
16.31651389
17.16586667
17.83640833
18.86457222
19.57981667
19.75862778
19.40100556
19.04338333
18.01521944
17.52348889
17.16586667
17.16586667
17.52348889
17.34467778
17.34467778
16.31651389
14.43899722
12.33796667
9.968719444
7.733580556
5.140819444

2.592761111
0.536433333
0
0
0
0
0
0
0
0
0.357622222
4.112655556
6.660713889
8.135905556
9.924016667
12.15915556
14.03667222
15.10953889
16.62943333
18.23873333
19.66922222
20.69738611
21.27852222
22.127875
22.88782222
23.69247222
24.31831111
24.85474444
25.21236667
25.07825833
25.12296111
24.94415
24.63123056
24.31831111
24.22890556
24.31831111
24.22890556
23.91598611
23.37955278
23.24544444
23.20074167
23.15603889
23.20074167
23.24544444
23.46895833
23.87128333

24.541825
25.39117778
26.28523333
27.08988333
27.84983056
28.69918333
29.59323889
30.30848333
31.02372778
31.47075556
31.56016111
31.60486389
31.42605278
30.48729444
29.72734722
29.01210278
28.47566944
27.93923611
27.26869444
26.50874722
25.79350278
25.03355556
24.36301389
23.60306667
22.88782222
22.127875
21.45733333
20.69738611
19.66922222
18.37284167
17.34467778
16.85294722
16.36121667
15.78008056
13.41083333
10.90747778
8.85115
6.928930556
4.8279
2.816275
1.430488889
0.938758333
0.536433333
0
0
0

0
0
0
0
0
1.206975
4.112655556
7.197147222
10.14753056
13.05321111
15.28835
17.34467778
19.22219444
20.25035833
20.9209
21.45733333
22.127875
22.48549722
23.02193056
23.33485
23.51366111
23.69247222
24.05009444
24.05009444
24.05009444
24.40771667
25.16766389
25.43588056
25.97231389
26.10642222
26.64285556
26.77696389
26.91107222
27.04518056
26.68755833
26.06171944
25.97231389
25.83820556
25.61469167
25.70409722
25.30177222
25.48058333
25.30177222
25.25706944
25.12296111
25.21236667

25.30177222
25.21236667
25.07825833
25.03355556
24.98885278
24.49712222
24.22890556
24.40771667
23.33485
24.45241944
24.89944722
25.48058333
25.92761111
25.97231389
26.55345
26.77696389
27.26869444
27.44750556
27.67101944
27.93923611
27.93923611
28.02864167
27.80512778
27.93923611
28.20745278
28.02864167
28.07334444
28.16275
28.65448056
28.565075
28.65448056
28.74388611
28.83329167
29.01210278
29.19091389
29.50383333
29.50383333
29.68264444
28.65448056
28.43096667
28.565075
28.65448056
28.47566944
28.74388611
28.69918333
28.565075

28.69918333
28.34156111
28.60977778
28.565075
28.60977778
28.52037222
28.60977778
28.29685833
28.34156111
28.565075
28.60977778
28.74388611
28.9674
29.10150833
28.60977778
28.69918333
28.20745278
28.47566944
28.20745278
28.47566944
28.38626389
28.16275
28.20745278
28.16275
28.29685833
28.34156111
28.29685833
27.93923611
27.93923611
28.11804722
28.07334444
27.80512778
27.89453333
27.84983056
27.84983056
27.89453333
27.760425
27.93923611
28.07334444
27.84983056
27.84983056
27.89453333
27.67101944
28.07334444
28.07334444
27.84983056

28.07334444
27.89453333
27.760425
27.67101944
27.62631667
27.760425
27.760425
27.760425
27.71572222
27.89453333
27.80512778
27.80512778
27.89453333
28.02864167
27.98393889
28.47566944
28.74388611
28.9674
29.10150833
29.45913056
29.54853611
29.95086111
30.04026667
30.174375
30.53199722
30.53199722
30.75551111
30.88961944
31.02372778
32.05189167
32.23070278
33.41172168
32.45421667
32.27540556
32.27540556
32.186
32.40951389
32.54362222
32.49891944
32.09659444
31.91778333
31.783675
31.783675
31.69426944
31.73897222
31.73897222

31.82837778
32.23070278
32.45421667
32.90124444
33.43767778
33.84000278
34.55524722
35.04697778
35.44930278
34.95757222
33.97411111
33.7953
34.15292222
34.68935556
34.86816667
35.35989722
35.53870833
35.71751944
35.71751944
35.89633056
35.89633056
35.53870833
35.53870833
35.35989722
35.18108611
34.68935556
34.197625
33.21416389
32.45421667
31.64956667
30.21907778
29.68264444
29.81675278
29.54853611
29.45913056
29.59323889
29.54853611
29.99556389
30.12967222
30.53199722
30.53199722
30.71080833
30.48729444
30.44259167
30.39788889
29.99556389

29.68264444
29.54853611
29.369725
29.50383333
29.68264444
29.50383333
29.63794167
29.95086111
30.174375
30.35318611
30.44259167
30.62140278
30.80021389
30.66610556
31.02372778
31.02372778
31.02372778
31.29194444
31.47075556
31.56016111
31.69426944
31.42605278
31.56016111
31.42605278
31.15783611
31.24724167
31.33664722
31.11313333
30.979025
31.24724167
31.15783611
31.06843056
31.24724167
31.38135
31.38135
31.38135
31.73897222
31.64956667
31.69426944
31.60486389
31.69426944
31.82837778
31.87308056
31.64956667
31.82837778
32.05189167

32.14129722
32.45421667
32.32010833
32.32010833
32.23070278
32.186
32.14129722
32.45421667
32.54362222
32.72243333
32.23070278
31.96248611
31.69426944
31.47075556
31.51545833
31.69426944
31.38135
31.73897222
31.38135
31.42605278
30.88961944
30.75551111
30.48729444
30.53199722
30.48729444
30.26378056
30.08496944
30.174375
30.21907778
30.21907778
30.04026667
29.95086111
29.63794167
29.77205
29.59323889
29.68264444
29.45913056
29.54853611
29.28031944
27.80512778
27.80512778
27.44750556
27.31339722
27.44750556
27.31339722
27.44750556

27.44750556
27.62631667
27.62631667
27.62631667
27.62631667
27.80512778
27.62631667
27.80512778
27.98393889
27.80512778
27.98393889
27.80512778
27.98393889
27.98393889
28.16275
27.98393889
27.80512778
27.31339722
26.59815278
26.28523333
25.39117778
24.89944722
24.18420278
23.02193056
21.99376667
21.81495556
21.27852222
20.07154722
18.55165278
16.62943333
15.46716111
14.75191667
13.05321111
9.968719444
7.912391667
7.733580556
6.258388889
4.470277778
2.682166667
0.894055556
0
0
0
0
0
0

0
0
0.089405556
1.966922222
4.514980556
6.973633333
9.298177778
11.22039722
12.38266944
12.60618333
11.98034444
11.08628889
10.01342222
7.644175
5.051413889
3.084491667
3.352708333
4.962008333
6.884227778
8.895852778
10.81807222
12.11445278
12.74029167
12.60618333
11.44391111
9.700502778
7.733580556
5.409036111
3.352708333
2.592761111
1.072866667
0.536433333
0.849352778
2.995086111
5.274927778
7.510066667
9.700502778
11.57801944
12.38266944
12.51677778
12.11445278
10.90747778
9.029961111
6.794822222
4.157358333
2.235138889

1.296380556
1.072866667
3.755033333
6.034875
7.957094444
9.924016667
11.71212778
13.41083333
13.32142778
11.62272222
9.521691667
7.24185
5.096116667
2.950383333
1.162272222
0
0
0
0
0
0
0
0
0.134108333
2.860977778
5.677252778
8.582933333
10.63926111
12.60618333
15.60126944
16.76354167
18.01521944
20.11625
22.30668611
23.06663333
22.88782222
22.61960556
22.30668611
21.36792778
19.93743889
18.41754444
16.89765
14.93072778
12.51677778
10.59455833
8.404122222

```
5.766658333
2.771572222
0.983461111
0
0
0
0
0
0
0];

velocity6=repmat(velocity,6,1);
velocity12=repmat(velocity,12,1);
velocity48=repmat(velocity,48,1);
```

Motor speed look-up table:

```
%Motor speed [rad/sec]

mc_spd_motor=[0
52.33333333
104.6666667
157
209.3333333
261.6666667
314
366.3333333
418.6666667
471
523.3333333
575.6666667
628
680.3333333
732.6666667
785
837.3333333];
```

Motor torque look-up table:

```
% motor torque [Nm] as a function of motor speed

mc_trq =[135.1886078
131.5143412
130.1585232
129.4806142
129.2094506
```

127.4468873
124.9928568
105.7538001
81.349077
61.01180775
51.5210821
40.6745385
31.18381285
25.76054105
17.62563335
14.91399745
13.80222673];

10.2.2.3 Simulink Post calculation function

```
%Post_calculation _file
figure(2);
plot(time,acceleration);
xlabel ('time (sec)');
ylabel ('acceleration (m/s^2)');
title('Acceleration');

figure(3)
plot(time, power/1000)
xlabel('time [sec]')
ylabel('power [kw]')
title('Power')

figure(4)
plot(time, energy/1000/3600)
xlabel('time [sec]')
ylabel('energy [kwh]')
title('Energy')

figure(5)
plot(time, H2_consuption/1000)
xlabel('time [sec]')
ylabel('Hydrogen [kg]')
title('Hydrogen Consuption')

figure(6)
plot(time,motor_current)
xlabel('time [sec]')
ylabel('current [amps]')
title('Motor Current')
```

```matlab
figure(7)
plot(time,Battery_current)
xlabel('time [sec]')
ylabel('current [amps]')
title('Battery Current')

figure(8)
plot(time,Voltage)
xlabel('time [sec]')
ylabel('Voltage [volt]')
title('Battery Voltage')

figure(9)
plot(time/60,SOC*100)
xlabel('time [min]')
ylabel('persentage of charge [%]')
title('State of Charge')

figure(10)
plot(Range, SOC*100)
xlabel('range [miles]')
ylabel('state of charge [%]')
title('Range as Fnc of SOC')

figure(11)
plot(time/60, Motor_speed_RPM)
xlabel('Time [min]')
ylabel('Motor speed [rpm]')
title('Motor Speed')

figure(12);
plot(time, Actual_vehicle_velocity);
hold on
plot(time, velocity);
xlabel('time');
ylabel('velocity [m/s]');
title('velocity');
legend('Actual vehicle speed', 'drive cycle')
hold off

figure(13);
plot(time, actual_motor_trque, 'g');
hold on
plot(time,Trq_req_motor, 'r --');
hold off
xlabel('Time [sec]');
```

```matlab
ylabel('Torque [Nm]');
title('Requested vs Actual Torque');
legend('Actual Motor Torque','Requested Motor Torque')
```